UNDERSTANDING RESERVOIR MECHANISMS USING PHASE AND COMPONENT STREAMLINE TRACING

A Thesis

by

SARWESH KUMAR

Submitted to the Office of Graduate Studies of
Texas A&M University
in partial fulfillment of the requirements for the degree of

MASTER OF SCIENCE

August 2008

Major Subject: Petroleum Engineering

UNDERSTANDING RESERVOIR MECHANISMS USING PHASE AND COMPONENT STREAMLINE TRACING

A Thesis

by

SARWESH KUMAR

Submitted to the Office of Graduate Studies of
Texas A&M University
in partial fulfillment of the requirements for the degree of

MASTER OF SCIENCE

Approved by:

Chair of Committee,	Akhil Datta-Gupta
Committee Members,	Yalchin Efendiev
	Daulat D. Mamora
Head of Department,	Stephen A. Holditch

August 2008

Major Subject: Petroleum Engineering

ABSTRACT

Understanding Reservoir Mechanisms Using Phase and Component Streamline Tracing.

(August 2008)

Sarwesh Kumar, B.Tech., Indian School of Mines, Dhanbad, India

Chair of Advisory Committee: Dr. Akhil Datta-Gupta

Conventionally streamlines are traced using total flux across the grid cell faces. The visualization of total flux streamlines shows the movement of flood, injector-producer relationship, swept area and movement of tracer. But they fail to capture some important signatures of reservoir dynamics, such as dominant phase in flow, appearance and disappearance of phases (e.g. gas), and flow of components like CO_2.

In the work being presented, we demonstrate the benefits of visualizing phase and component streamlines which are traced using phase and component fluxes respectively. Although the phase and component streamlines are not appropriate for simulation, as they might be discontinuous, they definitely have a lot of useful information about the reservoir processes and recovery mechanisms.

In this research, phase and component streamline tracing has been successfully implemented in three-phase and compositional simulation and the additional information obtained using these streamlines have been explored. The power and utility of the phase and component streamlines have been demonstrated using synthetic examples and two field cases. The new formulation of streamline tracing provides additional information about the reservoir drive mechanisms. The phase streamlines capture the dominant phase

in flow in different parts of the reservoir and the area swept corresponding to different phases can be identified. Based on these streamlines the appearance and disappearance of phases can be identified. Also these streamlines can be used for optimizing the field recovery processes like water injection and location of infill wells. Using component streamlines the movement of components like CO_2 can be traced, so they can be used for optimizing tertiary recovery mechanisms and tracking of tracers. They can also be used to trace CO_2 in CO_2 sequestration project where the CO_2 injection is for long term storage in aquifers or reservoirs. They have also other potential uses towards study of reservoir processes and behavior such as drainage area mapping for different phases, phase rate allocations to reservoir layers, etc.

DEDICATION

To my always encouraging family and my friends.

ACKNOWLEDGMENTS

First of all, I'd like to sincerely thank my advisor and committee chair, Prof. Akhil Datta-Gupta, for his guidance, support, and for funding this project. I'd also like to thank Dr. Michael King for his ideas and Dr. Eduardo E. Jimenez for his previous work in this area, which provided a really strong base to carry my work forward. I am also thankful to Mr. Kim Jong and Mr. Ajitabh Kumar for their continuous help in executing this project.

Last but not least, I would also like to thank all of my friends in the Department of Petroleum Engineering, especially Prannay Parihar. Their encouragement and support have made my journey through my M.S. degree a truly pleasant experience.

This work was supported in part by the industrial partners of the MCERI (Model Calibration and Efficient Reservoir Imaging) Joint Industry Project at Texas A&M University.

Thank you very much.

NOMENCLATURE

V_x	X-direction velocity of the phase in the cell under consideration
$V_{E/W/N/S/T/B}$	Average velocity components in the east/west/north/south/top/bottom directions respectively
$\Delta x / \Delta y / \Delta z$	Dimensions of the grid cells in the x/y/z directions
$Q_{E/W/N/S/T/B}$	Volume flow rate components in the east/west/north/south/top/bottom directions respectively
$v(x, y, z, t_0)$	Velocity field which is independent of time and depends on the location in the grid only
α, β, γ	Fractional distance along x/y/z directions respectively (for corner point grid to unit cube cell conversion)
$Q_{x/y/z}$	Principal velocity at points within unit cube cell in x/y/z directions respectively
F_{Tni}	Total flow rate from cell 'i' into neighbouring cell 'n'
$\mu_{o/w/g}$	Oil /water/gas viscosity, cp
$\rho_{o/w/g}$	Oil/water/gas density,lbm/cu ft
ϕ	Porosity of the cell
τ	Time of flight, day(s)
k_{rp}	Relative permeability of the phase *p,* (e.g. k_{ro} is the relative permeability of oil)
G	Acceleration due to gravity

D	Cell center depth
$d\tau$	Time of flight for the streamline for the given cell
dx	Distance traveled by the streamline in *x, y, z* directions
x_p^c	Mole fraction of component *c* in phase *p*
dP_{pni}	Potential difference of phase p between cells *n* and *i*
	Where,
	$dP_{pni} = P_{pn} - P_{pi} - \rho_{pni}\, G(D_n - D_i)$
	or
	$dP_{pni} = P_{pn} - P_i - P_{cpn} - P_{cpi} - \rho_{pni}\, G(D_n - D_i)$
P_{cp}	Capillary pressure for the phase *p*
P_p	Pressure for the phase *p*
ρ_{cp}	Mass density of phase *p*
T_{ni}	Transmissibility between cells *'n'* and *'i'*
S_{ij}	Phase saturation
ξ_{ij}	Phase molar density
x_{ij}	Mole fraction
k_{rj}	Relative permeability
μ_j	Phase viscosities
P_j	Phase pressure
ρ_j	Phase density
r_i	Molar flow rate per unit bulk volume for component *i*

TABLE OF CONTENTS

CHAPTER Page

CHAPTER Page

LIST OF FIGURES

FIGURE Page

FIGURE Page

FIGURE Page

CHAPTER I

INTRODUCTION

Streamline Simulation is now an established reservoir engineering tool, particularly useful for geologically complex and heterogeneous systems and for convection dominated flow. As it decouples the underlying geological model from the solution process of the transport equations, it is a computationally efficient alternative of conventional finite-difference simulation and has been successfully implemented for fast simulation of waterflood cases[16-23] and effective assisted history matching[30-38]. The comparative performance of finite difference method with numerical & analytical streamline simulator for a water flood case has been described in detail[7].

In addition to the regular simulation uses, the streamlines have the added feature of visualizing the flow and thus it can be used for identifying swept and un-swept regions in waterflood[16-23], for establishing injector-producer relationship[1,21,25] and tracer transport[25-29], for water-flood allocation[3,21], for predicting water breakthrough[1], for optimizing water injection and management of waterflood[16,18], for identifying reservoir compartmentalization[24], for statistical ranking of stochastic geo-models[39-41]. Using the concept of effective density, streamline simulation has also been successfully used for compositional simulations[24].

This thesis follows the style of *Society of Petroleum Engineers Journal.*

Streamlines have also been used with API tracking which can be compared to miscible gas injection (like CO_2)[26-27]. The ranking process of geostatistical models involving streamlines have been modified to incorporate production history and as well as to preserve the geological information[41].

Traditionally streamlines have been traced using total flux which can be used to trace the movement of the fluid as total. As discussed in detail in the above mentioned references, in addition to the regular simulation uses, total flux streamlines are great tool for study of reservoir dynamics due to visualization of the flow in the reservoir. They can be used for heterogeneity assessment of the reservoir[1,3] e.g., calculation of heterogeneity indicators such as Dynamic Dykstra Parson Coefficients and Lorentz coefficients for the reservoir. They are useful in upscaling because we can identify the layers having identical flow behavior[1, 3, 8]. But they fail to capture some of the important signatures of the reservoir dynamics, e.g. the dominant phase in flow in different regions of the reservoir and appearance & disappearance of phases cannot be identified. Streamlines based on total flux do not provide conclusive evidence of reservoir drive mechanism operating in different parts of reservoir and they cannot be used for tracking components like CO_2.

In this research, application of streamlines, as a flow visualization and reservoir dynamics study tool, have been broadened by tracing streamlines corresponding to the individual phases and components along with streamlines corresponding to the total flux. It would be demonstrated that some of the drawbacks of total flux streamlines can be addressed by this new approach of streamline tracing.

I .1 Motivation and Literature Review

Streamline simulation has been in use for quite some time now and it has been used for almost all stages of reservoir evaluation and monitoring. In addition to fast simulation that streamline simulation technology provides, flow visualization is one of the other most important benefit of streamlines. The literature on use of streamline simulation as a reservoir engineering tool is voluminous. Use of streamline simulation ranges from quick evaluation and ranking of geostatistical models, upscaling to get optimal layer simulation model, identification of un-swept reserves, and as source of novel information like injector-producer relationship. In spite of all the attention that streamlines have been getting recently as a simulation and flow visualization tool, we feel that still a lot need to be done to explore all the information that streamlines have to offer. The current study is a step towards that attempt.

The modeling of convection dominated flow in the reservoir has seen at least four other technologies[1] that have preceded streamline simulation. These are Line-source/sink methods, streamtube methods, particle tracking, and tracer & two phase flow using concept of stream-functions and potential-function.

A very important development, which enabled the decoupling of the underlying geological model and makes streamline simulation computationally efficient, is the concept of "time of flight" introduced by Datta-Gupta & King[1]. The 3D problem of saturation calculations can be reduced to 1D transport equations along the streamlines using transformation to time of flight coordinates. The solution in this transformed

coordinates is not restricted by CFL (Courant, Fredrichs, and Levy) criteria and hence large time-steps can be taken leading to overall faster simulation[1, 5, 7].

Pollock's algorithm[11], that suggests piece-wise linear interpolation of the velocity field within a grid block, forms the basis of streamline tracing in rectangular grid. Later this was extended to more complex geometries by several researchers and now streamline simulators can practically handle most of the geological complexities[9].

Broadly the application of streamlines can be divided into two categories depending on their special properties, which are:

1) Flow Visualization Applications
2) Faster Flow Computation Applications

Most of the projects undertaken by researchers and industry professionals exploit both the benefits of the streamlines, some of which are being listed below:

1) Flow Visualization Applications:
    a) Swept Volume Calculations: As streamline time of flight is directly related to the movement of flood front and mapping of TOF (τ) on the streamlines at different cut-offs gives an intuitive and visually appealing representation of the swept area[1, 2]. It also gives the connected volume that can be used for swept volume calculations for the geological model under various scenarios of well location and completions. **Fig. 1** presents the streamlines traced using total flux and the corresponding grid cells intersected at a particular cut-off of time-of-flight. As shall be discussed in

detail in Chapter II, time-of flight although given in unit of time, is used as a spatial coordinate in streamline simulation. So TOF can be treated as that linear distance along streamline till where the reservoir has been contacted in that many days (e.g. the penetrated cells presented in the right panel of the figure represent swept area in 10,000 days). It is significant to point out that the swept area in pattern is not uniform and is a function of heterogeneity and the well rates. So it would not be imprudent to conclude that a visualization tool like streamline is of immense help in reservoir management.

Streamline based drainage volumes can also be used to infer reservoir compartmentalization and flow barriers[24]. This process is based on matching the drainage volumes associated with the streamlines with their counter-parts from the decline curve analysis. Discrepancy in the two drainage volumes suggests some flow barrier or compartment not accounted in the geological model. Here for primary depletion or compressible flow, the concept of diffusive TOF is utilized.

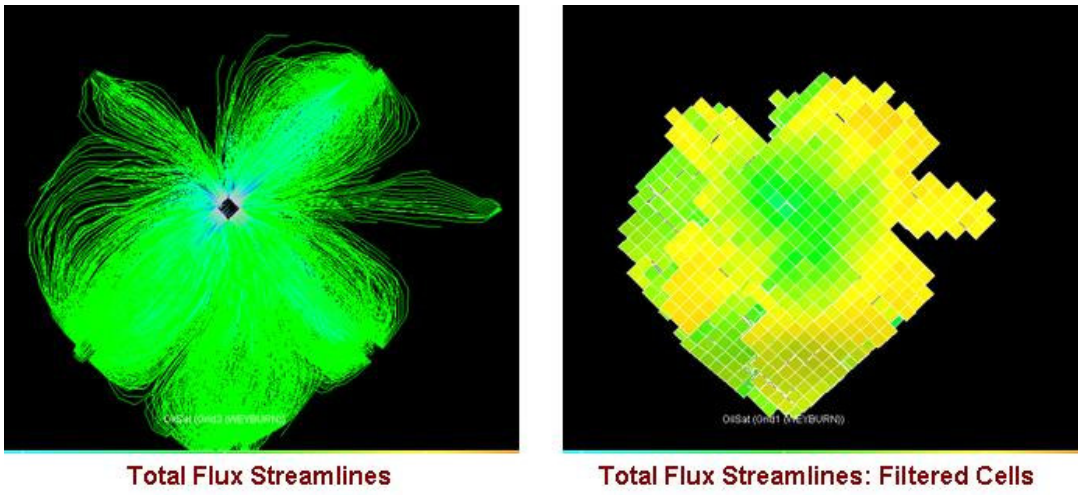

Fig. 1 – Swept Volume Calculation Using Streamline TOF Cut-Off (Here TOF Cut-Off of 10,000 Days is used)

b) Rate Allocation and Pattern Balancing: Due to the way the streamlines are constructed, they establish a direct relationship between the injectors and producers. Finite difference methods focus on where the fluid is and what the components involved are, whereas streamline simulation focuses on where the fluid is going. So streamline simulation can be used for rate allocation in producer-injector relationship and for balancing of patterns to minimize the water-cut. The use of streamlines to calculate Dynamic Injection Pattern Allocations[21] has been demonstrated to describe waterflood patterns through time. Here the author has highlighted the advantage of streamlines over the conventional finite difference simulation in finding out inefficiencies in the waterflood and to set injection targets. This dynamic process is better than static allocation methods like using angle open to flow

or volume distance weighting methodology which rarely represent the flow behavior or flow paths. The author has concluded that use of streamline generated dynamic allocation leads to reduced water cycling and increased efficiency of patterns.

The ability to quantify and visualize reservoir flow using streamline simulations and their use to define dynamic well allocation factors (WAFs) between injector and producers has been demonstrated in numerous previous works[1-4,6, 18]. They have also shown how the streamlines allow well allocation factors to be broken down into phase rates at either end of each injector/producer pair. The streamlines account for out of pattern flow which was a handicap of the previous methods. In this paper the authors have used streamlines derived injection efficiency, which has been defined as volume of offset oil production per unit volume of water being injected, to optimize the injection-production pattern.

c) Waterflooding: The single biggest area of application of streamlines is waterflood monitoring and optimization. This is due to the favorable nature of the problem in water-flood, of convection based flow regime with slighty compressible flow. Streamlines are also good for study of water floods due to visual depiction of movement of water front along the streamlines and have been used for optimal waterflood management[16]. Here the approach used is to equalize the arrival times of the water-front at all the producers within a selected sub-region of waterflood to minimize water recycling and

to maximize sweep efficiency. Streamline simulation has also been proactively used to manage waterflood[19]. Pattern optimization by actively using streamlines leads to gain in the offset oil producers. The streamlines were used to quickly build the history matched model by delineating which regions of the reservoir were responsible for low/high water-cuts and also gave some idea about the order of permeability change required at those regions. Then the streamlines in the history matched model guided the pattern optimization by indicating (i) where to increase injection rate, (ii) where to control the production rate, (iii) which high gross rate wells to close so as to divert the flow towards offset oil producers, (iv) assessment of unswept reservoir for infill, (v) which producer-injector pairs to be converted and (vi) estimation of water-cut for development location. In streamline based reservoir management[22], the balanced and unbalanced patterns can be identified, swept volume can be calculated and the kind of water drive present can be checked.

d) Modeling Tracer Flow: Streamlines have also been used to investigate inter-well connectivity and tracer transport[25]. Streamline simulation has also been used to simulate API tracking and it is mathematically similar to miscible gas injection[26]. Although this paper talks about the CO_2 injection as a possible candidate, but does not mention how CO_2 or for that matter any other component can be tracked using streamline. Also it does not talk about study of streamline as a visualization tool for CO_2 injection. These concerns

have been addressed in the work being presented as part of this thesis. Streamlines have also been used for IOR (Incremental Oil Recovery) evaluation process[27]. Here the approach is to calibrate 'recovery curves' that capture the characteristics of oil mobilization and returned solvent volumes as a function of gas injected. These calibrated curves are then used as tracers using streamline front tracking simulation to scale up to full field response.

2) Faster Computation Applications:

a) Up-gridding and Upscaling: Streamlines are useful in upgridding because we can identify the layers having identical flow behavior[1-3]. Application of streamlines to propose non-uniform up-gridding and to evaluate efficiency of this method, have been studied by Kurelenkov et al[8]. It has been established that non-uniform grids generated using the streamline technology better captures reservoir heterogeneity and that they are more efficient. Also, irrespective of whether the streamlines are used for upgridding and upscaling or not, the validity of the upgridding and upscaling process can be checked using streamline simulation because of their flow based approach and fast computation[5].

b) Ranking Geostatistical Models: Streamline simulation can handle geological models without upscaling. As the flow simulation is comparatively faster, they have been used for statistical ranking of stochastic geo-models[39, 40]. In one of the approaches the streamline properties like time-

of-flight for the geological realizations are compared with that of a history matched model to rank them[36].

c) History Matching/ Production Data Integration: As streamlines not only visualize the flow and establish injector-producer relationship but also their properties are directly related to the permeabilities, they can be used in assisted history matching[30-36]. Its use as an effective assisted history matching tool relies on sensitivity calculation using the fact that the modifications to reservoir properties needed to match production data can be estimated by using streamline TOF. The TOF, in turn, is inversely proportional to the average permeability along the streamline.

d) Primary Recovery, Compressible Flow and Compositional Simulation: Streamline simulation loses some of its computational advantages when used with compressible flow although in favorable cases it can be substantially faster than finite-difference methods. Also they have unique flow visualization capabilities which are not available with finite difference simulation[1,2]. For application to primary recovery or compressible flow concept of diffusive TOF is used whereas the compositional simulations are carried out using the concept of effective density[1, 31].

It can be observed that a lot of work is available in literature illustrating the use of total velocity streamlines but to our best knowledge no attempt has been made to extend the theory and implementation of streamline tracing to use of phase and component fluxes in streamline tracing. The nearest attempt is the use of tracer analogy

to model miscible gas injection. But this requires upscaling to 2D and although it is faster, it can not be used for visualization tool in general. Also the major challenge associated with this tracer analogy is the process of building up and validating the 2D layered field tracer model for the use by the streamline simulation.

I .2 Objective of Study

The objective in this research is to implement phase and component streamline tracing using the output of black oil and compositional simulators. Then these streamlines have been interpreted and analyzed along with the conventional streamlines to see how this added information helps us in better understanding of the reservoir flow mechanisms. Attempt has also been made to list the various purposes that they can be used for. The obvious motivation was to overcome the limitations of the conventional streamlines in terms of flow visualization.

Here the output of conventional black oil and compositional simulator has been used for streamline tracing. Thus by use of our post-processing tool to trace streamlines, the benefits of the finite difference simulator, in terms of accuracy of solutions, and reservoir flow visualization benefits of streamlines have been combined.

CHAPTER II

STREAMLINE-BASED SIMULATION

Reservoir simulation is the process of modeling the flow behavior of fluids through the porous media. The steps in reservoir simulation mainly consists of (i) Building up of the fine geostatistical model using all the available petrophysical parameters (porosity, permeability, seismic data, etc.), well locations & completions and other information (e.g. analogy to some other reservoirs), (ii) Upscaling to a coarse simulation model suitable for handling by simulators, (iii) Allocating the dynamic parameters such as well rates and production control parameters, (iv) Computation of the flow rates and pressure using mass conservation equation and Darcy's law, (v) Calibration of the simulation model by tuning to match the production history, (vi) Using the calibrated model to predict the future reservoir performance. Before advent of streamline simulation, the finite difference simulator dominated both the theoretical and practical work of reservoir simulation. Finite difference simulators are popular due to their robustness and due to their ability to simulate a lot of reservoir effects, e.g. capillary pressure and production parameters such as surface group constraints.

But finite-difference simulation methods have not been able to cope up with the advancement in the geological model building capacity. With advancement of computing technology and recent developments in geosciences, multi-million cell models can be easily made. But finite difference methods typically cannot handle such detailed models, so the geological models need to be upscaled and generally this

upscaling process leads to loss of information and often, introduction of unrealistic features. Also recently focus has shifted to have multiple realizations of the reservoir so that the range of uncertainty in the data and the modeling processes can be addressed. But all the hard work done in the uncertainty incorporation in the geological modeling can be incorporated in the business and operation decision making process only when flow simulations can be done to rank them or to generate multiple realizations of reservoir performance based on them. But finite difference simulators, due to the computational requirement, are of little help here.

Streamline simulation is IMPES in solution process because the pressure solution is implicit at each time step and the saturation is solved explicitly along each streamline. Streamline simulation are particularly useful for modeling large, complex and heterogeneous geological systems where the factors pre-dominantly affecting the flow are well positions and rates, static properties (porosity, permeabilities, faults, etc.), fluid mobility and gravity. They are computationally efficient, particularly for the cases where the time-steps in finite-difference simulation are restricted due to CFL criteria. This is due to decoupling of heterogeneity from saturation solution process.

Streamline simulation consists of the following steps:

1) Computation of velocities across the cell faces: This involves solution of pressure and saturation equations to get the phase velocities.
2) Tracing of streamlines is done using the total velocity and computation of time of flight is done on fly while tracing streamlines. By construction streamline density is more in high flow region and hence streamlines tend to resolve the area of

higher flow density in better way and the regions of flow stagnancy are allocated relatively fewer streamlines.

3) The initial saturation at that particular time-step is mapped to the streamlines.

4) After initialization of streamlines, the saturation equations are solved along streamlines in time of flight coordinates. This transformation from the actual geological grid coordinates to the time of flight coordinates decouples the effect of the heterogeneity and variation in grid dimensions. As the underlying grid does not matter during time-step selection, the time steps can be much larger than the ones for finite difference simulations.

5) Streamlines are periodically updated to honor the change in mobility conditions due to drastic change in saturation. Also change in field conditions like infill wells warrant update of the streamlines. After each update the time of flight is computed and the saturation calculations are carried forward in the updated time of flight coordinates.

6) Mapping of saturation from streamlines to the geological grid or vice-versa is a potential source of error in streamline simulation. This problem is addressed by having sufficient number of streamlines in each grid cell so that the computation efficiency is not lost whereas the saturation error are less than the allowable tolerance.

II .1 Basic Governing Equations

For tracing of streamlines and computation of time of flight along streamlines, velocities of the phases are required. Pressure equations need to be derived to obtain phase pressures and phase fluxes.

The general mass conservation equation for component *i* can be written as,

$$\frac{\partial W_i}{\partial t} + \nabla \cdot \overrightarrow{J_i} = R_i \quad \text{.....(1)}$$

Where, W_i, $\vec{J}_i$ and R_i are the accumulation, flux and the source or sink terms respectively[1]. Expanding the accumulation term, expressing the flux of component *i* in terms of convective and dispersive terms, and source or sink terms in molar flow rate per unit bulk volume for component *i*, the general conservation equation for component *i* can be written as[1] :

$$\frac{\partial}{\partial t}(\phi \sum_{j=1}^{n_p} \xi_j S_j x_{ij}) + \nabla \cdot \sum_{j=1}^{n_p} (\xi_i x_{ij} \overrightarrow{u_j} - \phi \xi_j \overrightarrow{\overrightarrow{K_{ij}}} \cdot \nabla x_{ij}) = r_i, i = 1,...,n_c \quad \text{.....(2)}$$

Where,

ϕ = Porosity

ξ_j = Molar density of phase *j*

S_j = Saturation of phase *j*

x_{ij} = Mole fraction of component *i* in phase *j*

$\overrightarrow{\overrightarrow{K}}$ = Dispersion tensor

Here the phase fluxes $\vec{u_j}$ are related to the phase pressures through a multiphase version of Darcy's law,

$$\vec{u_j} = -\vec{\vec{k}}_{ij} \cdot \lambda_{rj}(\nabla P_j - \rho_j g \nabla D) = -\vec{\vec{k}}_{ij} \cdot \lambda_{rj} \nabla \Phi_j, \quad \text{.....(3)}$$

Where,

λ_{rj} = Given as (k_{rj}/μ_j) are the relative phase mobilities

P_j = Phase pressure

ρ_j = Phase density

D = Depth from a reference pressure datum

g = Acceleration due to gravity

ϕ_j = Phase potential

For incompressible flow and ideal mixing, the above conservation equation can be represented in terms of volume of component *i* per unit bulk volume per unit time as follows,

$$\frac{\partial}{\partial t}(\phi \sum_{j=1}^{n_p} S_j C_{ij}) + \nabla \cdot \sum_{j=1}^{n_p} (C_{ij} \vec{u_j} - \phi S_j \vec{\vec{k}}_{ij} \cdot \nabla C_{ij}) = q_i, i = 1,...,n_c \quad \text{.....(4)}$$

Where, the accumulation, flux and source terms become respectively,

$$W_i = \phi \sum_{j=1}^{n_p} S_j C_{ij}, \quad \text{.....(5)}$$

$$\vec{J_i} = \sum_{j=1}^{n_p} (C_{ij} \vec{u_j} - \phi S_j \vec{\vec{K}}_{ij} \cdot \nabla C_{ij}) \text{ , and } \quad \text{.....(6)}$$

$$R_i = q_i, \quad \text{.....(7)}$$

Where,

q_i = Specific flow rate, i.e., volumetric flow rate of component *i* per unit bulk volume

C_{ij} = Concentration of component *j*

S_j = Saturation of phase *j*

Summing up the component conservation **Eq. 4** over all components leads to the following,

$$\sum_{j=1}^{n_p} \nabla \cdot \vec{u}_j = q_i \quad \text{.....(8)}$$

Where q_t represents the total specific rate, that is, total volumetric injection/production rate per unit bulk volume. Substituting Darcy's Law into **Eq. 8** leads to the following pressure equation,

$$-\nabla \cdot \sum_{j=1}^{n_p} \overrightarrow{\overrightarrow{k_{ij}}} \cdot \lambda_{rj} (\nabla P_j - \rho_j g \nabla D) = q_t \quad \text{.....(9)}$$

Using the capillary pressure relations to express all other phase pressure in terms of the aqueous phase pressure as given below,

$$P_j = P_w + P_{cwj} \quad \text{.....(10)}$$

Leads to the equation describing the aqueous phase pressure distribution:

$$-\nabla \cdot \vec{\vec{k}} \cdot \lambda_{rt} \nabla P_w = -\nabla \cdot \sum_{j=1}^{n_p} \vec{\vec{k}} \cdot \lambda_{rj} \rho_j g \nabla D + \nabla \cdot \sum_{j=2}^{n_p} \vec{\vec{k}} \cdot \lambda_{rj} \nabla P_{cwj} + q_t \quad \text{.....(11)}$$

The above equations can be solved numerically to obtain the phase pressure and phase velocities for incompressible flow. During simulation, typically finite difference methods are used to solve these equations.

II .2 Coordinate Transformation to TOF Coordinates

Streamlines are defined as integrated curves that are locally tangential to the direction of the velocity. The relationship between streamline and velocity is expressed schematically in **Fig. 2**. Here the velocity used for tracing streamline is instantaneous velocity at a particular time step. The actual simulation problem which can be unsteady state is treated as a series of steady-state problems at each time step.

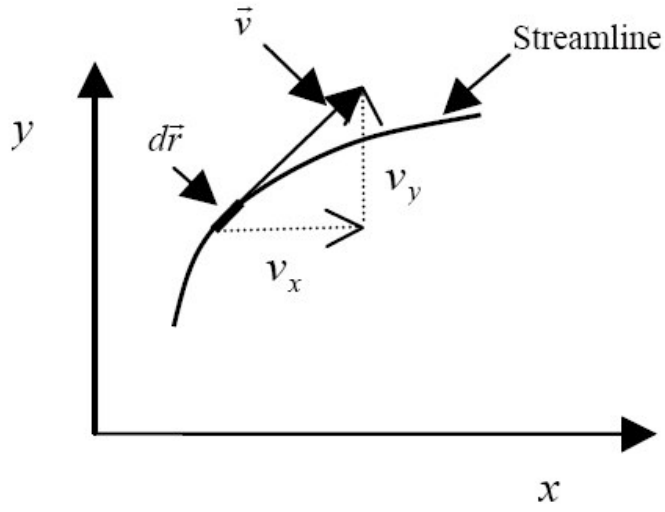

Fig. 2 – Relationship Between Streamline and Velocity in Planar Flow (after Bear, 1972)

Streamline should not be confused with pathline which is the actual trajectory of a neutral tracer particle as it moves through space and time. For a steady state flow streamline and pathline describe the same path but not for an unsteady state flow. For unsteady state flow, streamlines are a representation of the instantaneous velocity, not a physical trajectory.

Time of Flight: Time of flight is a very important parameter along the streamlines. By definition, it is the time taken by a neutral tracer to travel from the origin (sources like injectors or aquifer) to the point under consideration. **Fig. 3** schematically presents the concept of the time of flight.

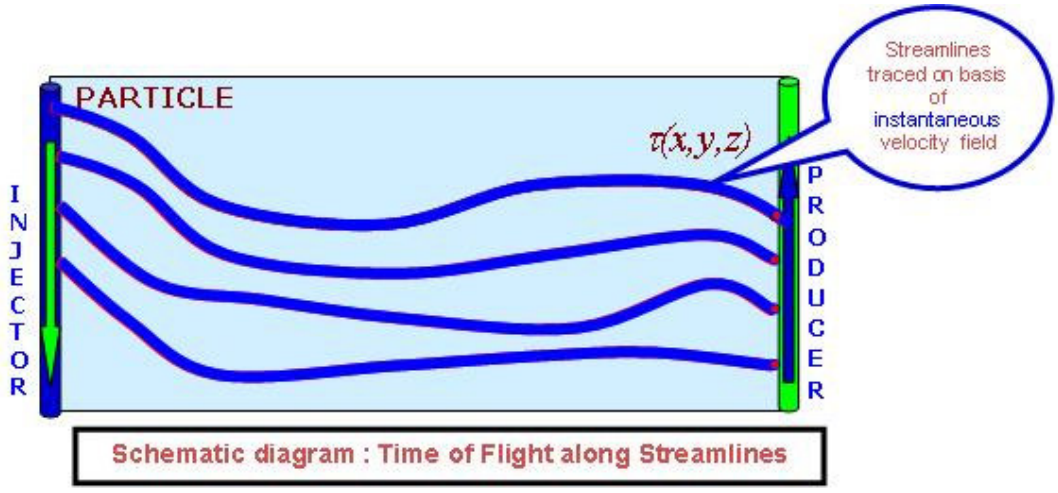

Fig. 3 – Schematic Diagram to Illustrate "Time of Flight"

Tracing of streamlines using total velocity will be discussed in detail in the next chapter. Without loss of continuity, it can be stated here that once the phase velocities are available they are summed up to get the total velocity which is used for tracing. For

each grid cell the time of flight is calculated and streamlines are traced on fly from source to sinks.

Once the streamlines are traced the transport equations are solved along the streamlines which is basically a transformation of the Euclidian coordinates to time of flight coordinates which is very crucial in terms of making the simulation process computationally efficient. Time of flight can also be used to represent the movement of fluid along streamline and hence can be used for swept volume calculation.

Time of flight is represented by the following integral:

$$\tau = \int_0^s \frac{\phi}{\left|\vec{u}\right|} ds \quad \text{.....(12)}$$

The test particle moves at the interstitial velocity, $\vec{u}/\phi$, and s is the spatial distance along streamline. Rewriting **Eq. 12** as a differential relationship,

$$\vec{u} \cdot \nabla \tau = \phi \quad \text{.....(13)}$$

Or as,

$$\frac{\vec{u}}{\phi} = \frac{\Delta s}{\Delta \tau} \quad \text{.....(14)}$$

This can be rewritten as in terms of the operator identity,

$$\left|\vec{u}\right| \frac{\partial}{\partial s} \equiv \vec{u}_t \cdot \nabla = \phi \frac{\partial}{\partial \tau} \quad \text{.....(15)}$$

The **Eq. 15** presents the operator identity at the heart of transformation from physical coordinates to the streamline time-of-flight coordinates. The power of the transformation of Euclidean coordinates to the time of flight *(τ)* coordinates can be

shown by application of this concept to the conservation equation for water phase in two-phase incompressible flow away from source and sink, (neglecting gravity and capillarity) as follows,

$$\phi \frac{\partial S_w}{\partial t} + \nabla \cdot (F_w \vec{u}_t) = 0, \quad \text{.....(16)}$$

Where F_w is the fractional flow term, $F_w = \lambda_w / \lambda_t$, Using the operator identity as derived in **Eq. 15** to transform from the physical space to the time of flight coordinates,

$$\nabla \cdot (\overrightarrow{F_w u_t}) = \vec{u}_t \cdot \nabla F_w = \phi \frac{\partial F_w}{\partial \tau} \quad \text{.....(17)}$$

Thus, the conservation equation can be written as,

$$\frac{\partial S_w}{\partial t} + \frac{\partial F_w}{\partial \tau} = 0, \quad \text{.....(18)}$$

As a result of this coordinate transformation, the 3D fluid flow has been decomposed into a series of 1D (in TOF coordinates) evolution equation for S_w along streamlines. This transformation includes all the effects of the heterogeneity and the dimensions of the problem (1D, 2D or 3D). The transport equation in TOF coordinates do not suffer from CFL restriction so can take large time-steps. The gravity and capillarity effects can be inducted in the transport calculations by use of operator splitting. Therefore, this transformation leads to order of magnitude of efficiency in computation[7, 20]. With all these background information about streamline simulation we are ready to compare streamline simulation viz-a-viz conventional finite difference simulation.

II .3 Streamline Simulation vs. Finite Difference Simulation

Streamline simulations are computationally more efficient than the finite difference simulations due to the following reasons:

1) As streamlines need to be updated only when there is some drastic change in saturation conditions or field conditions, the streamlines are updated infrequently.

2) Transport equations along the streamlines can be often solved analytically.

3) The solution of 1D transport equations along the streamlines are not constrained by the underlying geological grid-stability criterion (CFL criteria), thus allowing larger time-steps.

4) For displacements dominated by heterogeneity, computation time with streamline simulation varies linearly with the number of grid cells involved whereas for finite difference simulation it is order of magnitude more.

In addition to the computational advantage, the streamline simulation gives intuitive depiction of fluid flow due to their visualization capability which is not possible with finite difference methods. Also the streamlines give novel information like injector-producer relationship, swept area, well allocation factors and dynamic resolution of flow regions (i.e. higher streamline density in areas of higher flow compared to that of lower flow) which can be used in non-uniform up-gridding and upscaling. All these information is not available from finite-difference simulation methods directly or in most cases not even indirectly.

CHAPTER III

STREAMLINE TRACING USING TOTAL FLUX

By definition, streamlines are integrated curves that are locally tangential to the velocity field. It is same as the particle trajectory for steady state flow but not for unsteady state flow[1].

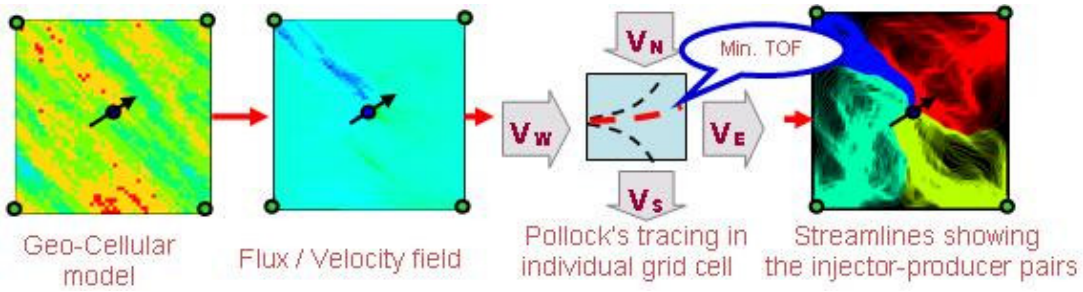

Fig. 4 – Streamline Tracing Using Total Flux

Fig. 4 shows a schematic workflow for streamline tracing using the total flux. The geo-cellular (earth) model is read into the standard simulator, which solves the pressure equations implicitly at each time step. After the calculation of pressure, flow equations are solved to obtain the fluxes of each phase at the cell faces. The phase fluxes (oil / gas/ water) across the cell faces are summed up to get the total flux which is used for streamline tracing. The streamlines are traced using the Pollock's or Modified Pollock's algorithm depending upon the kind of grid involved (rectangular or corner point grid) [9-11].

III . 1 Streamline Tracing in Cartesian Grid

For the streamline tracing in the conventional way, the total velocity is used. The tracing algorithm depends on the type of underlying grid. In this exercise, the grid used is corner point grid (CPG), but to understand the tracing in CPG we need to first go through the rectangular grid streamline tracing[9].

III .1.1 Pollock's Algorithm

Pollock's algorithm assumes that the total velocity varies linearly between the values on the opposing cell faces.

The Convention used in this exercise is as given in the **Fig. 5**.The average linear velocity component across each face is given as in **Eq. 19**.

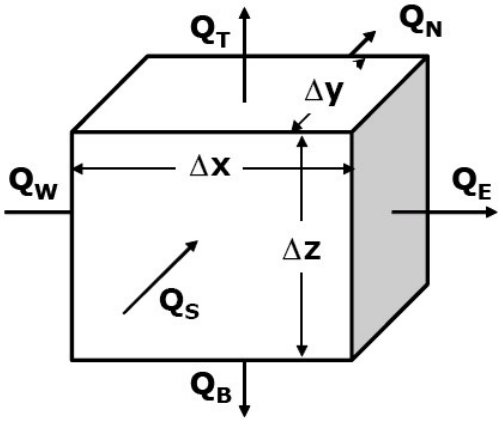

Fig. 5 – Finite Difference Cell Showing xyz Definitions[9]

$$V_E = \frac{Q_E}{\phi \cdot \Delta y \cdot \Delta z}, V_W = \frac{Q_W}{\phi \cdot \Delta y \cdot \Delta z}$$
$$V_N = \frac{Q_N}{\phi \cdot \Delta x \cdot \Delta z}, V_S = \frac{Q_S}{\phi \cdot \Delta x \cdot \Delta z} \quad \text{.....(19)}$$
$$V_T = \frac{Q_T}{\phi \cdot \Delta x \cdot \Delta y}, V_B = \frac{Q_B}{\phi \cdot \Delta x \cdot \Delta y}$$

Where Q is volume flow rate across a cell face and Δx, Δy and Δz are the dimensions of the cell in the respective coordinate directions. By the Pollock's interpolation, the principal velocity components at points within a cell can be obtained as follows:

$$V_x = A_x(x - x_1) + V_w$$
$$V_y = A_y(y - y_1) + V_N \quad \text{.....(20)}$$
$$V_z = A_z(z - z_1) + V_T$$

Where, A_x, A_y and A_z are constants that correspond to the components of the velocity gradients given as,

$$A_x = \frac{(V_W - V_E)}{\Delta x}$$
$$A_y = \frac{(V_N - V_S)}{\Delta y} \quad \text{.....(21)}$$
$$A_z = \frac{(V_T - V_B)}{\Delta z}$$

The movement of the particle is tracked through the grid cell. In the grid cell, the rate of change in the particle's *x-component* of velocity is given by:-

$$\left(\frac{dV_x}{dt}\right)_p = \left(\frac{dV_x}{dt}\right)\left(\frac{dx}{dt}\right)_p \quad \text{.....(22)}$$

Borrowing the definition of A_x from **Eq. 21** and denoting the time rate of change of the *x-location* of the particle, $(dx/dt)_p$, by V_{xp} we get,

$$\frac{1}{V_{xp}}\left(dV_x\right)_p = A_x dt \quad \text{.....(23)}$$

Integrating between times t_1 and t_2 leads to,

$$\ln\left(\frac{V_{xp}(t_2)}{V_{xp}(t_1)}\right) = A_x \Delta t \quad \text{.....(24)}$$

Putting the definition of the V_{xp} from the **Eq. 20** in the **Eq. 24** gives us the *x-position* of the particle as follows:

$$x_p(t_2) = x_1 + \frac{1}{A_x}\left[V_{xp}(t_1)e^{A_x \Delta t} - V_{x1}\right] \quad \text{.....(25)}$$

III .1.2 Steps of Streamline Tracing in Cartesian Grid

Now having established the equations for streamline tracing, the steps of the streamline tracing can be listed as follows:

a) The phase velocities are computed from the three dimensional solution of the pressure field and by application of Darcy's Law. The total velocity is the sum of these phase velocities in the appropriate units.

b) For the streamline tracing in the conventional way, the total velocity is used. The Pollock's Algorithm is used for the rectangular grid streamline tracing[9].

c) Here using **Eq. 24** corresponding to the respective faces, the time of flight taken by the particle to reach all the possible faces of exit are calculated.

d) Obviously, the actual streamline path would be the one with the minimum positive time of flight. For example, in the **Fig. 6** for a two-dimensional grid, the actual time is the smaller of Δt_x and Δt_y *(Time of Flight in x and y directions respectively)* and is denoted by Δt_e.

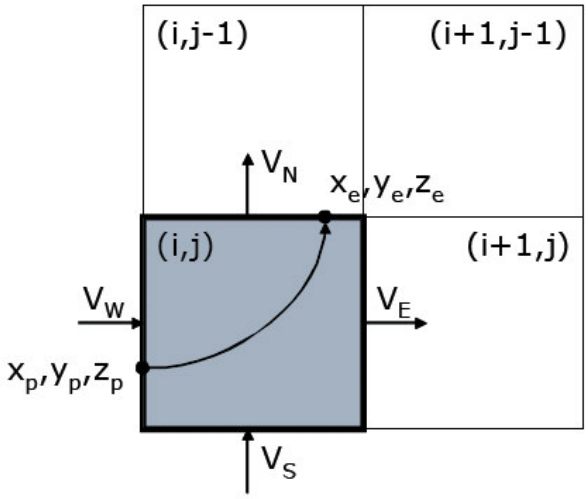

Fig. 6 – Computation of Exit Point and Travel Time in 2D[9]

e) This minimum of the positive time-of-flight, Δt_e, is used in **Eq. 25** to determine the exit coordinates (x_e, y_e) for the particle as it leaves the cell (i, j),

$$x_e = x_1 + \frac{1}{A_x}\left[V_{xp}(t_p)e^{A_x \Delta t_e} - V_{x1}\right] \quad \text{.....(26)}$$

$$y_e = y_1 + \frac{1}{A_x}\left[V_{yp}(t_p)e^{A_y \Delta t_e} - V_{y1}\right] \quad \text{.....(27)}$$

These steps are repeated for each grid cell that the particle enters until the particle reaches a sink or discharge point. Similarly for 3D these equations are repeated in all the three coordinates.

Equation of streamlines, which is the backbone of streamline tracing, is presented in the parametric form as follows:

$$\frac{d\tau}{\phi} = \frac{dx}{v_x(x,y,z,t_0)} = \frac{dy}{v_y(x,y,z,t_0)} = \frac{dz}{v_z(x,y,z,t_0)} \quad \text{.....(28)}$$

III .2 Streamline Tracing in Corner Point Grid (CPG)

Here the development by Cordes and Kinzelbach[12] (CK) as used by Eduardo Jimenz[10] is used as an extension to Pollock's algorithm. The streamline is traced in the unit cube cell using linear varying model of flux as discussed below. Then the unit cell coordinates, entry and exit coordinates are mapped back to the physical space in CPG using iso-parametric transformation.

III .2.1 Modified Pollock's Algorithm

For the unit cell, the Pollock's equation is re-written in dimensionless variables using the fractional distances through all three coordinate directions. The fractional distances are as represented in **Eq. 29**,

$$\alpha = \frac{x}{DX}$$
$$\beta = \frac{y}{DY} \quad \text{.....(29)}$$
$$\gamma = \frac{z}{DZ}$$

The directional interstitial velocities are converted into volumetric fluxes using the equations given as,

$$Q_x = u_x \cdot DY \cdot DZ$$
$$Q_y = u_y \cdot DX \cdot DZ \quad \text{.....(30)}$$
$$Q_z = u_z \cdot DX \cdot DY$$

Then a simple linear interpolation, similar to **Eq. 20** is applied to compute the principal velocity components at points within a cell. The linear interpolate for the volumetric flux in the *x-direction* is given as,

$$Q_j(\alpha_j) = A_j + C_j \cdot \alpha_j, \; j = 1, 2, 3 \quad \text{.....(31)}$$

Using the expression for the rate of change in the particle's velocity components as it moves through the cell, **Eq. 30** can be expressed as below,

$$\phi \cdot DX \cdot \frac{d\alpha}{d\tau} = \frac{Q_x(\alpha)}{DY \cdot DZ}$$
$$\phi \cdot DY \cdot \frac{d\beta}{d\tau} = \frac{Q_y(\beta)}{DX \cdot DZ} \quad \text{.....(32)}$$
$$\phi \cdot DZ \cdot \frac{d\gamma}{d\tau} = \frac{Q_z(\gamma)}{DX \cdot DY}$$

So in the transformed coordinates, the following relationships are obtained,

$$\frac{d\tau}{\phi \cdot DX \cdot DY \cdot DZ} = \frac{d\alpha}{Q_x(\alpha)} = \frac{d\beta}{Q_y(\beta)} = \frac{d\gamma}{Q_z(\gamma)} \quad \text{.....(33)}$$

This equation is similar to the streamline equation in the rectangular grid, **Eq. 28**; just the Pollock's model has been rescaled in terms of dimensionless distances and volumetric fluxes. For general corner point grids, the cell volume *(DX.DY.DZ)* in the **Eq. 33** is replaced by the Jacobian of the transformations $|J|$ as suggested by Cordes & Kinzelbach. So the time of flight can be determined by the following set of equations,

$$\phi \cdot \frac{d\alpha}{d\tau} = \frac{Q_x(\alpha)}{J(\alpha,\beta,\gamma)}$$
$$\phi \cdot \frac{d\beta}{d\tau} = \frac{Q_y(\beta)}{J(\alpha,\beta,\gamma)} \quad \text{.....(34)}$$
$$\phi \cdot \frac{d\gamma}{d\tau} = \frac{Q_z(\gamma)}{J(\alpha,\beta,\gamma)}$$

Here, as the Jacobian has the dimensions of volume and is a cross sectional area times a physical distance, the right side in the **Eq. 34** is essentially a Darcy velocity in the corresponding direction, scaled by cell length in that direction. But the solution of the **Eq. 34** to solve for the (α,β,γ) trajectories is quite difficult compared to similar operation in rectangular grid cells. This is so because the parameters (α,β,γ) are coupled through the Jacobian. To simplify the integration of the (α,β,γ) trajectories, the concept of pseudo-time-of-flight has been introduced[9].

III .2.2 Pseudo Time of Flight

The pseudo time of flight increases along a trajectory and acts as a time like variable. In the *x-direction* the equation for pseudo-time-of-flight would be,

$$\int_0^{T_E} dT = \int_{\alpha_0}^{\alpha} \frac{d\alpha}{Q_1(\alpha)} \quad \text{.....(35)}$$

Generalizing for the three directions the parametric equation for streamline is given as,

$$dT = \frac{d\tau}{\phi \cdot J(\alpha,\beta,\gamma)} = \frac{d\alpha}{Q_1(\alpha)} = \frac{d\beta}{Q_2(\beta)} = \frac{d\gamma}{Q_3(\gamma)} \quad \text{.....(36)}$$

For constant scaling factors, the equations for the (α,β,γ) in terms of the pseudo time of flight (T) are identical to the Pollock's equations in a three dimensional rectangular cell as given in **Eq. 28**.

III .2.3 Transformation to Real Space of CPG

Once the streamlines are traced in unit cube and we have the unit cube co-ordinates, the entry and the exit coordinates, then they are mapped to the real space of the CPG using iso-parametric transformation. For illustration, the transformation equations for the point 1 of the grid in **Fig. 7** are given as:

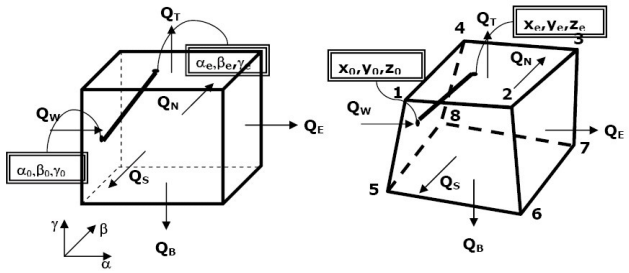

Fig. 7 – Iso-Parametric Transformation of Unit to Real Space[9]

$$x = P_{1x}\alpha + P_{2x}\beta + P_{3x}\gamma + P_{4x}\alpha\beta + P_{5x}\beta\gamma + P_{6x}\alpha\gamma + P_{7x}\alpha\beta\gamma + P_{8x}$$
$$y = P_{1y}\alpha + P_{2y}\beta + P_{3y}\gamma + P_{4y}\alpha\beta + P_{5y}\beta\gamma + P_{6y}\alpha\gamma + P_{7y}\alpha\beta\gamma + P_{8y} \quad \text{.....(37)}$$
$$z = P_{1z}\alpha + P_{2z}\beta + P_{3z}\gamma + P_{4z}\alpha\beta + P_{5z}\beta\gamma + P_{6z}\alpha\gamma + P_{7z}\alpha\beta\gamma + P_{8z}$$

Where,

$$\begin{aligned}
P_{1x} &= x_2 - x_1 \\
P_{2x} &= x_4 - x_1 \\
P_{3x} &= x_5 - x_1 \\
P_{4x} &= x_1 + x_3 - x_2 - x_4 \\
P_{5x} &= x_1 + x_8 - x_4 - x_5 \\
P_{6x} &= x_1 + x_6 - x_2 - x_4 \\
P_{7x} &= x_2 + x_4 + x_5 + x_7 - x_1 - x_3 - x_6 - x_8 \\
P_{8x} &\sim x_1
\end{aligned} \quad \text{.....(38)}$$

Similar equations are used for y and z coordinates of the point 1. Similarly transformations are carried out for all the points of the grid. After this transformation exercise we have the streamline entry and exit coordinates in the real space of the CPG.

III .2.4 Time of Flight Calculation in CPG

Actual time-of-flight in corner point grid is calculated as follows,

$$\tau = \phi \int_0^T J\big(\alpha(T), \beta(T), \gamma(T)\big)\, dT \quad \text{.....(39)}$$

Where the Jacobian of the real coordinates is expressed as follows:

$$J(x,y,z)=\begin{vmatrix}\frac{\partial x}{\partial \alpha} & \frac{\partial y}{\partial \beta} & \frac{\partial z}{\partial \gamma}\\ \frac{\partial x}{\partial \alpha} & \frac{\partial y}{\partial \beta} & \frac{\partial z}{\partial \gamma}\\ \frac{\partial x}{\partial \alpha} & \frac{\partial y}{\partial \beta} & \frac{\partial z}{\partial \gamma}\end{vmatrix} \quad \text{……...…….....…..(40)}$$

The Jacobian is a polynomial in α, β, and γ and they in turn are all known functions of the pseudo-time of flight. The resulting integrand is a sum of exponentials and constants which can be integrated numerically using the quadrature approach.

III .2.5 Steps of Streamline Tracing in CPG

a) To begin with, a unit cube is considered. The volumetric fluxes and its linear interpolate in unit cube and dimensionless distances are computed to be used in Modified Pollock's Algorithm as explained in Section (III.2.1).

b) The pseudo time of flight is computed for exit of particles from all the possible cell faces of the unit cube cell using **Eq. 35**.

For example, the time to reach the east face will be,

$$T_E=\int_{\alpha_0}^{\alpha}\frac{d\alpha}{A_j+C_1\cdot\alpha}=\frac{1}{C_1}\ln\left[\frac{a_1+C_1\cdot\alpha}{a_1+C_1\cdot\alpha_0}\right] \text{……...…….(41)}$$

Here, the volumetric flux has been replaced by its linear interpolate as given by **Eq. 31**.

c) Similarly time to exit from the other faces can be calculated and the actual pseudo-time of flight would be the one with the minimum positive value of the ΔT, i.e.,

$$\Delta T_e = Min\,(\Delta T_E, \Delta T_W, \Delta T_N, \Delta T_W, \Delta T_T, \Delta T_B)$$

Where, the subscripts 'e' corresponds to the actual time of flight taken to escape from the grid cell and subscripts E, W, N, S, T, B correspond to escape, east, west, north, south, top and bottom respectively.

d) Once the pseudo-time of flight is known the exit coordinate in the unit cube can be calculated in the similar fashion as that for the rectangular grid. The set of equations are as follows:

$$\alpha_e = \alpha_0 + (a_1 + \alpha_0 C_1)\left[\frac{e^{C_1 T} - 1}{C_1}\right]$$

$$\beta_e = \beta_0 + (a_1 + \beta_0 C_1)\left[\frac{e^{C_2 T} - 1}{C_2}\right] \qquad \text{.....(42)}$$

$$\gamma_e = \gamma_0 + (a_1 + \gamma_0 C_3)\left[\frac{e^{C_3 T} - 1}{C_3}\right]$$

Fig. 8 shows the exit coordinates computation in the unit cube, where the particle's time-of-flight is the minimum positive time to escape from the top face and hence the streamline is as shown by the curved line.

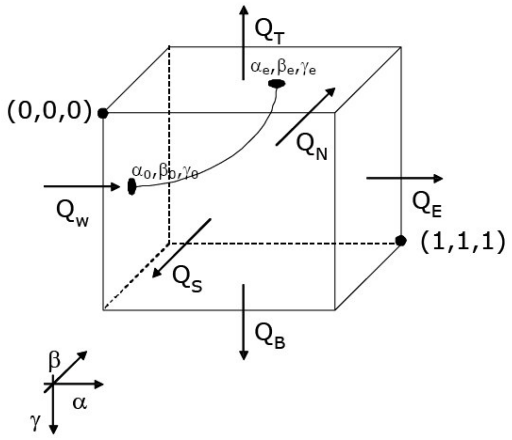

Fig. 8 – Computation of Exit Point and Time of Flight in a Unit Cube[9]

e) For each unit cube, the unit cube coordinates, entry and exit points for each streamline are transformed to the real space coordinates of CPG using equations similar to **Eq. 37** for each point.

f) The time of flight in real space is calculated as specified in Section (III.2.4).

Once streamlines are traced, the transport equations are solved along each streamline which in effect means transformation of coordinates from Cartesian grid to the time-of-flight coordinates. As the underlying geological model is decoupled, the selection of time step is not restricted by the CFL criteria and hence the saturation solution is computationally efficient[1]. Here the initial saturation is mapped from grid to streamline and after the solution of transport equation the final saturation is mapped back to the grid.

This research deals with only streamline tracing and does not concern with the saturation computation and mapping of saturation from streamlines to the grid. For

details of streamline simulation, solution of transport equation along streamlines and mapping of saturation from streamlines to grid, readers may refer to the several literature sources cited in the reference section.

Streamlines traced using the total flux, are great tool for study of reservoir dynamics due to visualization of the flow in the reservoir e.g. water flood front movement. Also they can be used for heterogeneity assessment of the reservoir. Dynamic Dykstra parson coefficients and Lorentz coefficients which are statistical indicators of heterogeneity for the reservoir can be calculated using streamlines. They are useful in upscaling because the layers having identical flow behavior can be identified. In upscaling the objective is to minimize the variation within an upscaled layer and maximize the variation between the layers. Using streamline the layers having similar flow properties can be clubbed together and thus optimal upscaling can be obtained. Also fast flow simulation can be done using streamline simulation to check the efficacy of upscaling. As mentioned in the references given in introduction, the total velocity streamlines are also useful for study of injector-producer relationship due to explicit visual depiction of their interaction, swept area calculation, ranking of geostatistical model based on swept area, and in AHM (Assisted History Matching) which involves the alteration of permeability as demarcated by the streamlines. But total velocity streamlines fail to capture some of the important signatures of the reservoir dynamics, e.g. the dominant phase in flow in different regions of the reservoir and also appearance & disappearance of phases cannot be identified. Streamlines traced using total flux do not provide conclusive evidence of reservoir drive mechanism operating in

different part of reservoir and also they cannot be used for tracking components like CO_2 in compositional simulation.

CHAPTER IV

STREAMLINE TRACING INVOLVING INDIVIDUAL FLUID PHASES AND COMPONENTS FLUXES

IV.1 Phase Streamline Tracing Using Output of Black Oil Simulators

In this exercise a standard commercial finite-difference black oil simulator has been used to compute the pressure and fluxes. The fluxes obtained as output along with array of other parameters written to the restart file have been used.

IV.1.1 Individual Phase Fluxes vs. Total Flux

The total flow rate from cell '*i*' into neighboring cell '*n*' is given by the sum of flow rate of all the phases.

$$F_{Tni} = F_{oni} + F_{wni} + F_{gni} \quad \text{.....(43)}$$

Where, F_{Tni} = Total flow rate from cell 'i' into neighboring cell 'n'

F_{oni} = Oil flow rate from cell 'i' into neighboring cell 'n'

F_{wni} = Water flow rate from cell 'i' into neighboring cell 'n'

F_{gni} = Gas flow rate from cell 'i' into neighboring cell 'n'

In the proposed approach, at the step when the individual phase fluxes are available, instead of summing them up to get the total velocity, they are treated individually for the tracing purpose.

IV.1.2 Streamline Tracing Using Phase Fluxes

Modified Pollock's algorithm for corner point grid (CPG) as discussed in Section (III.2.1) has been used for computing streamline trajectories and pseudo-time of flight following the steps as explained in Section (III.2.5). **Eq. 36** for all the phases in the unit cube is solved separately and phase streamlines are traced in the unit cube cell.

$$dT_i = \frac{d\tau_i}{\phi \cdot J(\alpha,\beta,\gamma)} = \frac{d\alpha}{Q_{1_i}(\alpha)} = \frac{d\beta}{Q_{2_i}(\beta)} = \frac{d\gamma}{Q_{3_i}(\gamma)} \quad \text{.....(44)}$$

Where, i = *oil, gas or water*

Then the coordinates are transformed from the unit cube to the corner point grid (CPG) using equations similar to **Eqs. 37** and **38** (chapter III) and TOF in CPG is computed using **Eq. 39** of the chapter III.

As generalized streamline tracing assumes nothing about the phase involved, streamlines for all the involved phases can be traced separately. The simulator is run only once and the phase fluxes stored can be used for tracing under different scenarios.

The phase streamlines need not lie along the total flux streamlines. For example, in regions with high gravity, the flow of water and oil can be totally different whereas the total velocity vector would be a result of vector addition of these two velocities.

Fig. 9 illustrates how phase streamlines can be different from the total velocity streamlines using a simple case of flow under effects of gravity. Here the streamlines would be locally tangential to the corresponding velocity vector. Similarly in areal sense also the water, oil, gas streamlines would show the regions of their respective dominance and orientation of flow. In real field cases, in addition to gravity, several other reasons could be in play causing the phase streamlines to be very different from each other and from total flux streamlines. These could be different zones of injection and production, different relative permeability resulting in differential flow of phases, alteration in injection schemes (e.g. Water Alternate Gas Injection Schemes), etc. The results discussed using the synthetic and field examples in Chapter V has tried to cover as many cases of such kind as possible.

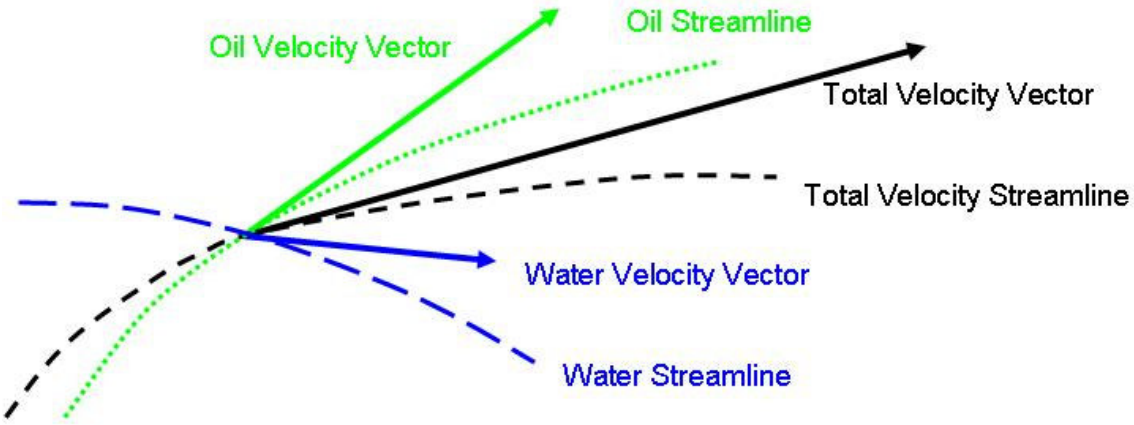

Fig. 9 – Schematic Diagram to Illustrate the Relationship between Phase and Total Velocity Streamline Tracing

The phase streamline tracing feature is not available in any of the commercial software. So a C++ based code (DESTINY), used to trace streamlines using total flux,

was modified to suit the need. Here, streamlines can be traced originating from sinks, which can be either the producers or individual cells having fractional flow (of the phase under consideration) greater than a specified value. For all practical purposes, the tracing from the individual cells is same as tracing from injectors onwards.

In our study, the fluxes are obtained from an industry standard finite difference simulator and the streamlines are traced by post processing the fluxes. The full flow physics involved has been honored by using finite-difference simulator and on the same hand the advantages of flow visualization and injector-producer connectivity information provided by the streamline analysis have been utilized. So this procedure has the benefits of both the streamline and finite difference simulation technologies.

IV.2 Component and Phase Streamline Tracing Using Output of Compositional Simulators

Standard compositional simulators give individual component fluxes as output instead of the phase fluxes. The component output is in moles/day. These along with other outputs such as phase potentials, molar density, mole fraction, relative permeability, etc. reported for each cell have been used in the following exercise to compute the component & phase streamlines.

IV.2.1 Component, Phase and Total Flux Calculations

As represented schematically in **Fig. 10**, the fractions of each component in different phases have been identified to get the phase fluxes which can then be used for tracing of streamlines.

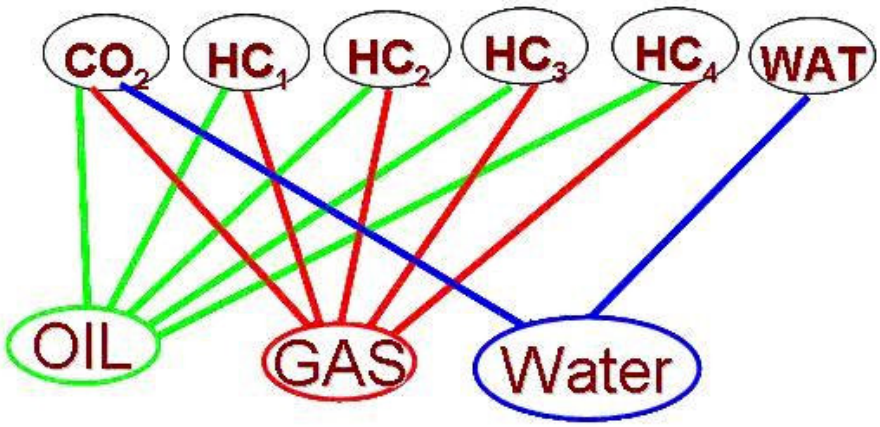

Fig. 10 – Schematic Diagram to Explain Component and Phase Flux Computation from the Component Fluxes Obtained as Compositional Simulator Output

The flow rate of component '*c*' embedded in a phase *p (p=o, w, g)* into cell '*i*' from a neighboring cell '*n*' is given as[13, 14, 15],

$$F^{c}_{Tni} = T_{ni}\,(M^{c}_{p})\,dP_{pni} \quad \text{.....(45)}$$

Where, M^{c}_{p} is the *generalized mobility* of component *c* in phase *p* given as,

$$M^{c}_{p} = x^{c}_{p} k_{rp}(S_p)\frac{b^{m}_{p}}{\mu_p} \quad \text{.....(46)}$$

Where, x^{c}_{p} = Mole fraction of component *c* in phase *p*

k_{rp} = Relative permeability of the phase *p*

S_p = Saturation of phase p

b_p^m = Molar density of phase p

μ_p = Viscosity of phase p

The fluid mobilities M_p^c are evaluated in the upstream cell for each phase (oil, water, gas) separately.

And, for the potential difference terms,

dP_{pni} = Potential difference of phase p between cells n and i defined as,

$$dP_{pni} = P_{pn} - P_{pi} - \rho_{pni}\, G(D_n - D_i)$$

or

$$dP_{pni} = P_{pn} - P_i - P_{cpn} - P_{cpi} - \rho_{pni}\, G(D_n - D_i)$$

where,

P_{pn} = Pressure for the phase p in cell 'n'

P_{pi} = Pressure for the phase p in cell 'i'

P_{cp} = Capillary pressure for the phase p

ρ_{cp} = Mass density of phase p

G = Acceleration due to gravity

Here **Eq. 45** has been used to identify the fraction of the components in different phases. Then it has been multiplied with the component flow rate across the cell faces in appropriate units to get the phase velocities. Then these phase velocities are used for streamline tracing. For total velocity streamlines, these phase velocities are summed up in the appropriate units to obtain the total velocity. If component tracking is required

then the component velocity in appropriate units is used. Also for each component, streamlines in different phases can be traced separately, i.e. CO_2 in aqueous phase and CO_2 dissolved in oil phase can be traced separately.

The streamlines corresponding to CO_2 in aqueous phase would be a great tool to study the movement of CO_2 in sequestration projects, in which the CO_2 is injected into aquifers for long time storage.

IV.2.2 Streamline Tracing Using the Phase(s) and Component Fluxes

Once the phase velocities and the component velocities are obtained in appropriate units for streamline tracing then the Modified Pollock's Algorithm for streamline tracing in the unit cube is used as explained in Section (III.2.1). Streamlines are traced using the steps outlined in Section (III.2.5) and then iso-parametric transformation is used to get the corresponding streamline coordinates in the real space corner point grid (CPG). The streamline TOF in CPG coordinates is calculates as explained in Section (III.2.4).

So, regarding tracing involving phases and components it can be summed that this new approach of streamline tracing is more or less same as the generalized streamline tracing in CPG with the only difference being in the way the fluxes are computed and treated for tracing.

CHAPTER V

RESULTS AND APPLICATIONS

V.1 Synthetic Model - Streamlines Using Output of Black Oil Simulator

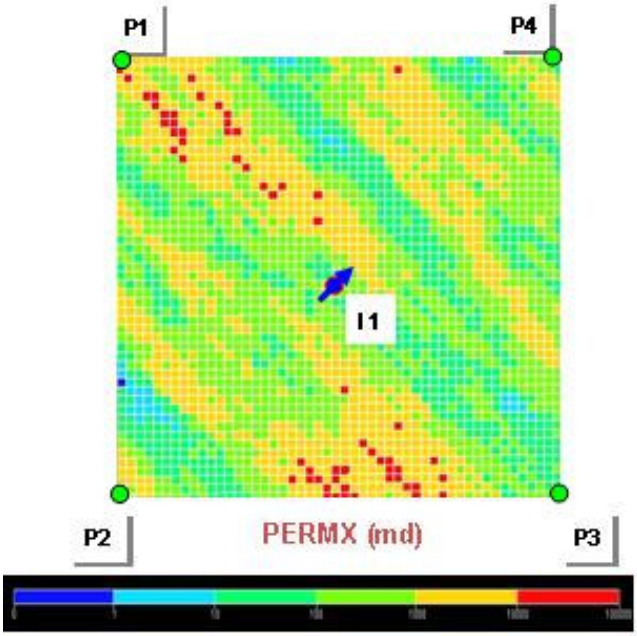

Fig. 11 – 2D Synthetic Model Used to Test the Formulation of Phase and Component Streamlines

Fig. 11 presents the two dimensional synthetic model which has been used to validate the phase streamline tracing. This model is a reservoir grid of (50X50X1) 2500 grid cells and has three phases, namely oil, water & gas in flow. This synthetic case was particularly chosen because although it is a simple model, yet it has different drive mechanism operating in different parts of the reservoir. It is a five spot pattern with four producers located at the corners & the injector at the center and the simulation study is

for 6 years. The porosity is same for all the cells at 22.5 % but permeability shows a high permeability trend in the north-west south-east direction. The pressure and fluxes were computed using the Eclipse©(Schlumberger) simulator and the streamline tracing was done using the in-house developed code "DESTINY".

V.1.1 Total Flux Streamlines (Fails to Capture Important Flow Effects)

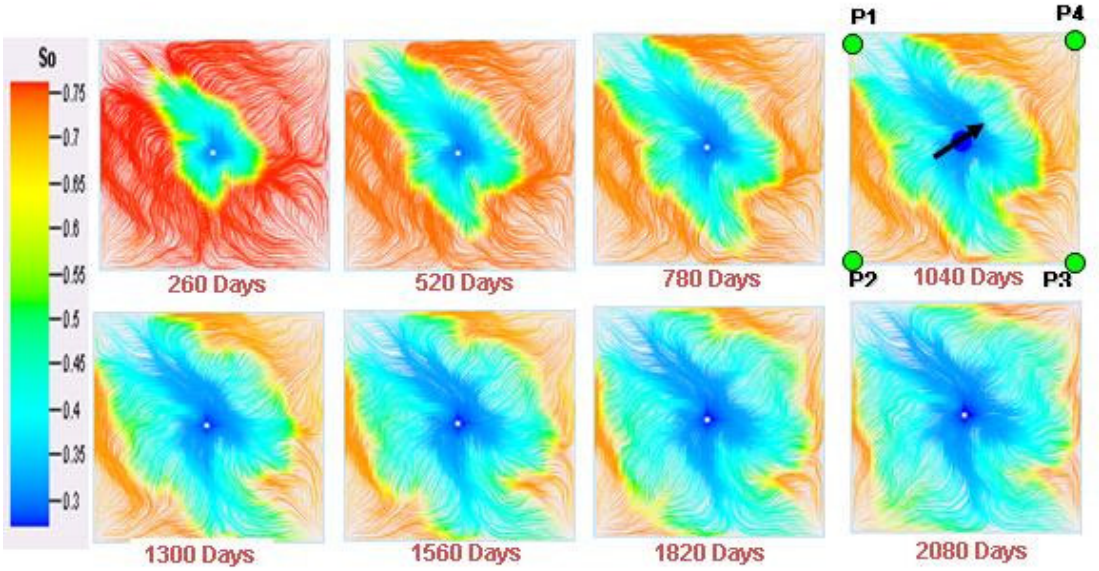

Fig. 12 – Synthetic Model: Total Flux Streamlines (Traced from Cells as Sinks, Oil Saturation Mapped on Streamlines)

In **Fig. 12**, the streamlines traced using the total flux have been presented. They have been traced from individual cells having fractional flow of the total flux greater than 0.1 (equivalent to tracing from injectors onwards to all the cells having fractional flow greater than the cut-off specified). For the total flux streamline this would include all the cells where the total flow is present because in all of those cells the fractional flow of the

total flow would be greater than 0.1. Oil saturation has been mapped along the streamlines and the streamlines along with saturation profile at eight consecutive time-steps, of 260 days each, have been shown.

The direction of sweep, as shown by oil saturation mapping on streamlines, can be easily linked to the permeability orientation. Although the movement of flood front can be visualized with time, we can not say for sure which regions have been stripped of oil and which regions have the dominant gas flow. We can not comment about the appearance and disappearance of gas in the history of field production. Also we are not able to distinguish between the drive mechanisms operating in different regions. We would try to address these issues with phase streamlines.

V.1.2 Phase Streamlines - Implementation and Significance

In this section, the streamlines have been traced separately for each phase (oil /water/ gas) & then they have been interpreted along with the total velocity streamlines. For each phase, streamlines have been traced from individual cells where the fractional flow of the phase under consideration is greater than 0.1 or from producers as sinks and corresponding saturation is mapped on the streamlines, e.g. water saturation on water streamlines and gas saturation on gas streamlines.

V.1.2.1 Water Streamlines (Explain Reservoir Drive Mechanism and Water-Cut of Producers)

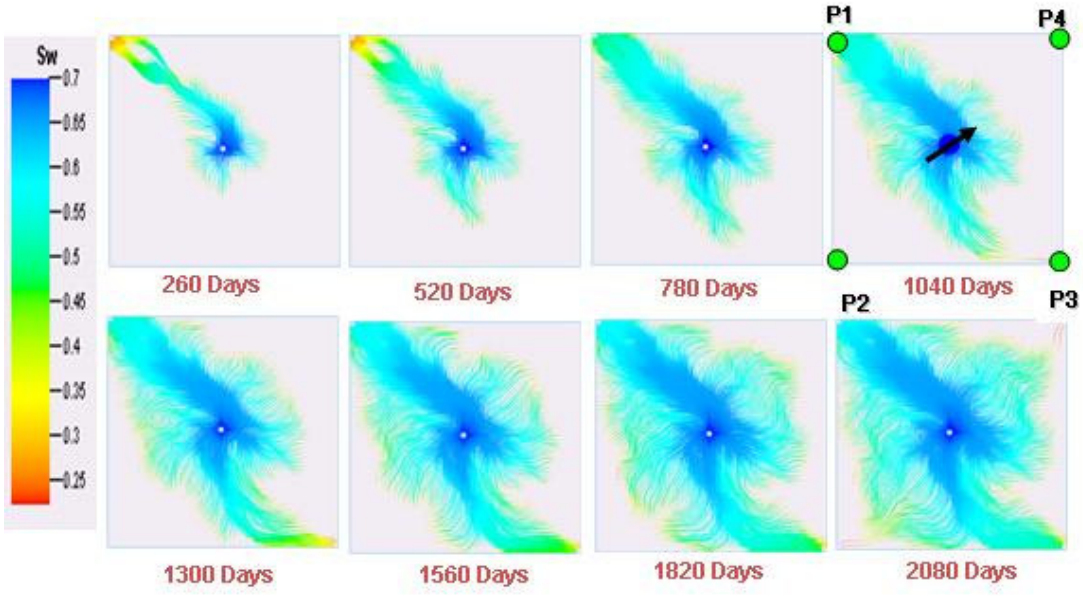

Fig. 13 – Synthetic Model: Water Streamlines (Traced from Producers and Cells as Sinks, Water Saturation Mapped on Streamlines)

In **Fig. 13** the streamlines based on water flux have been shown. Here the streamlines have been traced from producers as well as from individual cells having fractional flow of water greater than 0.1. So we see streamlines only in the regions of significant water flow along with water streamlines that have broken through at the producers.

Water streamlines suggest that the lion's share of water being injected is supporting the production from the well P1 and P3 whereas the wells P2 and P4 do not see effect of water drive until around 2000 days. From relative density of water

streamlines in near well regions, it is visually evident that the production at wells P1 and P3 is under water injection drive whereas production at well P2 and P4 is under natural depletion drive. The production from a well which is pressure supported by water being injected has been termed to be under water injection drive whereas production from a well which is driven by pressure depletion, without significant pressure support, has been termed as under natural depletion drive. Here using water streamlines the two different reservoir drive mechanisms can be identified and their existence can be distinguished from each other.

The water streamlines can also be used for explaining the water-cut of the producers. **Fig. 19** on page 56 shows the water-cut of all of the four producers. Well P1 & P3, at which the water streamlines have broken through, show early initiation of water-cut compared to the wells P2 & P4. The density of the water streamlines can also be used for explaining the water-cut magnitude in these wells. The well P1 having higher density of water streamlines has the higher water-cut compared to the well P3.

These streamlines can also be used for water flood front movement study. Thus, these streamlines are particularly effective for deciding on infill injection. As we can visually map the drainage area of the well with time, these streamlines can also be used for well test drainage area calculation.

They can also be used for assisted history matching of water cut. In history matching the approach is to honor the field production history without altering the prior model drastically. By using water streamlines, the regions whose static properties have direct bearing on the water production can be delineated. So to achieve a water-cut

match, the permeability only in the water streamline demarcated region is modified instead of using permeability multiplier for the entire model.

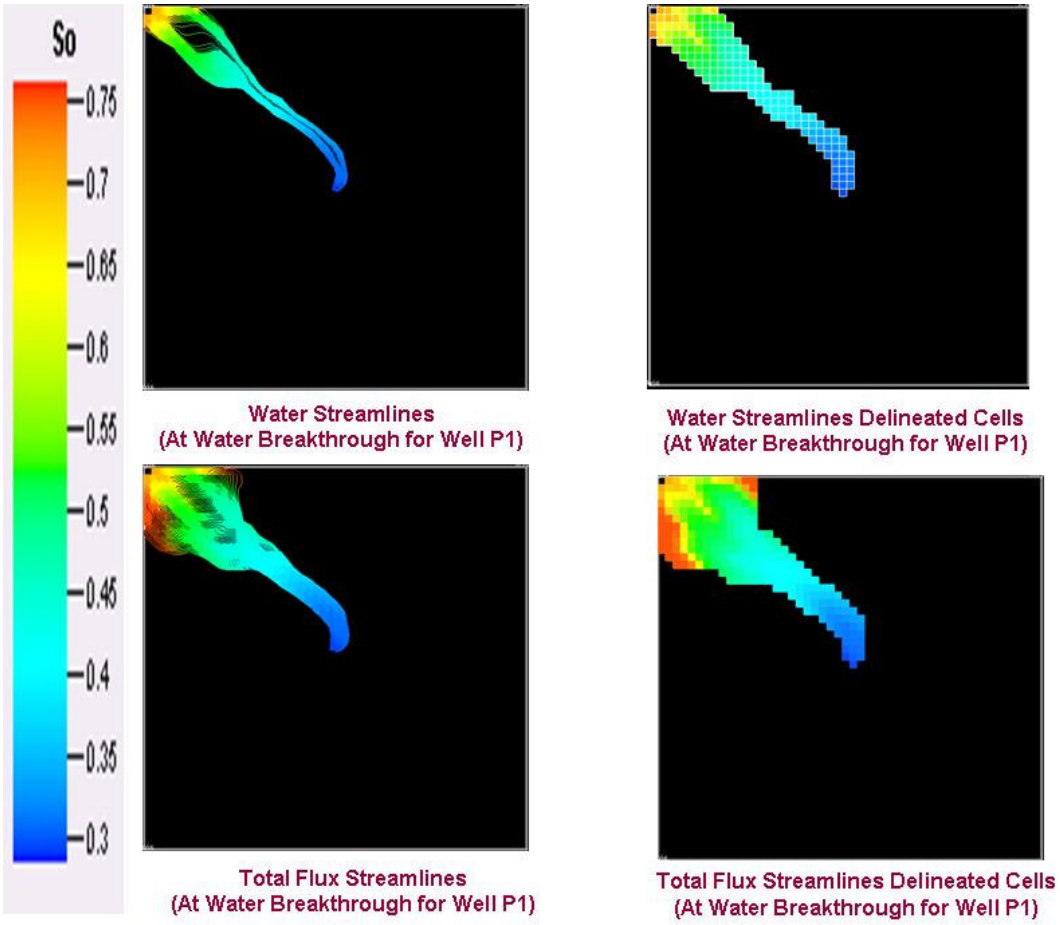

Fig. 14 – Synthetic Model: Streamline Delineated Cells for History Matching - Water Streamlines vs. Total Velocity Streamlines (Traced from Producers as Sinks, Oil Saturation Mapped on Streamlines)

In **Fig. 14** the water streamlines and total flux streamlines are presented for the time-step corresponding to water-breakthrough at well P1. It can be noted that water streamline delineated region for permeability alteration for matching water-cut is more localized than the region delineated by total flux streamlines (which breakthrough at the

producers). So water streamlines assisted history matching would have a higher tendency to preserve the prior model compared to total velocity streamlines. Please note that only streamlines which breakthrough at the producers should be used for assisted history matching.

V.1.2.2 Gas Streamlines (Show the Appearance & Disappearance of Gas with Time)

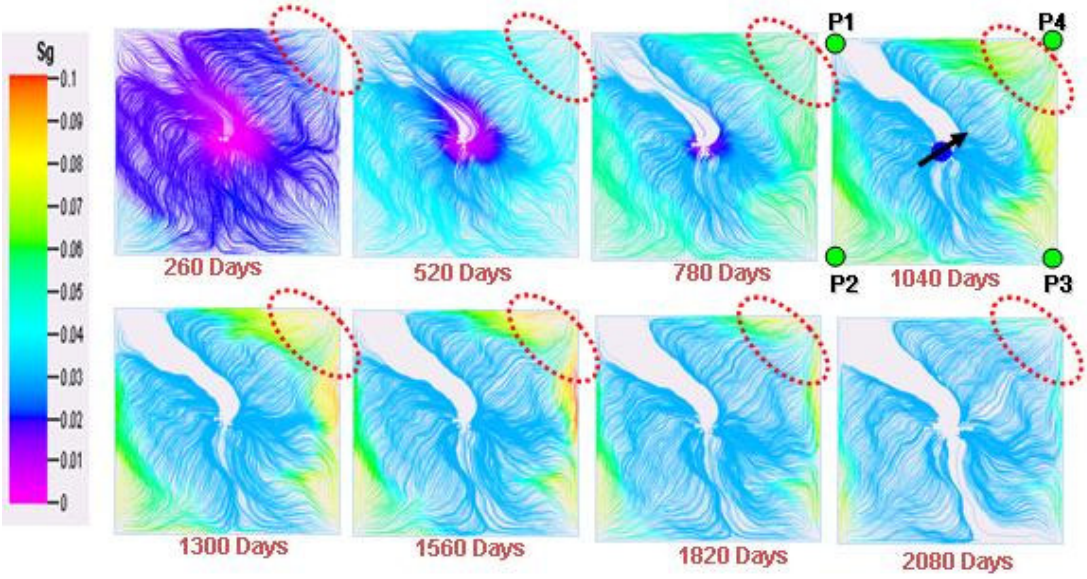

Fig. 15 – Synthetic Model: Gas Streamlines (Traced from Cells as Sinks, Gas Saturation Mapped on Streamlines)

In **Fig. 15** the gas streamlines from individual cells having fractional flow of gas greater than 0.1 have been shown. In the vicinity of the well P4 it can be noted that the gas saturation increases and then decreases with time. This increase in gas saturation can be

correlated to the natural depletion drive mechanism. In natural depletion drive, production is due to pressure drop and as there is little pressure support, reservoir pressure is more likely to go below bubble point pressure compared to regions of reservoir under pressure support. So high gas saturation because of release of solution gas is a typical signature of this kind of reservoir drive. Here the wells P2 and P4 which have been found to be producing under natural depletion show increase in gas saturation with time. But once the water being injected starts reaching these regions, with increase in reservoir pressure the gas is re-dissolved into the solution. This is also indicated by streamline density. High gas streamline density represents high gas flux near these wells. The regions with low or almost no gas streamlines specify the regions stripped of oil and hence having negligible or no mobile gas. On the same premises as using water streamlines for matching water-cut, the gas streamlines breaking through at producers can be used for assisted history match of gas-oil-ratio (GOR) of the producing wells.

V.1.2.3 Oil Streamlines (Identify Reservoir Drive Mechanism and Guide Water Flood Management & Well Location Optimization)

Fig. 16 shows the oil streamlines where the streamlines have been traced from the cells having fractional flow of oil greater than 0.1. Here by observing the distribution of oil streamlines, regions depleted of oil can be easily identified. Thus, the oil streamlines will be effective in identifying the infill producers. Near the wells P4 and P2 the oil saturation is decreasing but waterflood has not reached these regions so they are

producing under natural depletion whereas wells P1 and P3 are producing under water flood drive as shown by the streamlines. The two different reservoir mechanism of production, as were identified with water and gas streamlines, have now been verified using the oil streamlines.

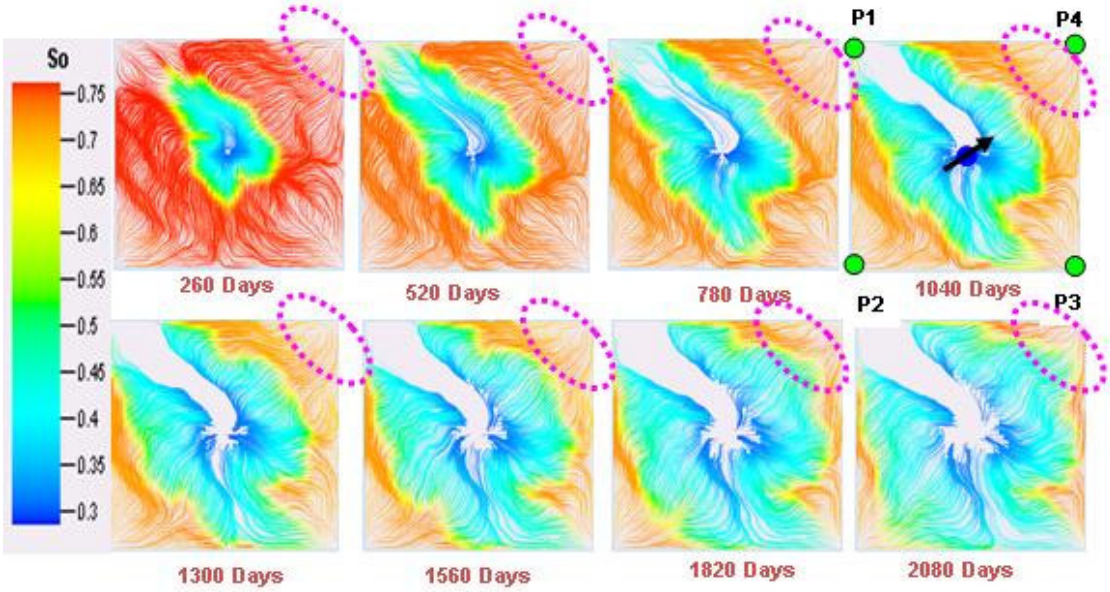

Fig. 16 – Synthetic Model: Oil Streamlines (Traced from Cells as Sinks, Oil Saturation Mapped on Streamlines)

Here it is noteworthy to observe that while regions of unswept oil remains in the reservoir, the water being injected is recycled through wells connected to injector through high permeability streaks without aiding oil recovery. So it can be concluded that considering the heterogeneity of the reservoir, the location of injector is not optimum and as most of the water injected is recycled by wells P1 and P3 after breakthrough, the location of injector should be changed (after 4th time step). Once we

have evaluated the base case, several scenarios can be created with different locations of injectors & producers and additional infill wells and then fast streamline simulations can be done to optimize the location of the wells to have maximum recovery. Thus, oil streamlines can be used to optimize the water injection well location and to locate infill wells to extract the un-swept oil.

V.1.2.4 Overlapping of Phase Streamlines (Helps in Determining the Reservoir Drive Mechanism)

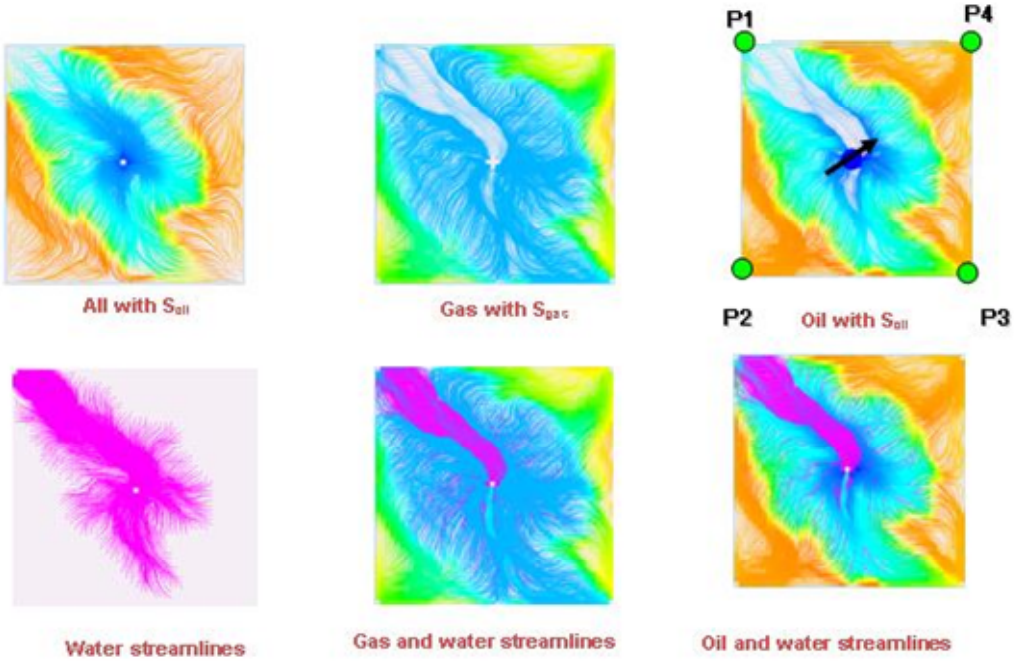

Fig. 17 – Synthetic Model: Overlapping of Phase Streamlines - Depicts Dominant Phase in Flow in Different Regions of the Reservoir

In **Fig. 17** oil and gas streamlines, at 1040 days (time-step 4), have been superimposed with water streamlines to show the selective regions of their dominance. It is quite evident that they complement each other. This is valuable information in a reservoir study for flood management and infill drilling location evaluation because the regions not benefitting from the current injection program can be identified.

V.1.3 Validation of Observations from Phase Streamlines Using the Pressure and Production Data

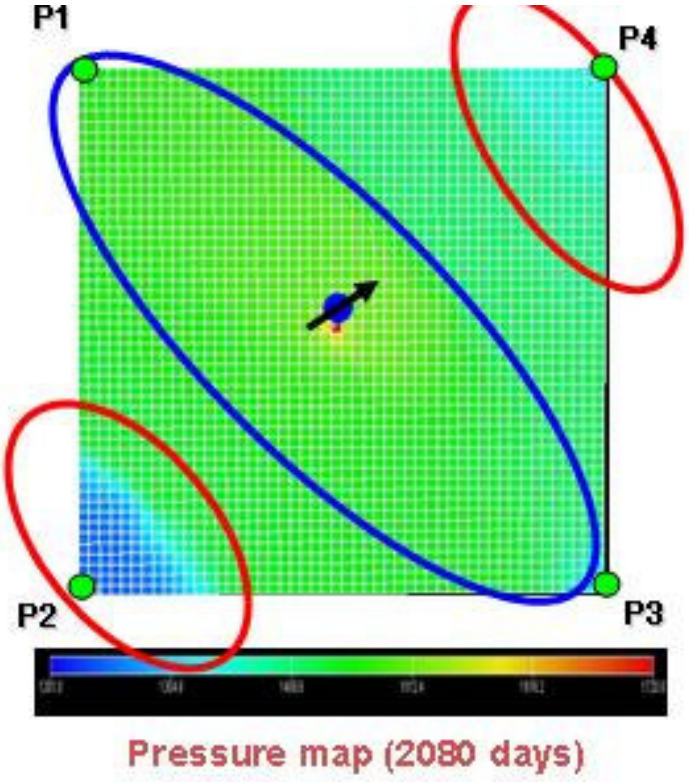

Fig. 18 – Synthetic Model: Pressure Map - Validates the Observations Made Using Phase Streamlines

Fig. 18 shows the average reservoir pressure map at the last time step (2080 days) for the model, which has been used to validate the observations about the GOR, water-cut and the drive mechanisms.

The wells P2 and P4 where we had dense gas streamlines show insufficient pressure support and high GOR (encircled in red), which are typical features of natural depletion whereas wells P1 and P3 have good pressure support and high water saturation which is in line with dense water streamlines at these wells suggesting water injection drive (encircled in blue).

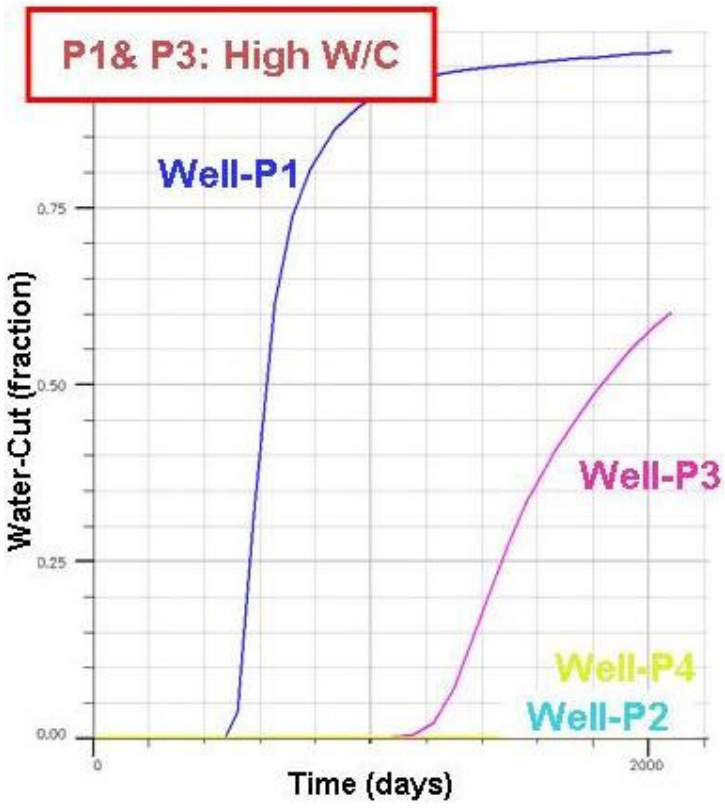

Fig. 19 – Synthetic Model: - Observed Water Cut in the Production Wells - Supports the Observations from Phase Streamlines

In **Fig. 19**, the water-cut for all the wells are presented. Here it can be noted that the wells where the water streamlines had broken through have high water-cut. Also the well P1 where the water streamlines had broken through earlier has early water-cut whereas P3 has water breakthrough after approximately 1000 days corresponding to 4th time step. The wells P2 and P4 where the water streamlines have not broken through show zero water-cut.

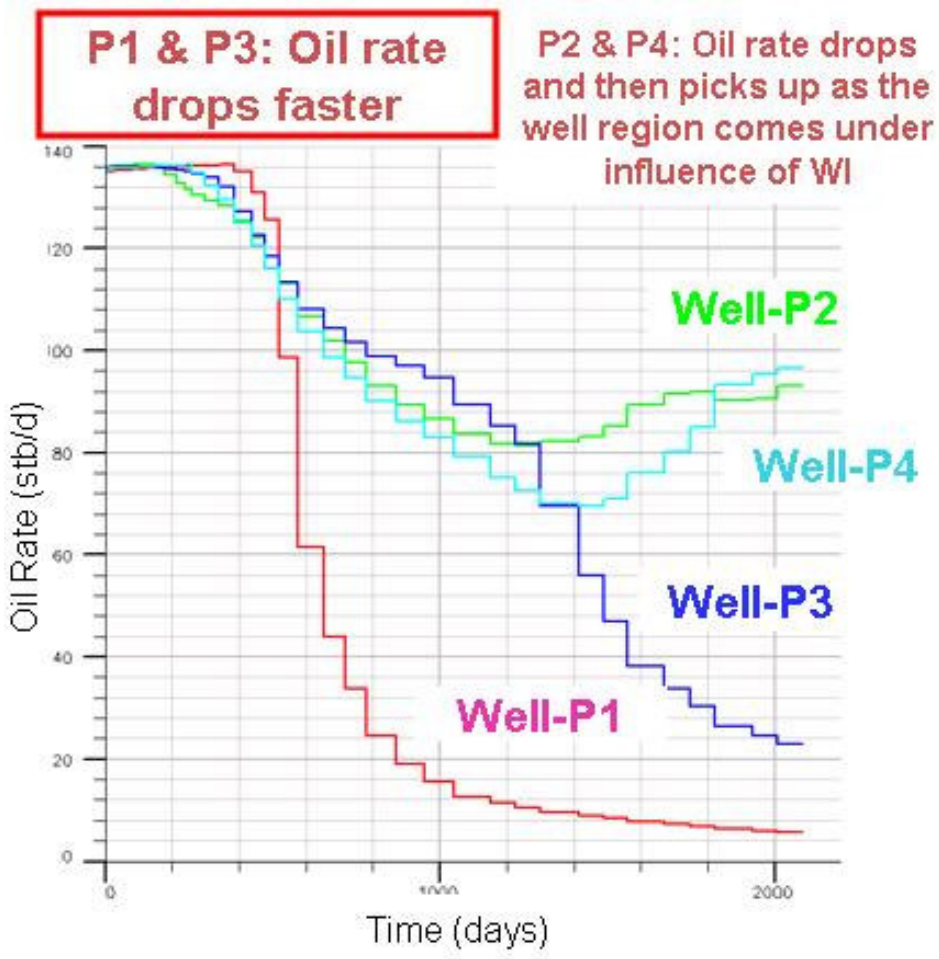

Fig. 20– Synthetic Model: Observed Oil Production Rate - Supports the Observations from Phase Streamlines

In **Fig. 20**, the oil production rates for all the wells are presented. At the wells P2 and P4 the oil rate drops till the 5th time step as it is producing under natural depletion whereas once they start getting pressure support due to water injected, the production rate increases again, which validates our observation about the drive mechanism from the phase streamlines. If the injection is continued for long time then eventually all of these wells would also come under water injection drive but before that a lot of water would be recycled without effecting any oil displacement.

V.2 Field Case - Streamlines Using Output of Black Oil Simulator

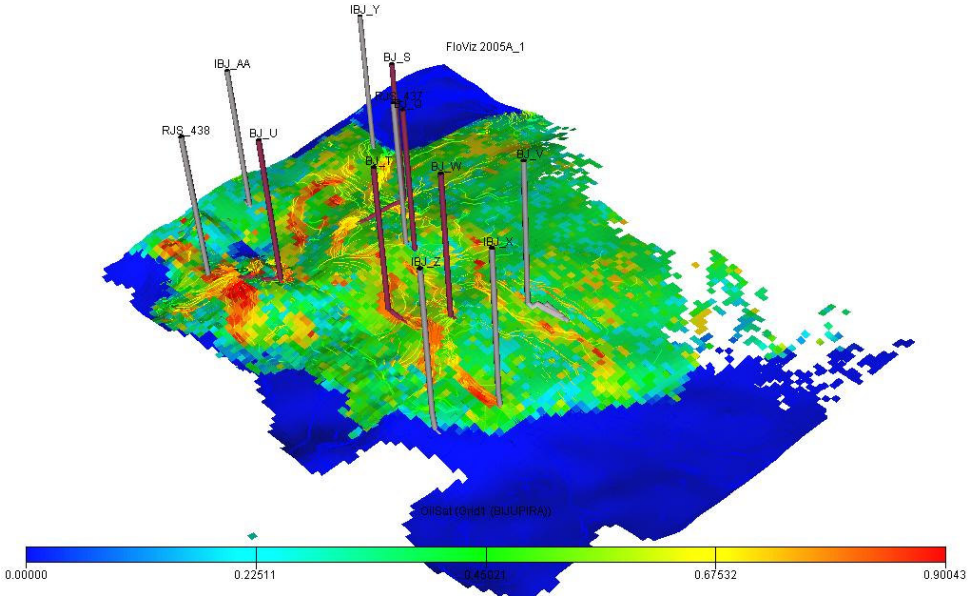

Fig. 21 – Field Case: South African Offshore Reservoir

For the field implementation of phase streamline tracing a South American Offshore Reservoir has been considered. The field is in water depth of 400 to 800 m. It is a turbiditic geological set-up with three partially connected Eocene deep-marine reservoirs (organized in sheet and channel sands) at a depth of approximately 3000 m. The OOIP was 500 MMSTB and the initial reservoir pressure was 4000 psi. The field was initially produced under natural flow conditions (primary depletion) from 2 wells for 6 years. It was then completely shut in and brought on production after re-development with 6 new producers and 4 water injectors, over a time frame of 3 years. After re-development another 3 years of production history were available. The quality of the sands is quite good with payzone thickness upto 70 m, porosity in range of 20-35 %, permeabilities up to 10 Darcy. The geological model with the location of wells is as presented in **Fig. 21**. The oil bearing zone is at the crest of the reservoir deposition and there is a surrounding aquifer. The 4 injectors are located along the periphery of the reservoir and the 8 producers are at the crest of the reservoir and production history of 11 yrs has been considered.

V.2.1 Total Flux Streamlines

In **Fig. 22**, the streamlines traced using total flux have been presented. Clearly they show the drainage area in the field and when presented for each producer individually they will represent the drainage area as a function of time for that particular well. These can be used for locating unswept regions for location of infill wells.

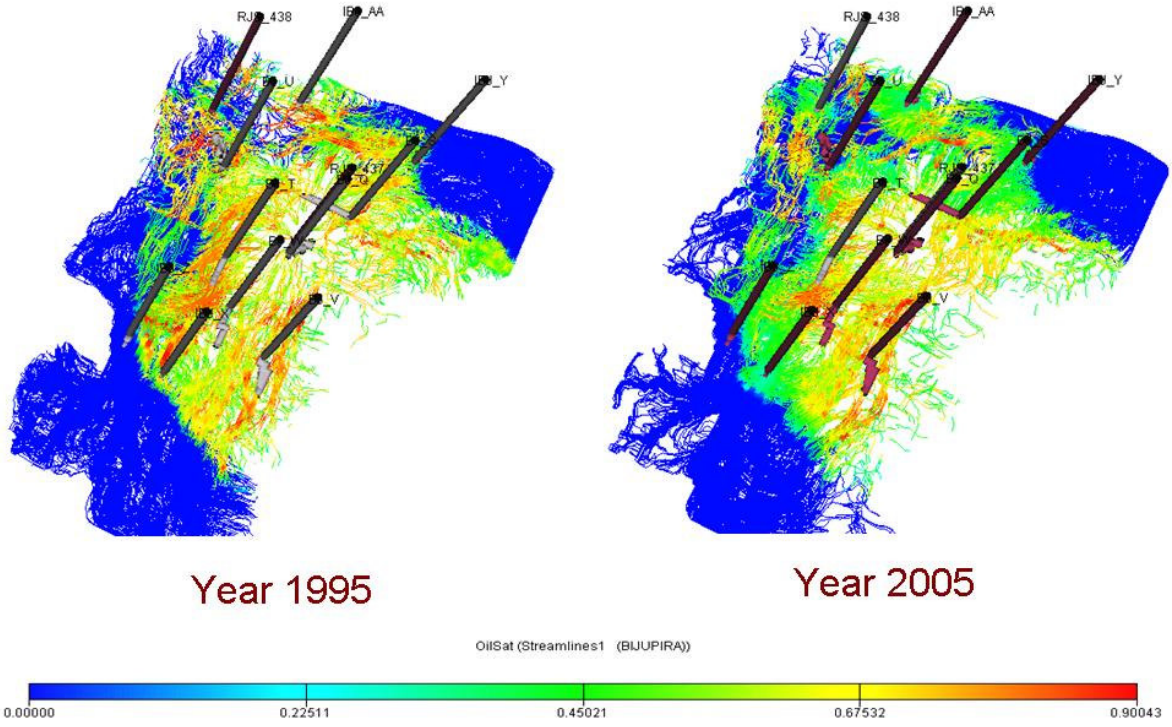

Fig. 22 – Field Case: Total Flux Streamlines - Show Drainage Area (Traced from Producers as Sinks, Oil Saturation Mapped on Streamlines)

In the **Fig. 23**, permeability in the reservoir is presented along with the streamlines traced using total flux. The permeability fields show presence of high permeability channels flanked by low-permeability overbanks. Clearly the effect of this permeability orientation has been captured by the streamlines. Also they can be used to establish the path of connected volume that would be swept with time.

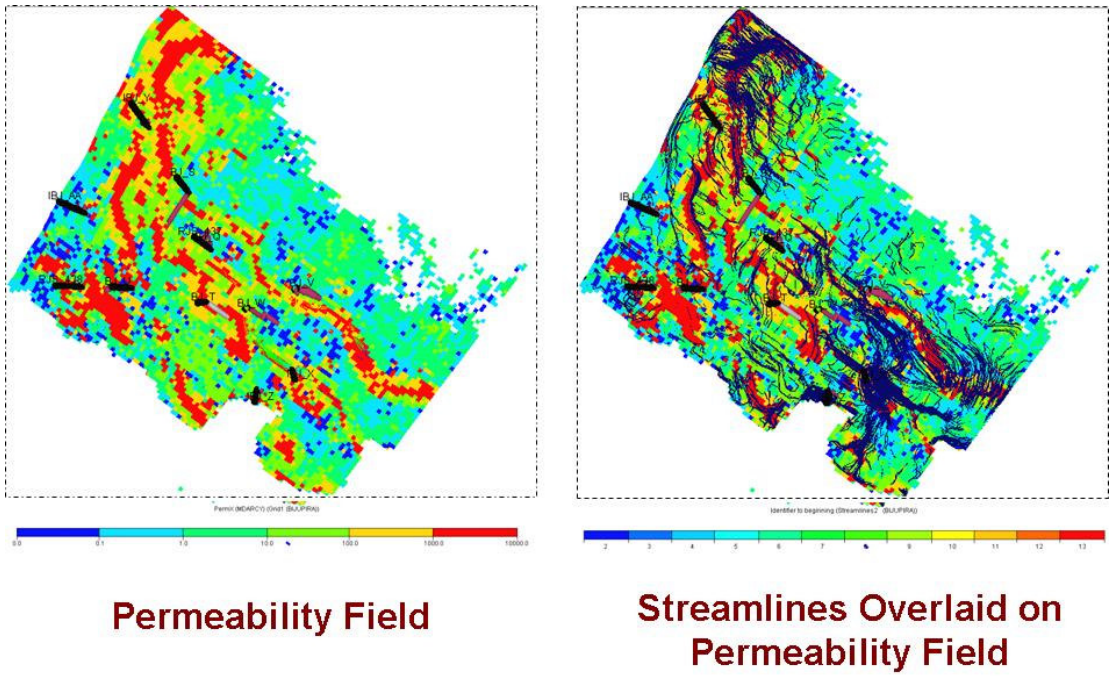

Fig. 23 – Field Case: The Total Flux Streamlines Capture the Effect of Permeability Orientation on the Fluid Movement

Figs. 24 and **25** show the permeability orientation and the injector producer relationship which manifests that the channel orientation is dictating the injector-producer relationship. This information can be obtained to tune the injection rates so that the water breakthrough is delayed at the producers and the water-flood influence area is maximized.

Although total flux streamlines present a lot of valuable information, they fail to ascertain the movement of aquifer, if any. Also we cannot segregate the areas based on dominance of water or oil flow. Please be reminded that the saturation mapped on the streamlines show the amount of phases present, not necessarily their movement. It might

be that the areas of high oil saturation do not have significant oil flow signifying their non-contribution to the field production and potential areas for locating infill wells.

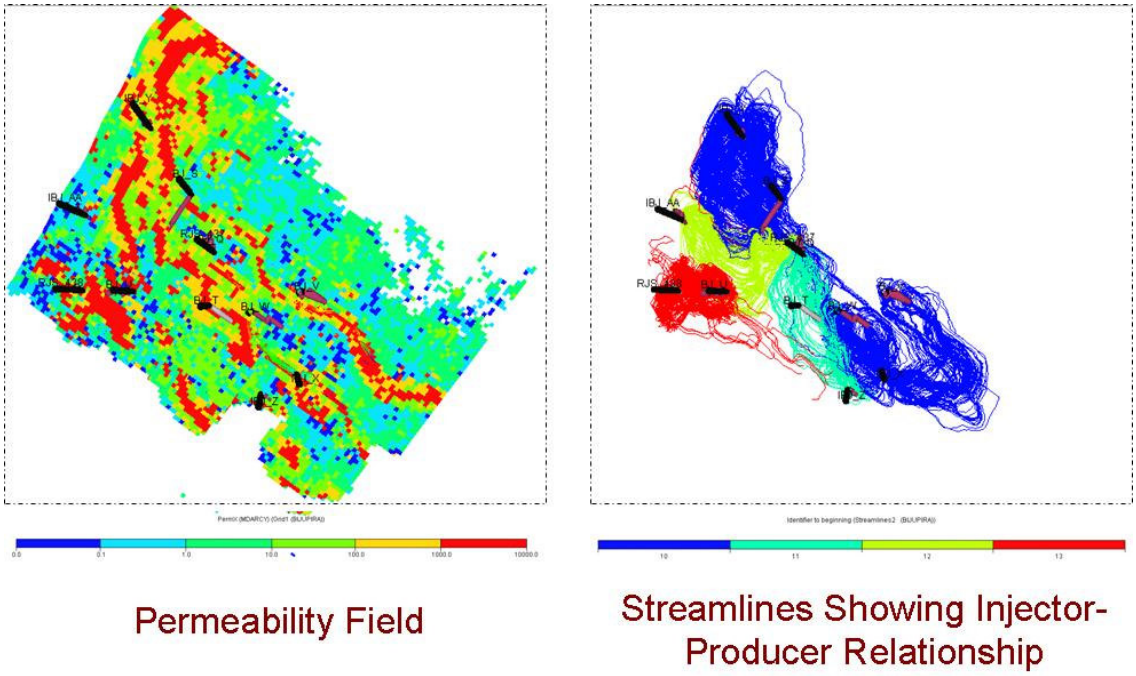

Fig. 24 – Field Case: Permeability Field and Injector-Producer Relationship

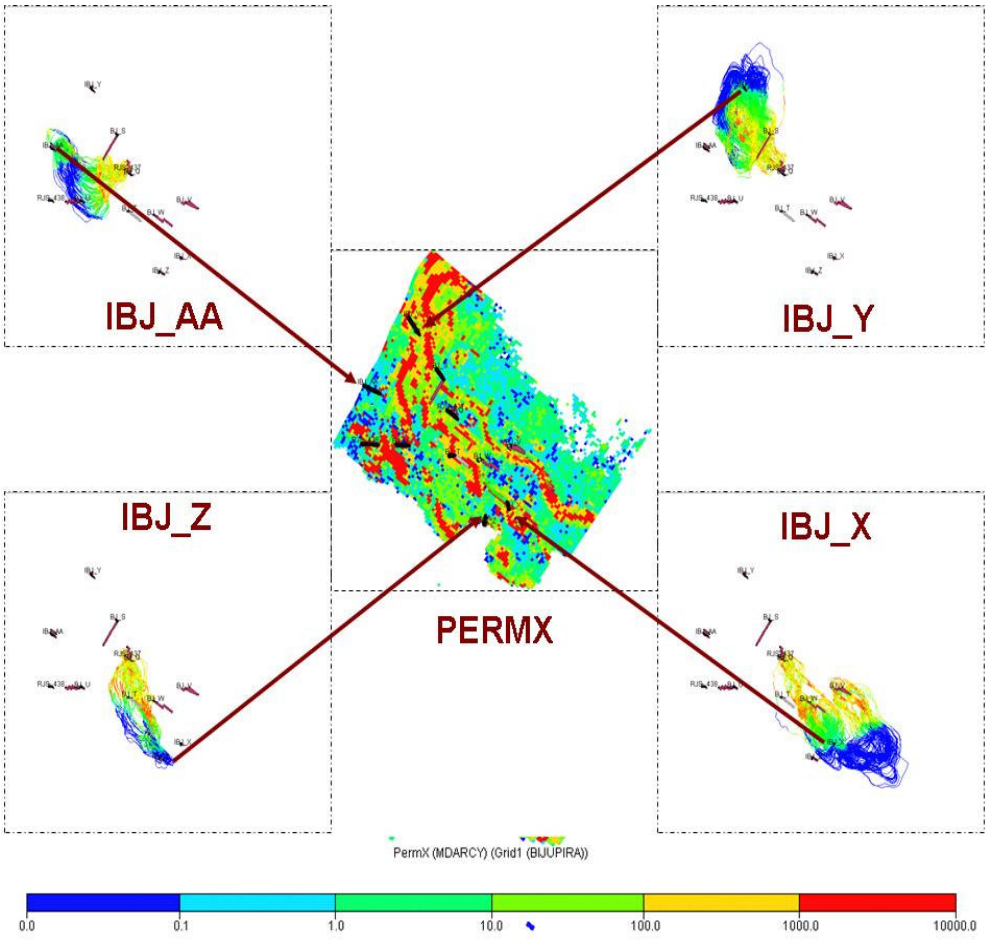

Fig. 25 – Field Case: Permeability Field and Injector-Producer Relationship on Well-by-Well Basis

V.2.2 Phase Streamlines

The issues that could not be addressed by the total flux streamlines would be explored with the phase (oil / water) streamlines and their relevance to the understanding of the reservoir processes would be presented. Streamlines have been traced from individual cells having fractional flow of the phase under consideration greater than 0.1.

V.2.2.1 Water Streamlines

The water streamlines are presented in **Fig. 26**. Here the streamlines have been traced from cells as sinks where the fractional flow of water is more than 0.1. It can be noted that the water streamlines are located in the periphery where aquifer is located and where most of the water injection is going on. When the water streamlines at lapse of 11 yrs are compared then the encroachment of water streamlines (marked with red) can be observed during the field life. Thus although very subtle, the movement of aquifer has been captured using the water streamlines. Streamlines from aquifer also suggest peripheral water drive.

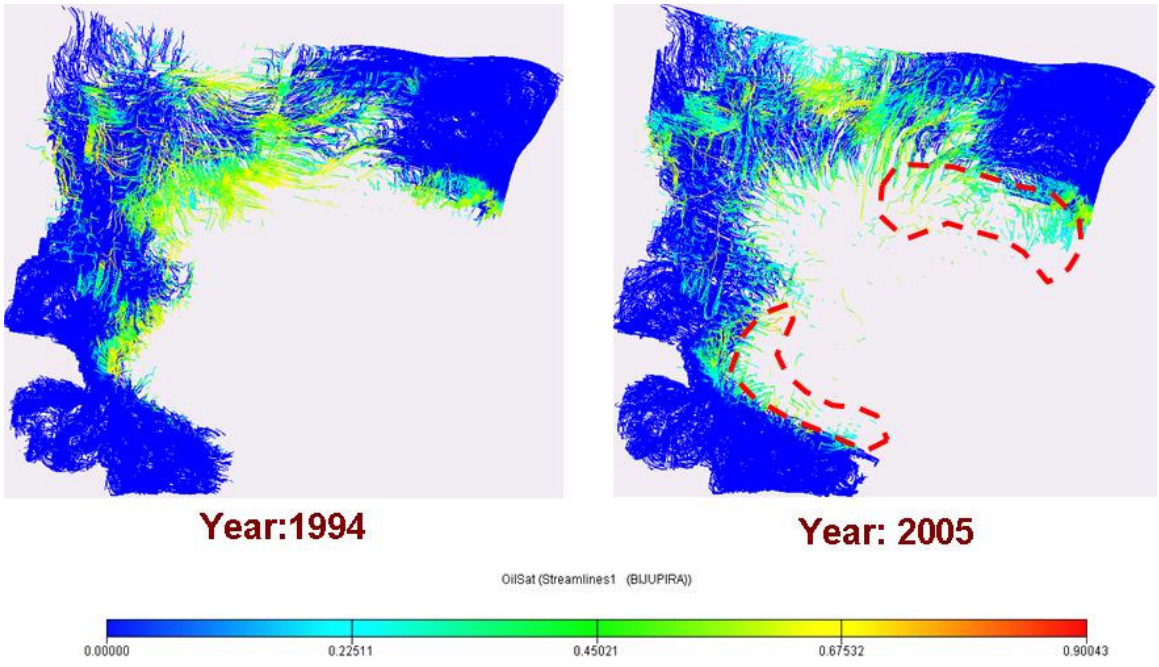

Fig. 26 –Field Case: Water Streamlines - Show Aquifer Movement (Traced from Cells as Sinks and Water Saturation Mapped on Streamlines)

V.2.2.2 Oil Streamlines

The oil streamlines are presented in **Fig. 27**. The oil streamlines are predominantly located at the crest of the reservoir. So by visual depiction of the phase streamlines, the dominant phase in flow in different regions can be established. The effect of encroachment of aquifer has been marked in red in the figure.

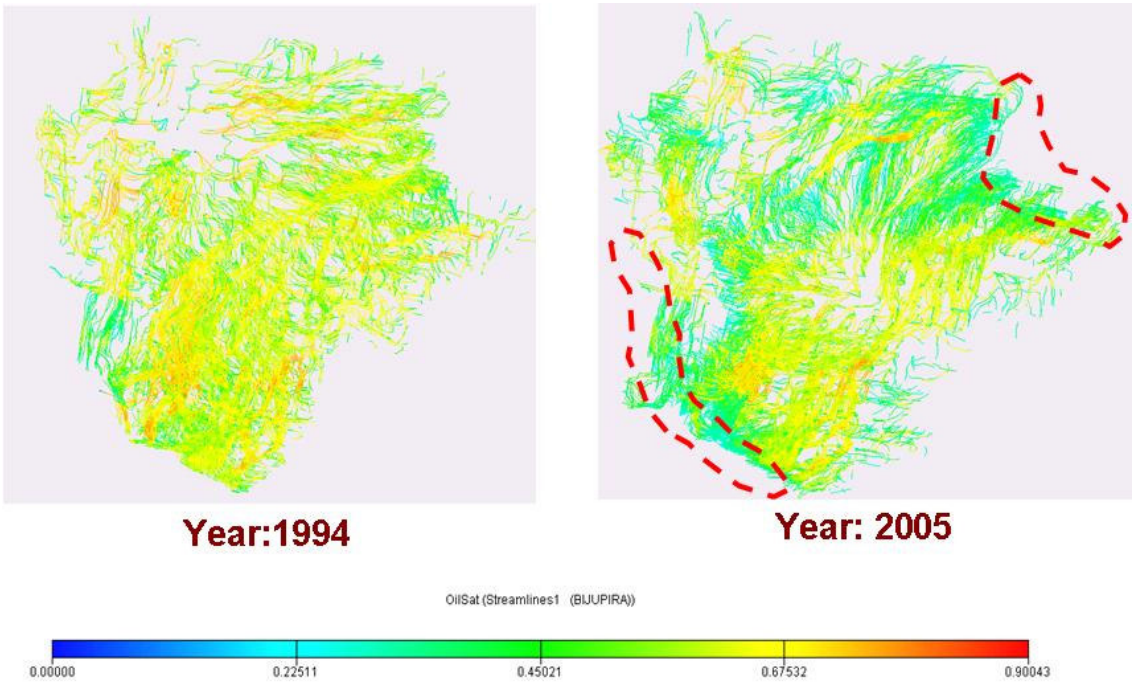

Fig. 27 – Field Case: Oil Streamlines - Useful for Infill Well Placement (Traced from Cells as Sinks and Oil Saturation Mapped on Streamlines)

Based on the aquifer movement as depicted by streamlines the location of next series of injectors can be decided. Overlap of oil and water streamlines can be used in selecting regions which would be suitable for locating further infill wells for production because regions having un-swept oil can be demarcated. Also as using phase streamlines the preferential path of movement of water being injected can be established, these can be used to plan orientation of the horizontal section, if horizontal injectors are planned. Similarly the orientation of horizontal section of producers can be planned to delay the breakthrough of water (by keeping it away from the direction of encroachment of aquifer or water channels)

V.3 Synthetic Model - Streamlines Using Output of Compositional Simulator

The component and phase streamline tracing has been applied to the synthetic case (the two dimensional synthetic case discussed previously). Here the static & dynamic parameters like permeability field, production & injection rates of the reservoir have remained unchanged. Only significant change is the replacement of the fluid being injected from water to CO_2.

V.3.1 Total Flux Streamlines

The streamlines traced using the total flux for the synthetic model have been presented in the **Fig. 28**. They have been traced from grid cells having fractional flow of the total

flux greater than 0.1 (for total flux streamlines all the grid cells would be used where the total flux is present), which is same as tracing from injector to the grid cells satisfying this criteria. Clearly they capture the movement of flood front but we cannot establish the region of dominant CO_2 or other phases flow. Also it cannot be ascertained where CO_2 is in gas phase at reservoir conditions or dissolved in oil. Also different drive mechanisms cannot be identified.

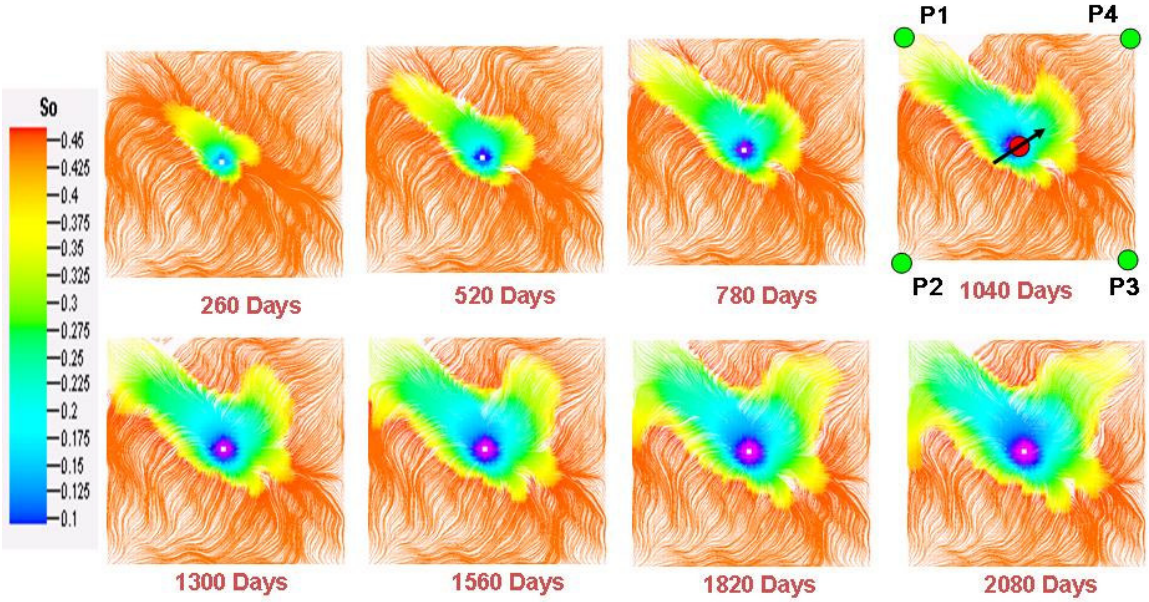

Fig. 28 – Synthetic Model: Total Flux Streamlines from Output of Compositional Simulator (Traced from Cells as Sink , Oil Saturation Mapped on Streamlines)

V.3.2 Phase and Component (CO_2) Streamlines

V.3.2.1 CO_2 Streamlines

The CO_2 streamlines and the corresponding oil streamlines have been presented in **Fig. 29**. They have been traced from grid cells having fractional flow of CO_2 greater than 0.1, which is same as tracing from injector to the grid cells satisfying this criteria. Clearly, the movement of CO_2 with time has been captured by the CO_2 streamlines but not with the total velocity streamlines.

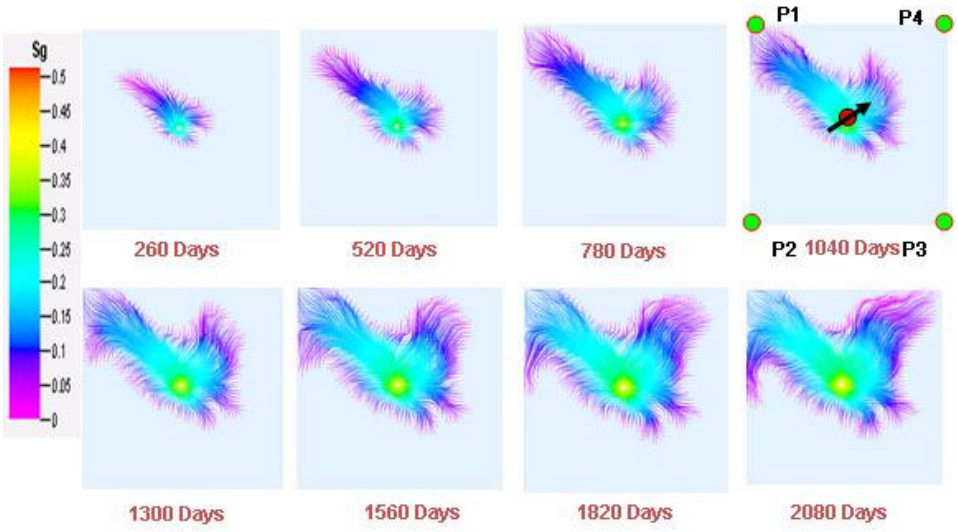

Fig. 29 – Synthetic Model: CO_2 Streamlines - Capture the Movement of CO_2 Flood (Traced from Cells as Sinks, Gas Saturation Mapped on Streamlines)

From study of CO_2 streamlines, it can be observed that the CO_2 breakthroughs at the well P1 much faster than at other wells, which shows the adverse effect of the permeability orientation. This can also be verified by the GOR plot of the wells (**Fig. 30**). Also it can be observed that only well P1 is benefitting from CO_2 flood whereas other wells are producing under natural depletion.

A very high GOR is observed at well P1 because CO_2 being injected is recycled through this well, bypassing the remaining oil in the reservoir. Thus, it can also be pointed out that the tertiary recovery mechanism is not augmenting the production from other wells.

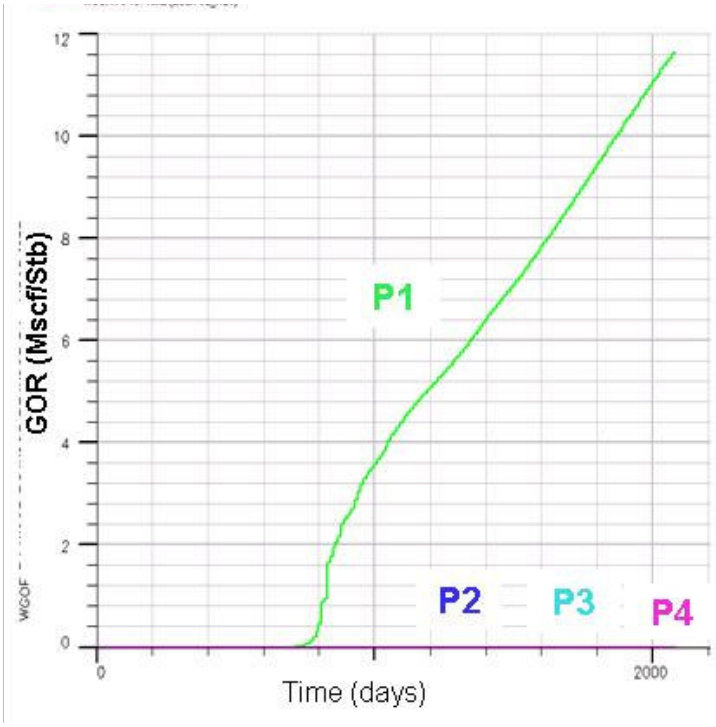

Fig. 30 – Synthetic Model: GOR for the Producers of the CO_2 Injection Synthetic Example

V.3.2.2 Oil Streamlines

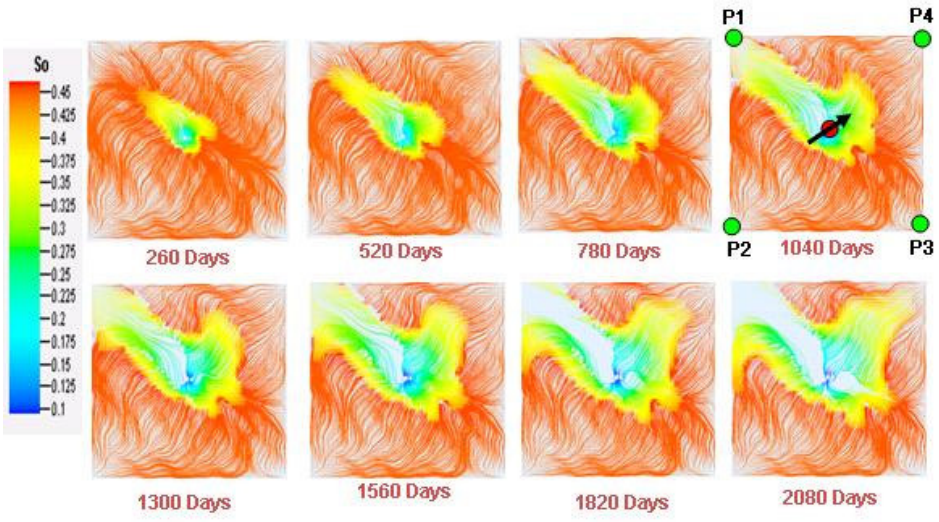

Fig. 31– Synthetic Model: Oil Streamlines for the CO_2 Flood - Show Poor Sweep Efficiency of Flood (Traced from Cells as Sinks, Oil Sat. Mapped on Streamlines)

The oil streamlines have been presented in **Fig. 31**. From these streamlines also it can be observed that only regions connected to well P1 have been swept whereas a lot of un-swept oil, as represented by dense oil streamlines, is still left in the other regions. For tertiary flood, the rule of thumb states that if it is a good waterflood then it is going to be a better CO_2 flood but reservoir showing poor response to waterflood will respond poorer to CO_2 flood. In the synthetic case under study, this rule of thumb appears to have been validated, because the spread of CO_2 is much less and sweep is poorer than the case of waterflood.

V.3.2.3 Gas Streamlines

Gas streamlines presented in **Fig. 32** show that the injected CO_2 movement path is same as the gas streamlines suggesting that the injected CO_2 is in gas phase and the reservoir pressure is below MMP (minimum miscibility pressure).

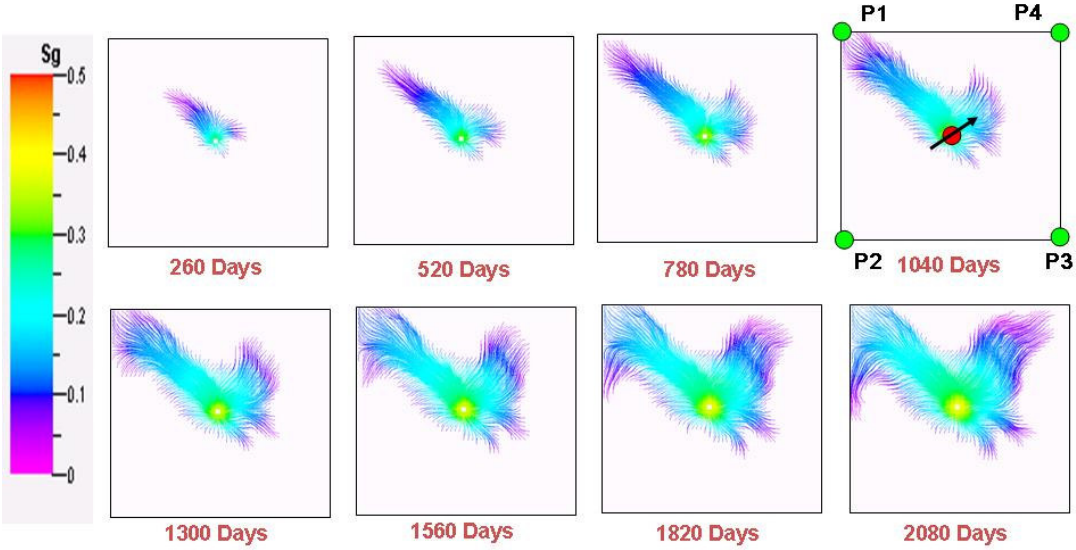

Fig. 32 – Synthetic Model: Gas Streamlines - Show That the Injected CO_2 Is in Gaseous Phase (Traced from Cells as Sinks, Gas Saturation Mapped on Streamlines)

From CO_2, oil and gas streamlines it can be concluded that wells P2. P3 and P4 are not getting pressure support and hence are producing under natural depletion. Also the regions of dominant flow for each phase can be identified.

V.3.2.4 Water Streamlines

Here the presence of water streamlines indicate that water is mobile although their contribution to total flow is not very significant. Comparing water streamlines (**Fig. 33**) with the oil streamlines presented in **Fig. 31** suggest that the water movement follows the movement of the oil in general. Comparing water streamlines with component (CO_2) streamlines tells that in the region of dominant CO_2 flow, water flow is quite less significant from other regions.

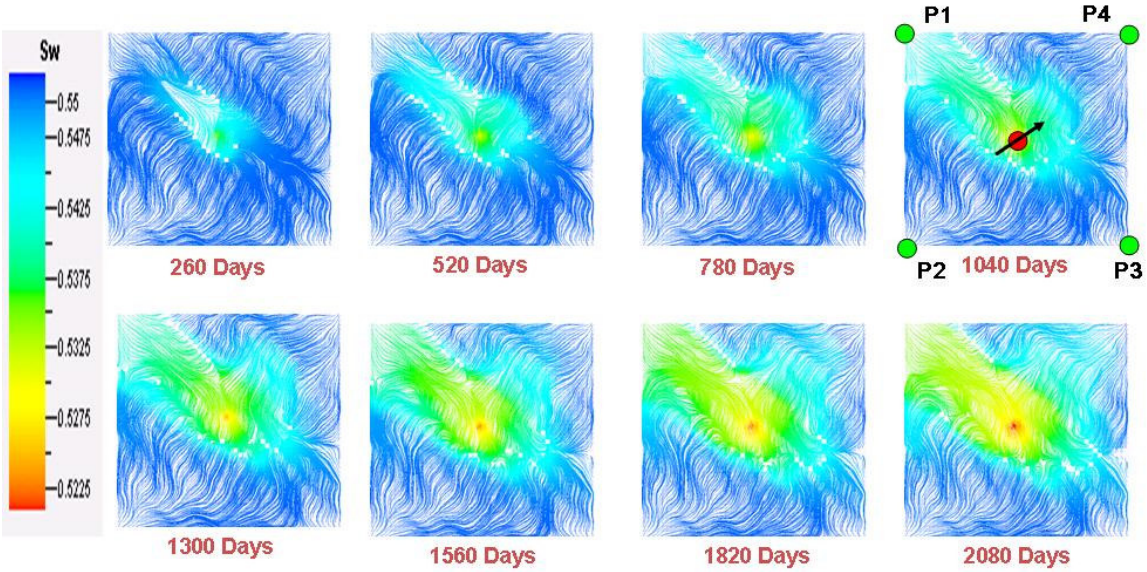

Fig. 33 – Synthetic Model: Water Streamlines - Show That the Flow in the Reservoir Is Two-Phase (Traced from Cells as Sinks, Water Saturation Mapped on Streamlines)

Also we can note the effect of injection as the orientation of water streamlines is along the CO_2 streamlines, i.e. diagonally towards well P1 (in the region of component CO_2 flow) whereas in other regions of the field, they are oriented along oil streamlines.

V.4 Field Case - Streamlines Using Output of Compositional Simulator

A Canadian Onshore Reservoir (**Fig. 34**) currently under CO_2 flood was selected as the pilot field project to validate the component and phase streamline tracing using the output of compositional simulator.

The field was discovered in 1954, put on waterflood in 1960s and tertiary recovery was implemented in 2003 with CO_2 flood. Original oil in place was about 1.5 billion barrels. After a peak production of about 50,000 STB/D, production declined steadily for the next 20 years dropping to 9,000 STB/D by the late 80's. Additional infill wells (horizontal and vertical) were drilled, increasing production to approximately to 22, 000 STB/D. By the end of the 90's, the recovery of oil was 23 % of OOIP. Production was declining again and it was envisaged that if no EOR methods are applied then the total recovery from the field would not be more than 25 %.

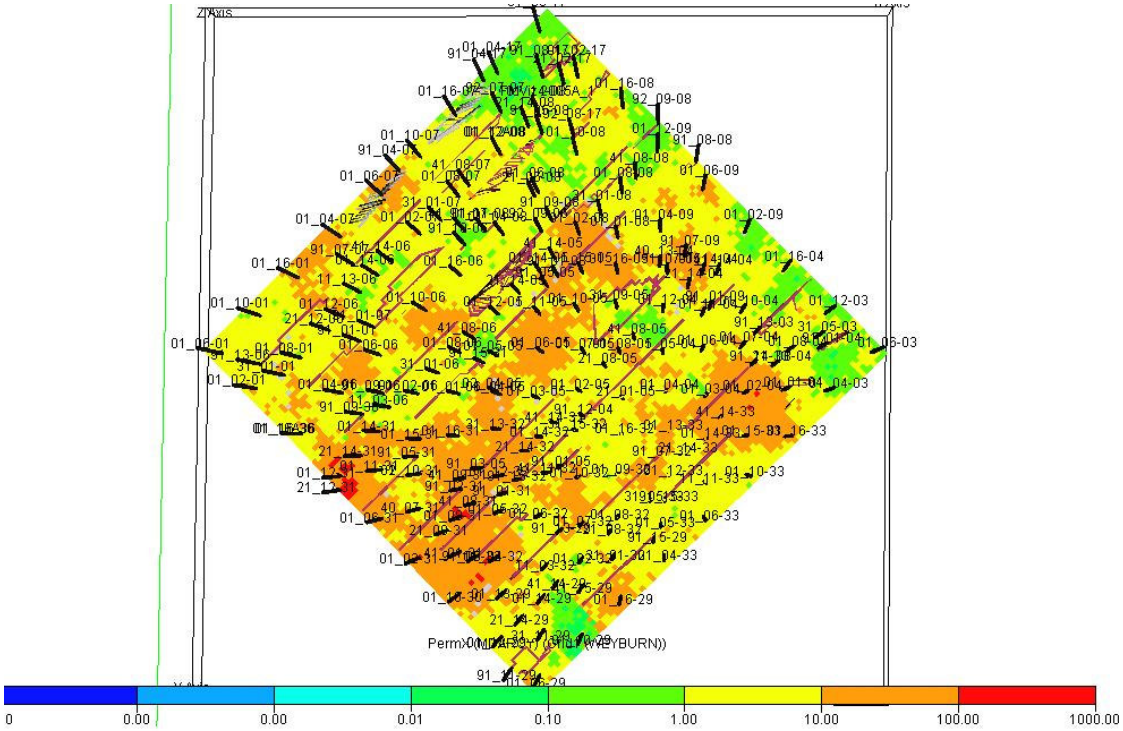

Fig. 34 – Field Case for CO_2 Flood Study: Canadian Onshore Reservoir

Detailed study suggested CO_2 injection to enable additional production. Injected CO_2 reduces the viscosity of oil and increases the transmissibility of oil. Also CO_2 swells oil and forces them out of tight pores where they are left as irreducible oil in waterflood. Water was pumped alternate to CO_2 (WAG process) to push the swelled oil towards the producer wells. The irreducible oil in case of CO_2 flood is of the order of 3-8% compared to 23-35 % in case of waterflood; thus, the difference is the targeted incremental oil. The success of EOR project will be measured not only by the additional production, but also by delivering the background work and example of field application necessary to encourage implementation of CO_2 geological storage. Total number of

wells in the field is 1016 in a 9-spot grid pattern. But for this project study, a section of reservoir where CO_2 injection is active was selected. This section has total of 213 wells (160 producers, 26 water injectors and 27 CO_2 injectors).

The streamline based reservoir management process is quite promising for such a field. Streamlines can be used to understand the well interactions (including injector-producer connectivity), to identify the bypassed oil zones useful to optimize the WAG process, to calculate allocation factors and to use the allocation factors for identifying the efficiency of injectors.

V.4.1 Streamlines during the Waterflood Regime

Here the case presents the opportunity to test our formulation and to investigate the additional information for waterflood period (starting in 1965) as well as for the tertiary recovery stage involving CO_2 injection (WAG).

V.4.1.1 Total Flux Streamlines

Fig. 35 shows the streamlines traced using total flux, during the period of waterflood. Streamline tracing is done from producers to injectors so they show all the streamlines that are breaking through at the producers. The streamlines show the drainage area for each pattern. Although most of the producers are draining from the patterns, flow is out of pattern for some of the others (particularly in the wells around the center of map).

Also the pattern performance can be judged on the basis of this, e.g. pattern on the left most corner are not performing as good as other patterns. Also we can identify the migration from 5-spot to 9-spot pattern as the infill wells are drilled gradually and so we can note the injector-producer relationship.

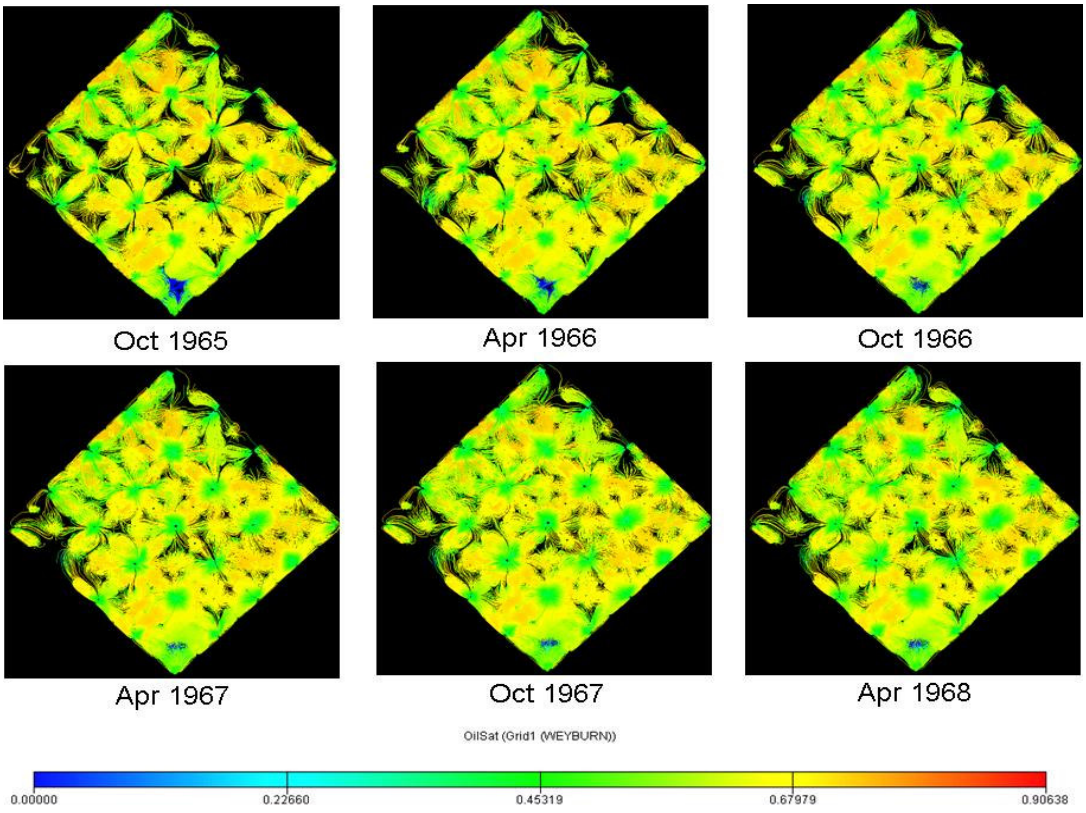

Fig. 35– Field Case for CO_2 Flood Study: Total Flux Streamlines during Waterflood Regime
(Traced from Producers as Sinks, Oil Saturation Mapped on the Streamlines)

V.4.1.2 Oil Streamlines

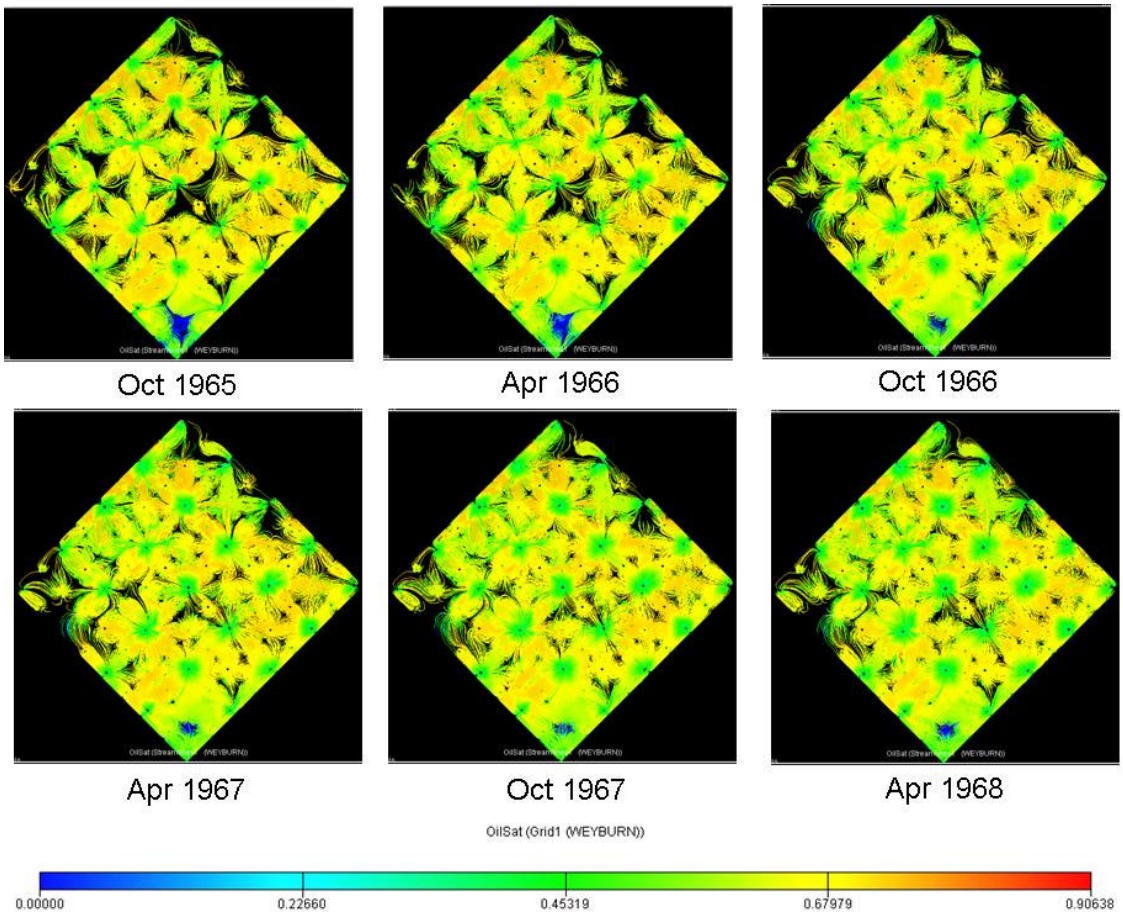

Fig. 36– Field Case for CO_2 Flood Study: Oil Streamlines during Waterflood Regime (Traced from Producers as Sinks, Oil Saturation Mapped on the Streamlines)

Fig. 36 presents the oil streamlines for the waterflood regime. Areal comparison to total flux streamlines reveal that for most of the areas they overlap. As we shall observe with a specific example, this statement cannot be generalized for all the phases. Here also we can see how the injectors and producers are interacting. Here as streamlines carry oil

only, so we can dynamically allocate oil production from each producer to the pressure supporting injectors. Also we can map the oil drainage regions areally as well as vertically.

V.4.1.3 Water Streamlines

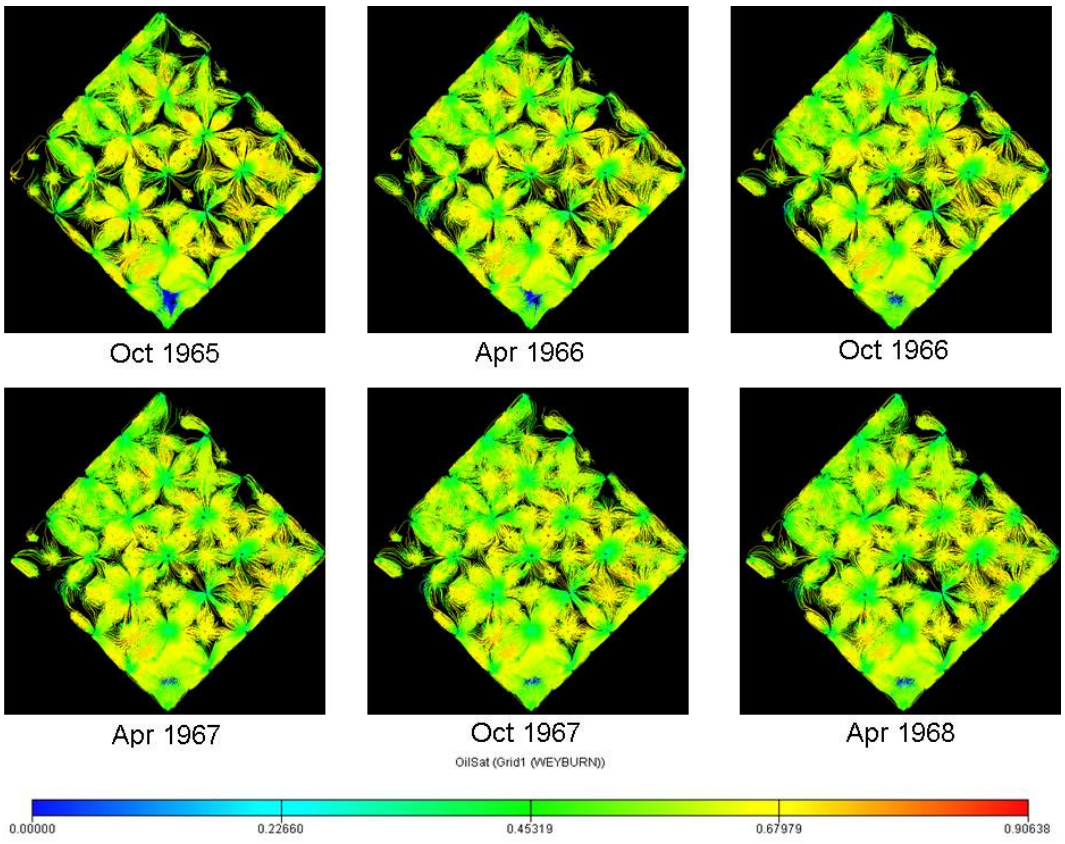

Fig. 37 – Field Case for CO_2 Flood Study: Water Streamlines during Waterflood Regime (Traced from Producers as Sink, Oil Saturation Mapped on the Streamlines)

In **Fig. 37** the streamlines traced using water flux are presented at the same six time-steps as the previous streamlines. Here we can see that water is not supporting few of the producers as given by holes (regions of no streamlines) in the map. Also the streamline density between the injector-producers can be taken as measure of the water-cut severity at the producers. Also they can be used as tool to dynamically allocate the injection volume to the producers in the patterns.

V.4.1.4 Comparison of Phase and Total Flux Streamlines

In **Figs. 38** and **39** the streamlines traced using total flux, oil flux, and water flux are compared at one particular time step. Although the top view shows some difference in the oil drainage pattern and water drainage patterns, the main difference is in the vertical positioning of the streamlines as seen in **Fig. 39**. The water streamlines are dominant in the lower region of reservoir where the injection is going on and hence water movement is dominant, whereas the oil streamlines are dominant at the upper layers where the production wells are completed. Thus the regions of dominant oil and gas flows can be demarcated on basis of their flow. Also we can see the injection is creating a pseudo bottom water drive to support pressure and production of oil.

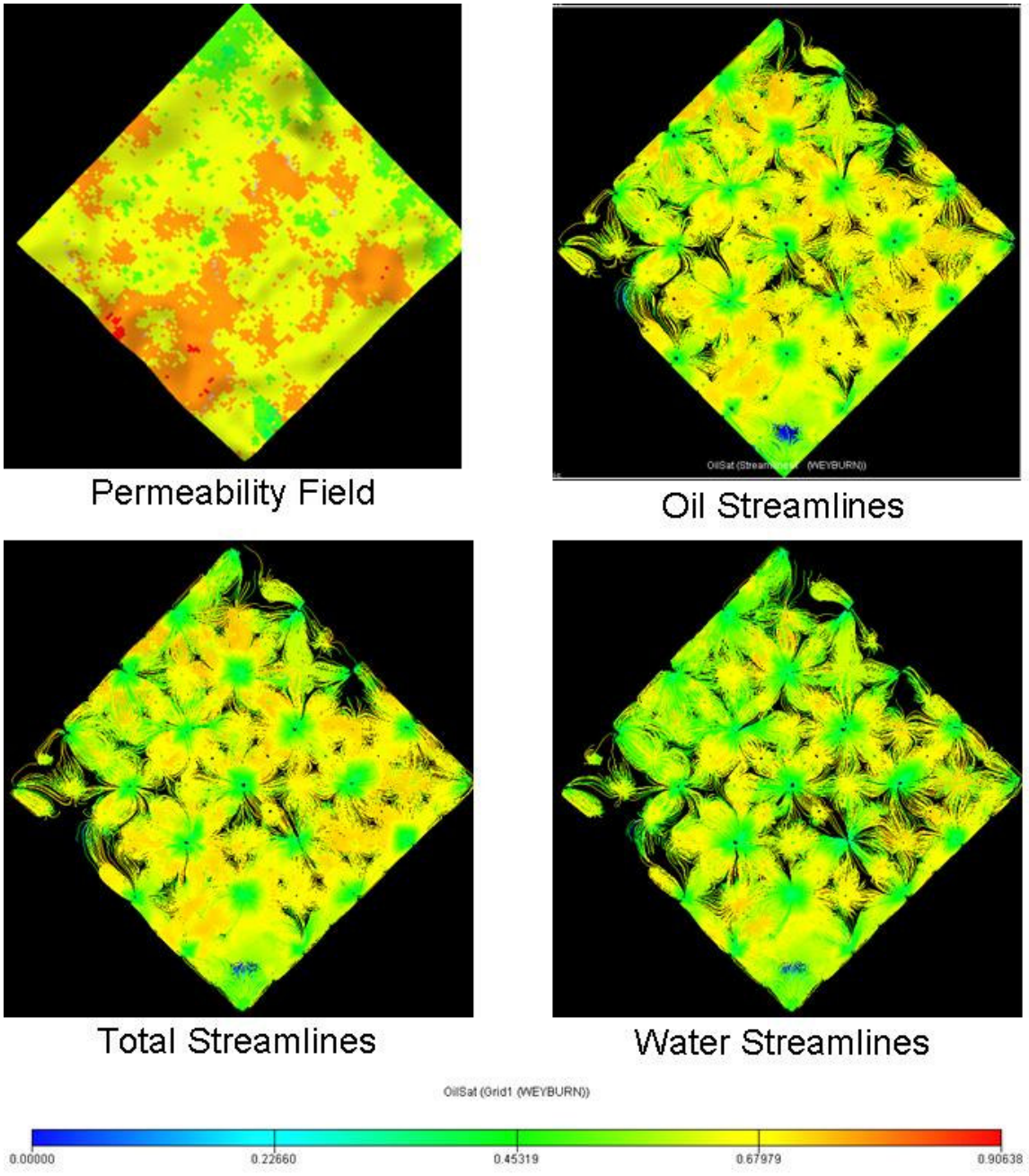

Fig. 38 – Field Case for CO_2 Flood Study: Comparison of Total Flux, Oil and Water Streamlines during Waterflood Regime (Top View)
(Traced from Producers as Sink, Oil Saturation Mapped on the Streamlines)

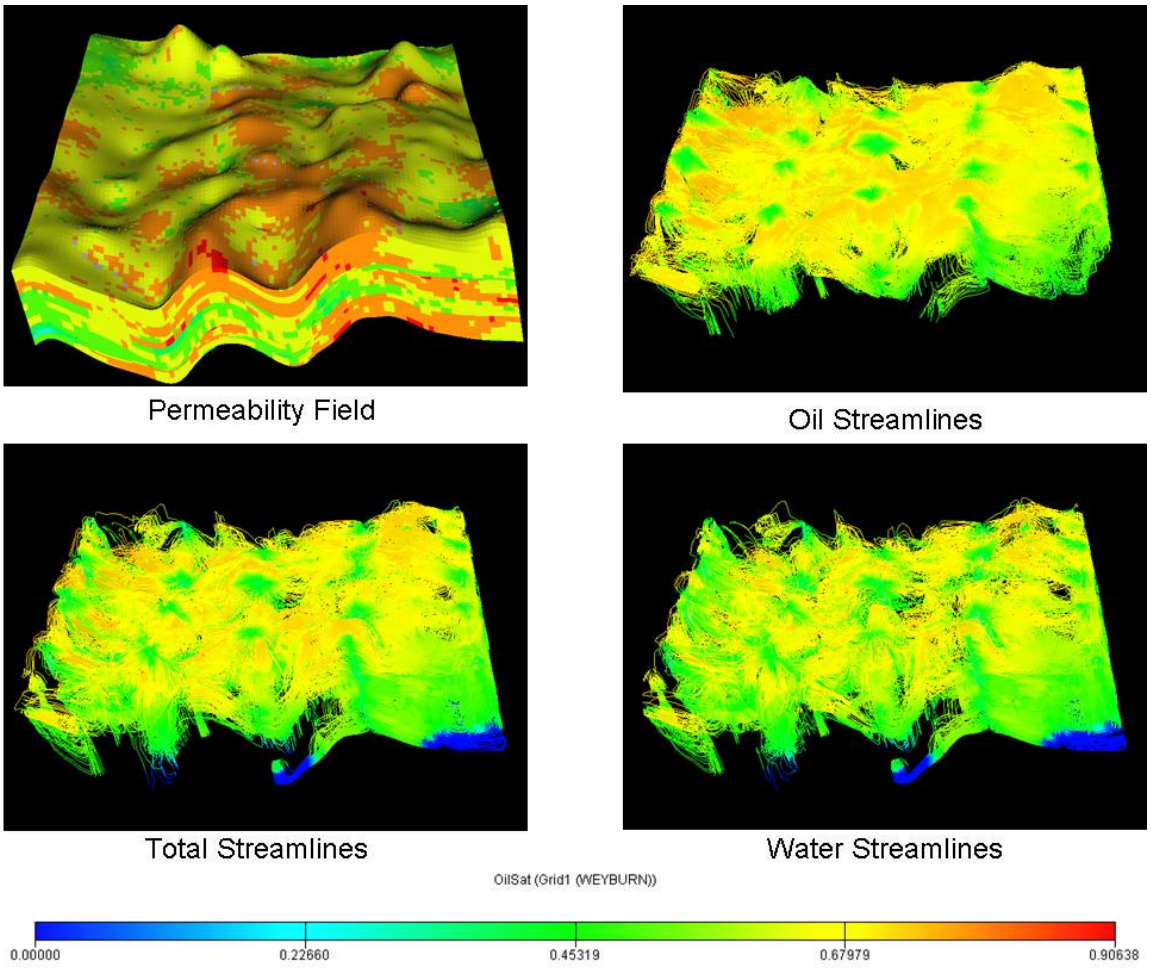

Fig. 39 – Field Case for CO_2 Flood Study: Comparison of Total Flux, Oil and Water Streamlines during Waterflood Regime (Side View)
(Traced from Producers as Sink, Oil Saturation Mapped on the Streamlines)

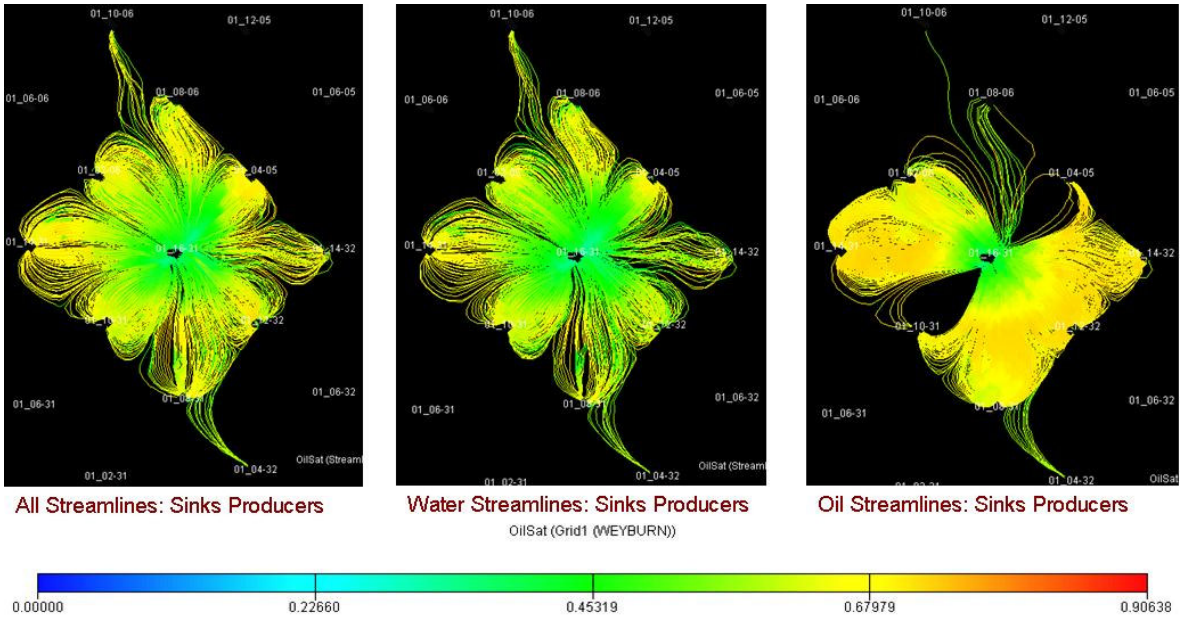

Fig. 40 – Field Case for CO_2 Flood Study: Total Flux, Water and Oil Streamlines Corresponding to a Pattern during Waterflood Regime (Traced from Producers as Sink, Oil Saturation Mapped on the Streamlines)

In **Fig. 40**, total flux, water and oil streamlines for a particular well are compared. It can be commented that the region between the well 01_16-31 & 01_04-05 and 01_16-31 & 01_10-31 is having water as the dominant phase in flow whereas for other injector-producer pairs the flow is two phase (water and oil). Information like these are not available using the total flux streamlines. Here based on these streamlines we can say which well is expected to get the highest water-cut and thus the candidates for re-completion can be identified.

From **Fig. 40** it can be noted that the injected water in the pattern is going out of pattern as well. Generally for well allocation it is difficult to account for out of pattern

flow, but streamlines can account for that. And with phase streamlines the out of pattern flow can be further broken down in oil and gas flows, in and out of pattern.

V.4.2 Streamlines During the CO_2 Flood Regime

The streamlines corresponding to the phases (oil, gas, water), component (CO_2) and total velocity has been traced and we are presenting the results at some time steps to demonstrate their significance.

V.4.2.1 Total Flux Streamlines

Fig. 41, presents the total velocity streamlines. Here the movement path of the fluid can be identified and also the regions which have negligible fluid movement can be identified. The pattern boundaries which are regions of flow stagnancy can be marked as they don't have any (or very few) total velocity streamlines.

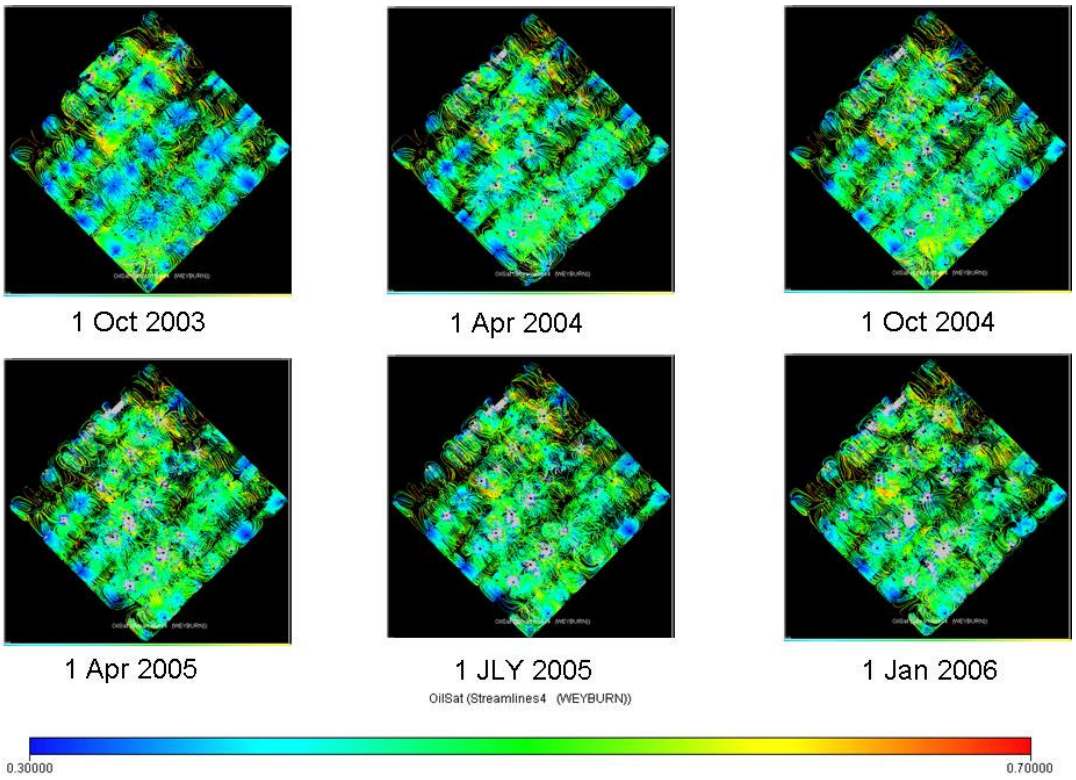

Fig. 41 – Field Case for CO_2 Flood Study: Total Velocity Streamlines during CO_2 Flood Regime
(Traced from Producers as Sink, Oil Saturation Mapped on the Streamlines)

V.4.2.2 Component (CO_2) Streamlines

Comparing CO_2 streamlines in the **Fig. 42** and the total velocity streamlines (**Fig. 41**) it can be noted that the flow of CO_2 was not captured by the total velocity streamlines.

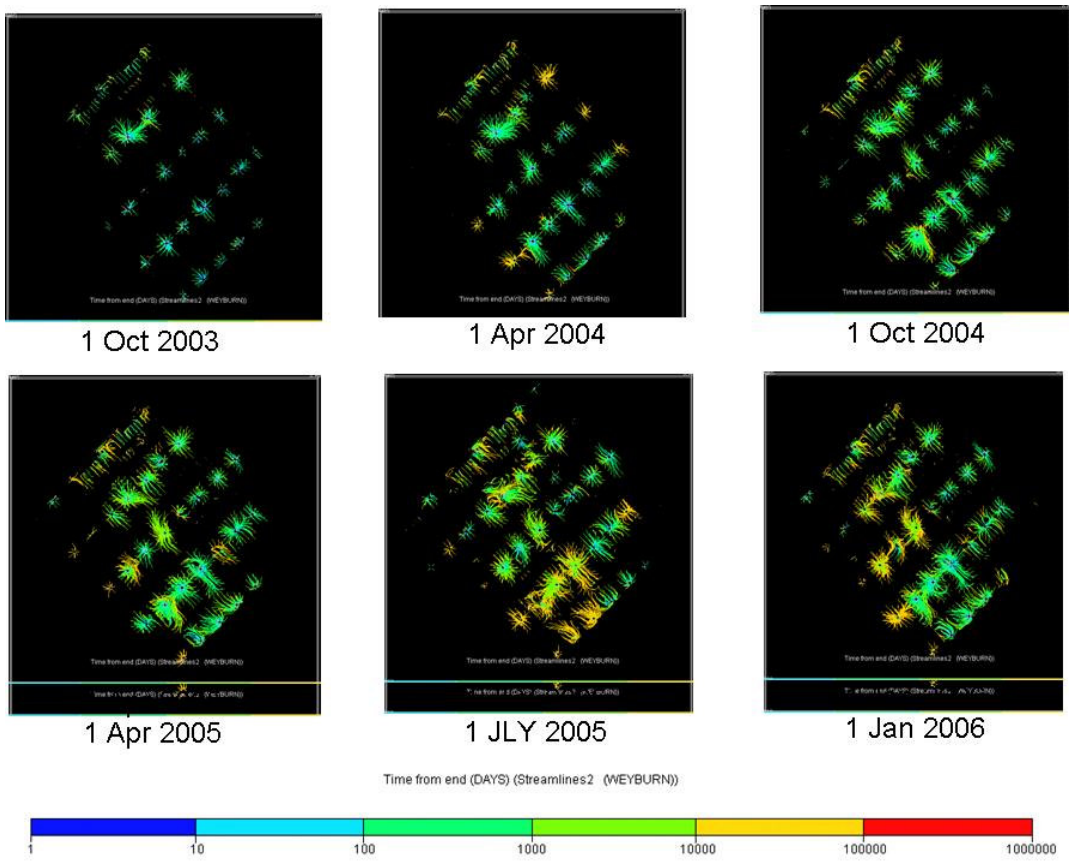

Fig. 42 – Field Case for CO_2 Flood Study: CO_2 Streamlines during CO_2 Flood Regime
(Traced from Cells as Sink, TOF Mapped on the Streamlines)

In the **Fig. 42**, the movement of injected CO_2 can be tracked with time and if the model is history matched with respect to waterflood regime, then we can also predict with reasonable accuracy as to which producers will see breakthrough of CO_2 and in which order. Accordingly the facilities to handle CO_2 production can be designed at the corresponding wells. Using the component tracking, the CO_2 dissolved in aqueous phase can be traced in CO_2 sequestration projects where it is injected for long time storage. Also from CO_2 streamlines density, the injection wells can be ranked in terms of the

injection rates vs. swept area. This ranking would be useful to identify the injectors to shut down when there is shortage of CO_2 on supply side or when CO_2 needs to be diverted to new locations.

From these streamlines, the regions which are not getting benefit of injection program, due to heterogeneity and bypass of flow, can be delineated and thus the component streamlines (CO_2) can be used for identifying the location of the CO_2 injectors in future. Also it can be noted that for some of the injectors the CO_2 influenced area extends beyond their pattern boundary as well indicating that assuming strictly pattern based allocation between injector and producer would be unjustified in these cases.

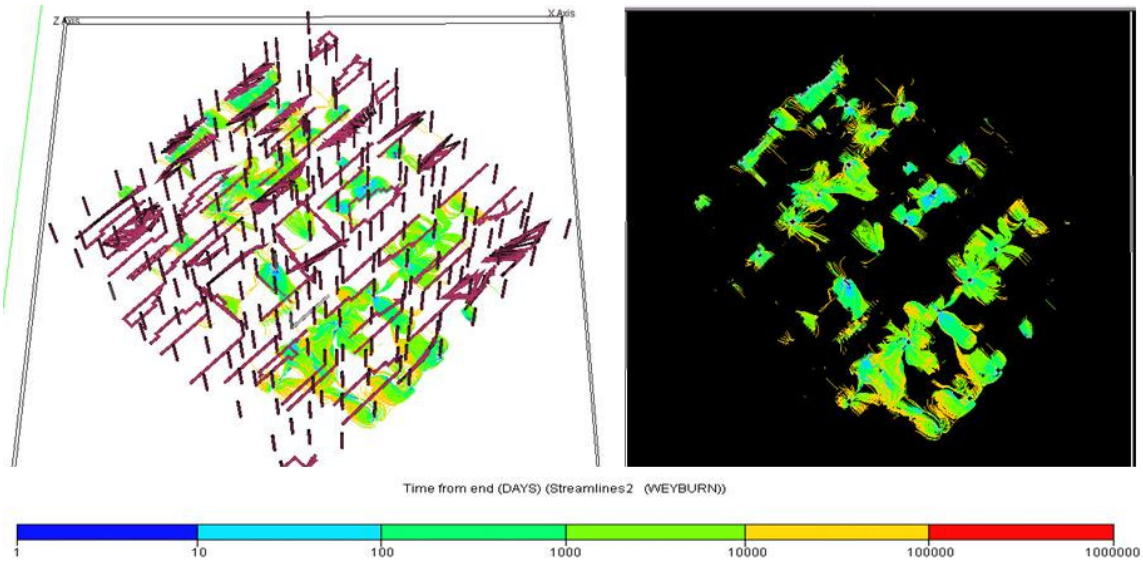

Fig. 43 – Field Case for CO_2 Flood Study: CO_2 Streamlines Showing the Movement Path and Injector-Producer Relationship (1 Oct 2005) (Traced from Producers as Sink, TOF Mapped on the Streamlines)

Fig. 43 presents the producers and injectors along with the CO_2 streamlines, thus explicitly showing the injector-producer relationship. It can be observed that the path of CO_2 is more controlled and directed in case of horizontal injectors (near the top regions of map) compared to the vertical injectors. Also the out of pattern flow can be observed. In **Fig. 44** few selected injector wells along with their corresponding producing partners are presented. The close up look at the CO_2 injectors and the movement of the injected fluid gives a fair idea about the variation in their flow paths, which could be interplay of various reservoir and well control parameters.

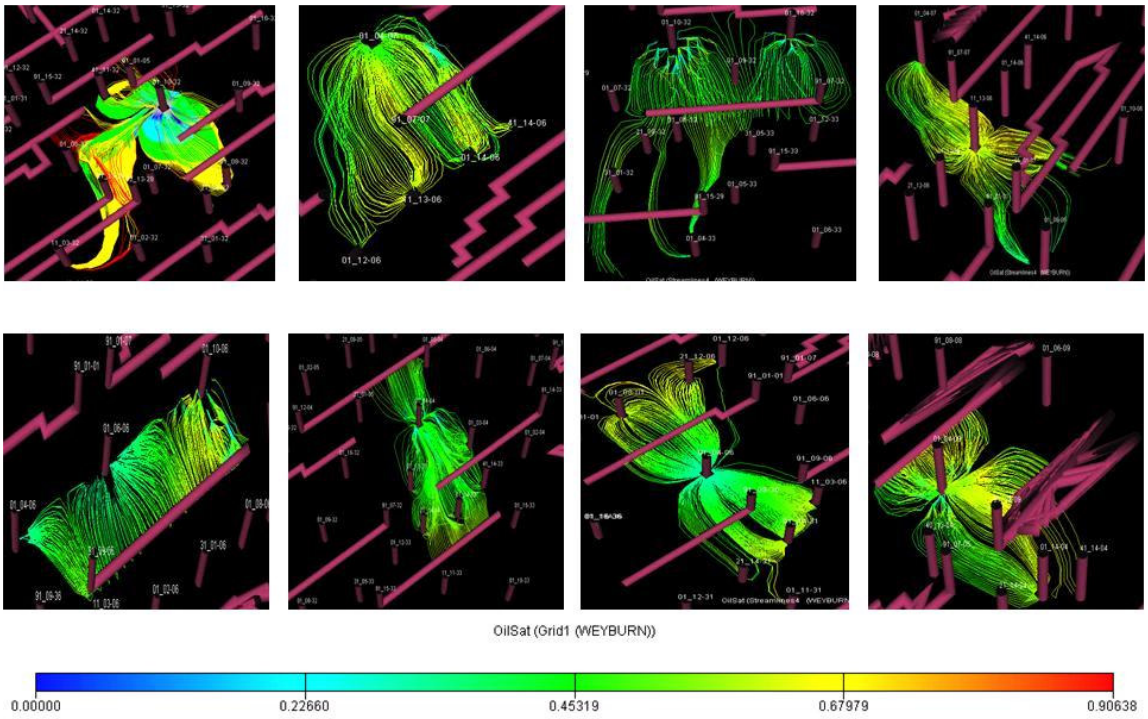

Fig. 44 – Field Case for CO_2 Flood Study: CO_2 Streamlines for Few Selected Wells to Demonstrate Their Unique Paths Instead of Pattern Flow (1 Apr 2004) (Traced from Producers as Sink, TOF Mapped on the Streamlines)

V.4.2.3 Oil Streamlines

Fig. 45 presents the oil streamlines at the same time steps as total flux streamlines. Here comparing the streamlines at gradually progressing time-steps, it can be noted that the regions where the density of oil streamlines have reduced are regions swept of oil. Also we can see that the borders of the patterns have high oil saturation and low streamline density suggesting un-swept oil is not benefitting from current reservoir production mechanism. The "holes" or regions with no streamlines near the injectors (CO_2) suggest that the injected CO_2 is in gas phase.

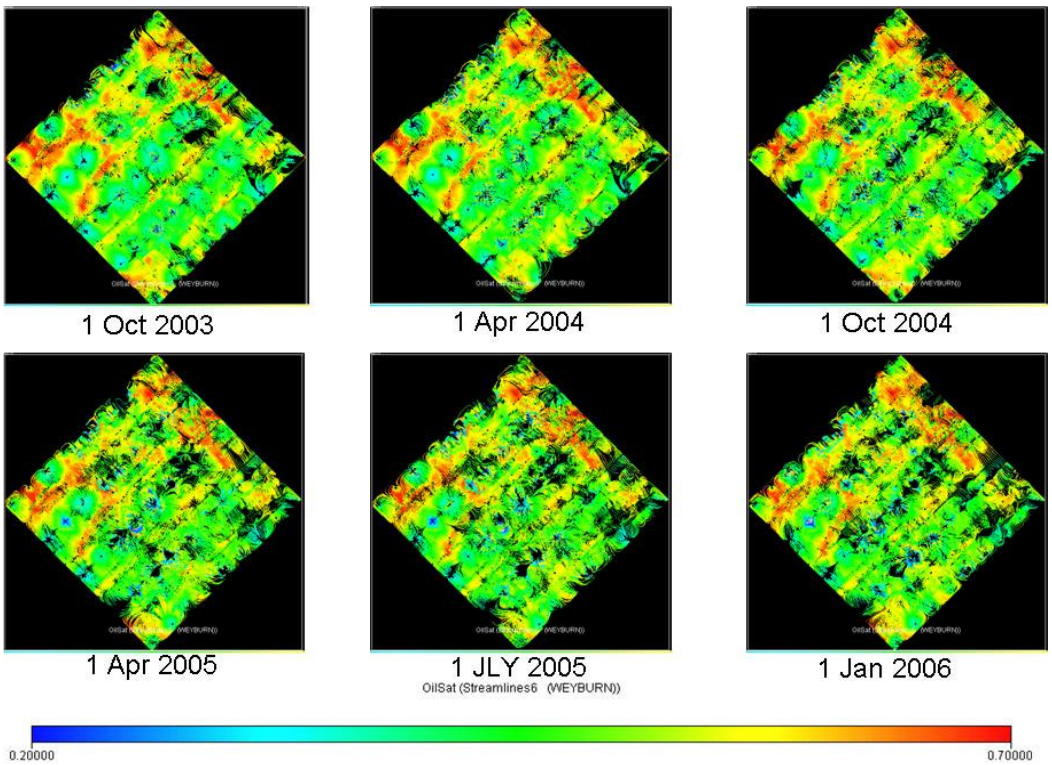

Fig. 45 – Field Case for CO_2 Flood Study: Oil Streamlines during CO_2 Flood Regime (Traced from Cells as Sinks, Oil Saturation Mapped on the Streamlines)

V.4.2.4 Water Streamlines

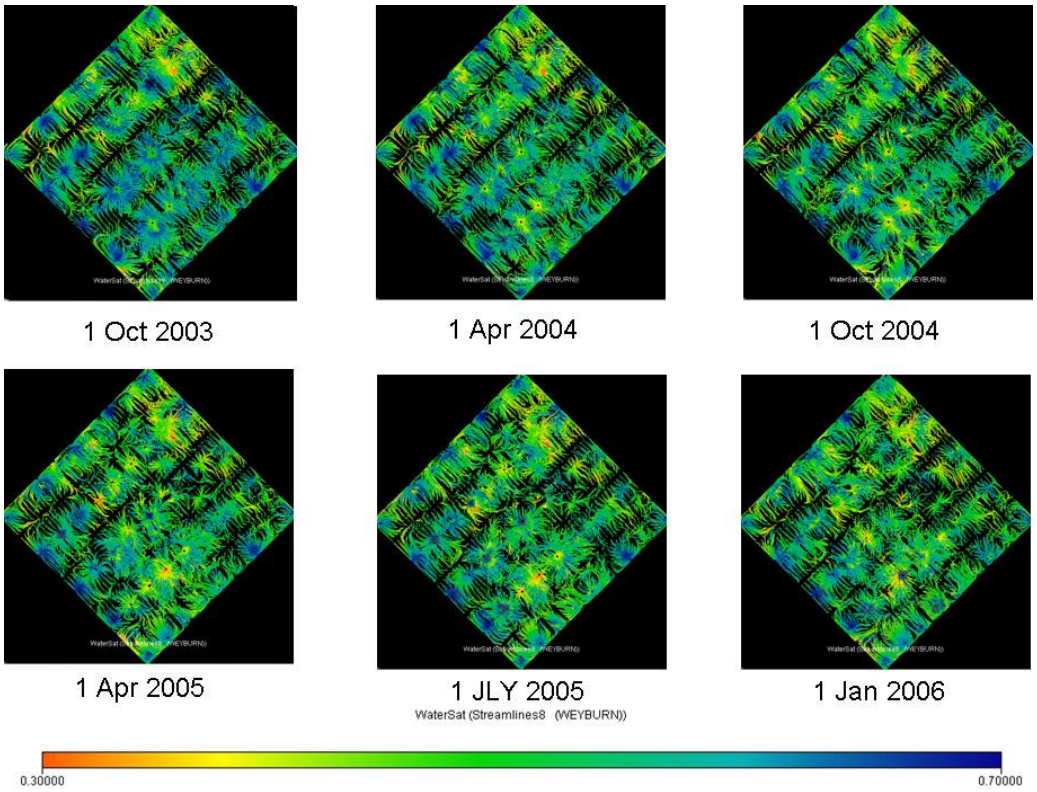

Fig. 46 – Field Case for CO_2 Flood Study: Water Streamlines during CO_2 Flood Regime (Traced from Cells as Sink, Water Saturation Mapped on the Streamlines)

In **Fig. 46**, the streamlines corresponding to water flux are presented and the streamlines are injector onwards to cells where fractional flow of water is greater than 0.1. Comparing with oil and total velocity streamlines, it can be noted that water is not a dominant phase of flow and in regions near the pattern boundaries the fractional flow of water is less than 0.1. The movement path of water being injected (during water cycle of WAG) can be observed and it can be noted that the flow is out of pattern for few of

them. Also the swept area vs. the volume of water allocated to the injectors can be used to rank them in terms of sweep efficiency.

V.4.2.5 Gas Streamlines

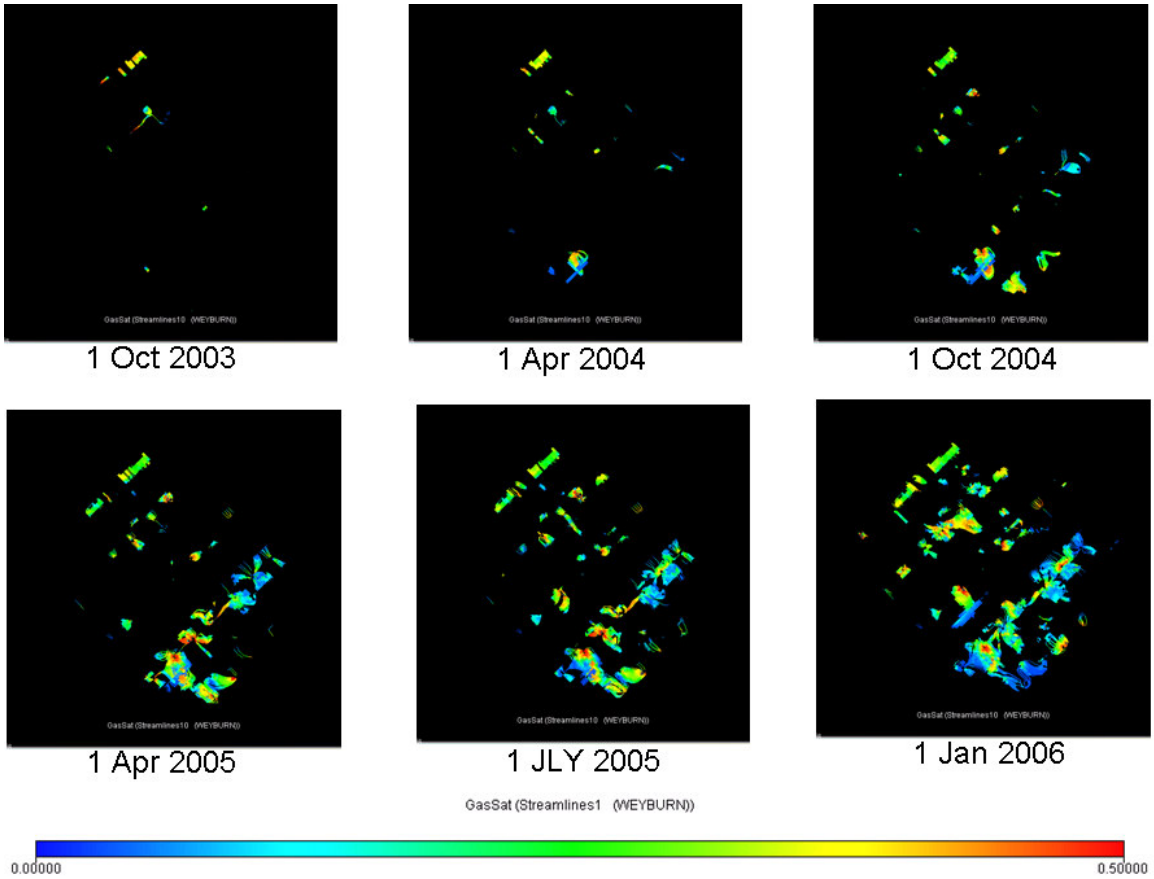

Fig. 47 – Field Case for CO_2 Flood Study: Gas Streamlines during the CO_2 Flood Regime (Traced from Cells as Sinks, Gas Saturation Mapped on the Streamlines)

Fig. 47 shows the gas streamlines traced from individual grid cells to the injectors. Here it can be observed that the gas streamlines almost overlap with the CO_2 streamlines suggesting that the CO_2 is in gaseous phase near the well and not much of it is in dissolved phase with oil. This indicates that the pressure is below MMP. Still there is some region in the middle of map where the CO_2 is in dissolved phase. The gas streamlines provides good information for the WAG cycles, because for efficient displacement of oil the CO_2 should swell oil, which is possible only when sufficient pressure and time is given for the process, thus in turn dictating the timing of CO_2 injection period and the following water injection period.

V.4.2.6 Comparison of Total Flux, Phase and Component Streamlines

Fig. 48 presents the total velocity streamlines and the CO_2 streamlines at the same time thus illustrating that the CO_2 movement was not captured by the streamlines traced using total flux.

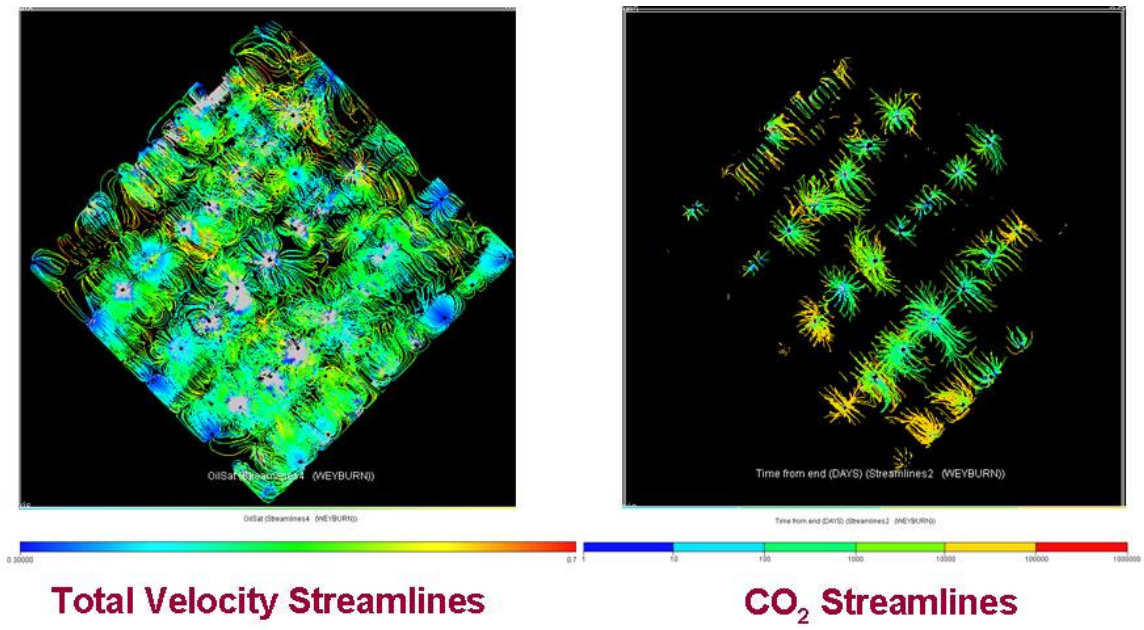

Fig. 48 – Total Velocity vs. CO_2 Streamlines for a Time-Step in CO_2 Flood (1st Oct 2005) (Traced From Cells as Sinks, Oil Saturation Mapped on Total Velocity Streamlines and TOF on the CO_2 Streamlines)

In **Fig. 49** and **Fig. 50**, the phase (oil, gas, water) and component streamlines at a specific time step have been compared. It can be noted that the regions with high density of CO_2 have dominant gas streamlines suggesting that the pressure of the reservoir is below MMP (minimum miscibility pressure) and hence CO_2 is not dissolved in oil and is in gaseous phase. By comparison of oil, water and gas streamlines it can be remarked that for all practical purposes water and oil streamlines are overlapping whereas gas streamlines are sparsely located suggesting that the flow in the reservoir is mostly two phase and most of the reservoir is above bubble point because of pressure maintenance

by water and CO_2 injection. All these information were not obtained by just using the streamlines traced using total flux.

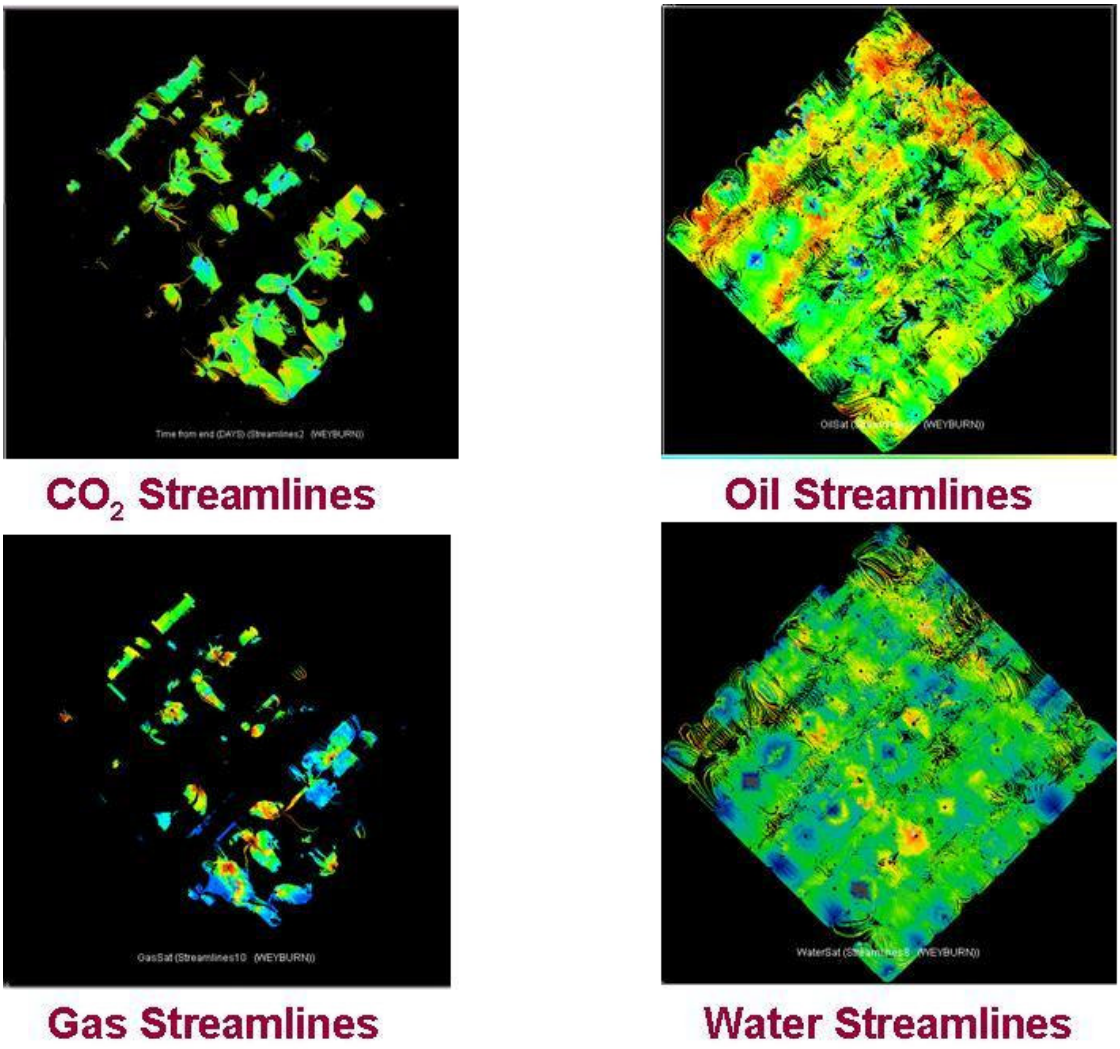

Fig. 49 – Comparison of CO_2 & Phase Streamline Tracing Provides Valuable Information for Tertiary Recovery Management
(Streamlines Traced on Time Step Corresponding to 1st Oct 2005)
(Traced from Producers as Sinks, TOF Mapped on the CO_2 Streamlines and Corresponding Saturations Mapped on the Phase Streamlines)
(For Scales Refer to their Respective Plots in Previous Sections)

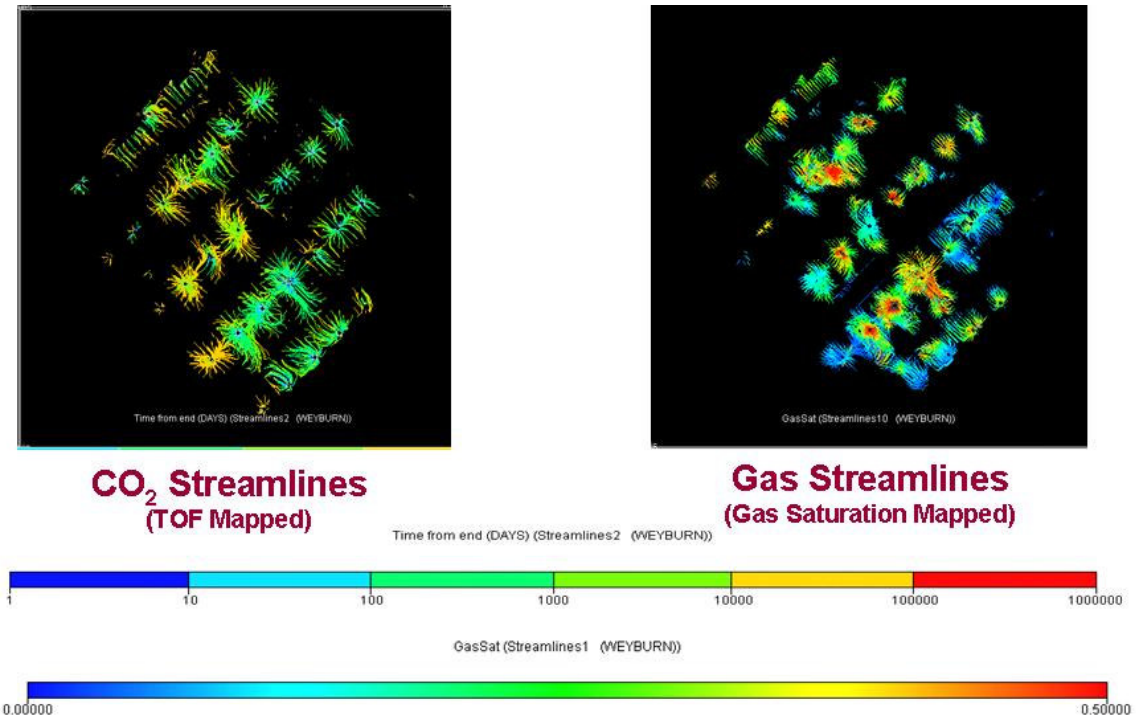

Fig. 50 – Comparison of CO_2 & Gas Streamline Tracing Shows That the CO_2 Is in Gaseous Phase (Streamlines Traced on Time Step Corresponding to 1st Oct 2005) (Traced from Cells as Sinks, TOF Mapped on the CO_2Streamlines and Gas Saturation on Gas Streamlines)

In **Fig. 51**, the phase and component streamlines for a hypothetical scenario of pressure regime and injection rates for the same field case is presented. The injection rates are significantly higher than the actual case and so is the reservoir pressure. This was done to demonstrate the condition in regions where the CO_2 is completely dissolved in liquid phases and does not exist in gaseous phase at the reservoir conditions. It can be noted that the regions with high density of CO_2 streamlines do not have dominant gas streamlines (in center of map) validating that the pressure of the reservoir is above MMP (minimum miscibility pressure) in those regions and hence CO_2 is dissolved in oil and is

not in gaseous phase. By comparison of oil, water and gas streamlines it can be remarked that water and oil streamlines are overlapping whereas gas streamlines are sparsely located suggesting that the flow in the reservoir is mostly two phase and most of the reservoir is above bubble point.

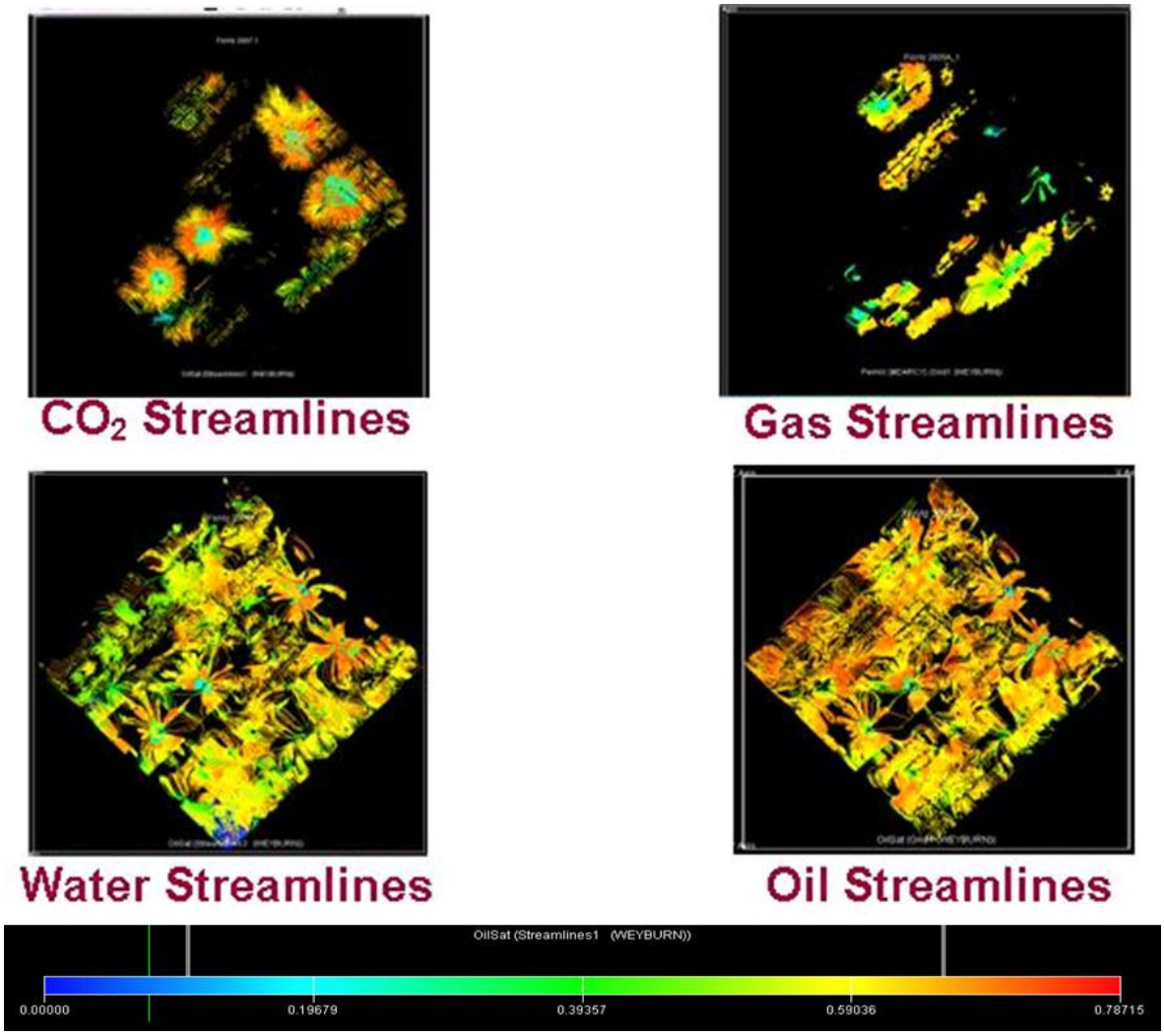

Fig. 51 – Comparison of CO_2 & Phase Streamline Corresponding to a Hypothetical Pressure and Injection Regime Where the CO_2 Is in Liquid Phase Dissolved in Oil Rather Than in Gaseous Phase under Some Conditions (1st Oct 2005) (Traced from Cells as Sinks, Corresponding Saturations Mapped on the Streamlines)

In **Fig. 52**, the CO_2 and water streamlines corresponding to different time-steps are presented for an injection well which is undergoing WAG (Water Alternate Gas) injection process. The corresponding injection schedule is presented in **Fig. 53**. It can be noted that the period of water and CO_2 injection can be differentiated based on water/ CO_2 streamlines. CO_2 Streamlines are not present at 1 July 2003 when there is no CO_2 injection, few water streamlines are at 1 Oct 2004 when CO_2 injection cycle is going on and again CO_2 Streamlines decrease when water injection cycle starts. We can also see that the preferential paths of movement of the two phases are different which is logical since different mechanisms are responsible for movement of CO_2 and water.

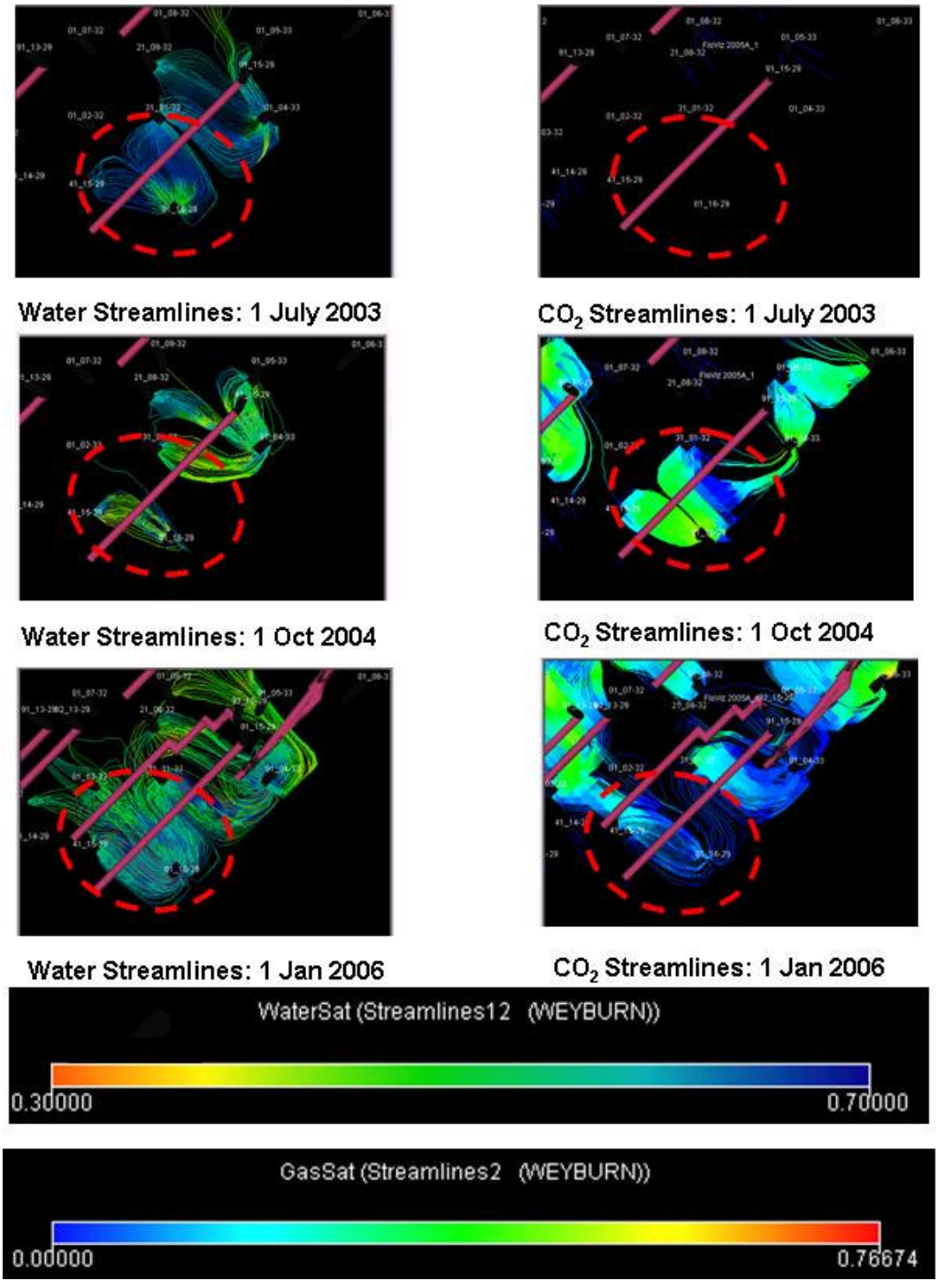

Fig. 52 – Water and CO_2 Streamlines for a Particular Injector at Different Timesteps to Demonstrate Their Use in Study of WAG Processes (Traced from Cells as Sinks, Water Saturation Mapped on Water Streamlines and Gas Saturation on CO_2 Streamlines)

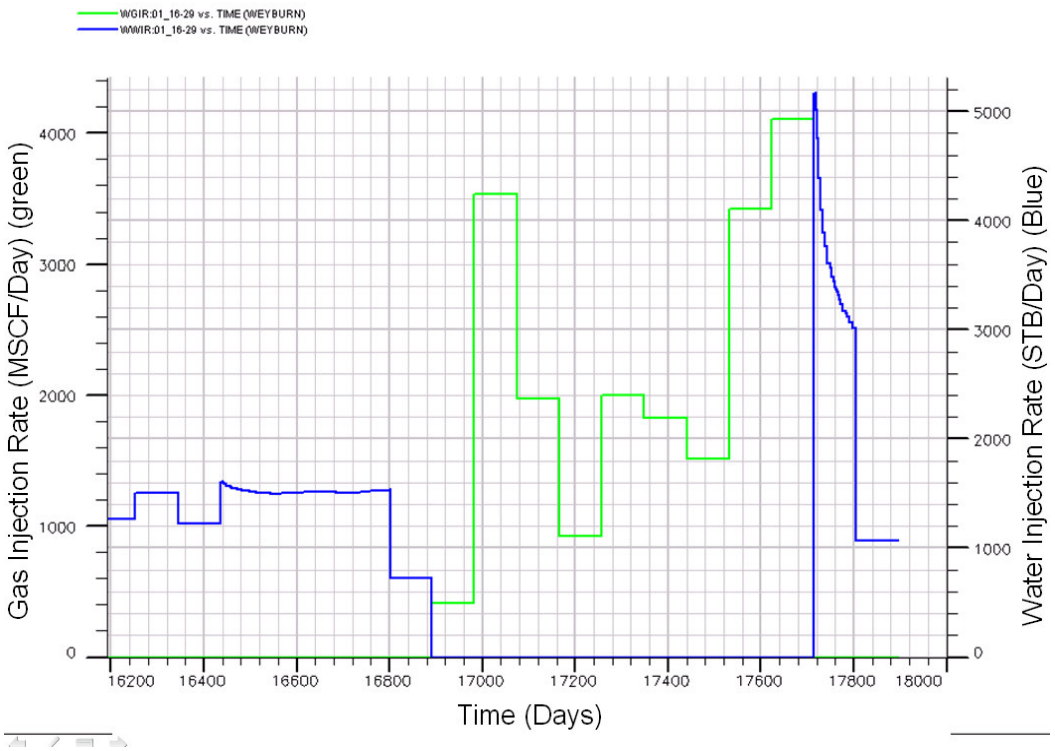

Fig. 53 – Water and CO_2 Injection Rates for a Particular Injector Showing the WAG Cycles

V.4.3 Rate Allocations and Drainage Area Mapping Using the Phase Streamlines

Fig. 54 presents the oil streamlines corresponding to a particular well from the CO_2 field case study. This time-step corresponds to the field under initial water injection drive in 1960s. From the oil streamlines it can be pointed out that the main contributors to oil flow are two different layers (one having streamlines with orange and the other with yellow colored streamlines) and using fraction of streamlines in each layer, share of production from the different layers can be found. Similar analysis for water streamlines

in injectors will lead to identification of thief zone taking most of the water injected. Water streamlines in producers will identify the zone to be shut off to reduce the water production. Here if only total streamlines are used then they would give the fraction of total production coming from different layers without differentiating between the phases.

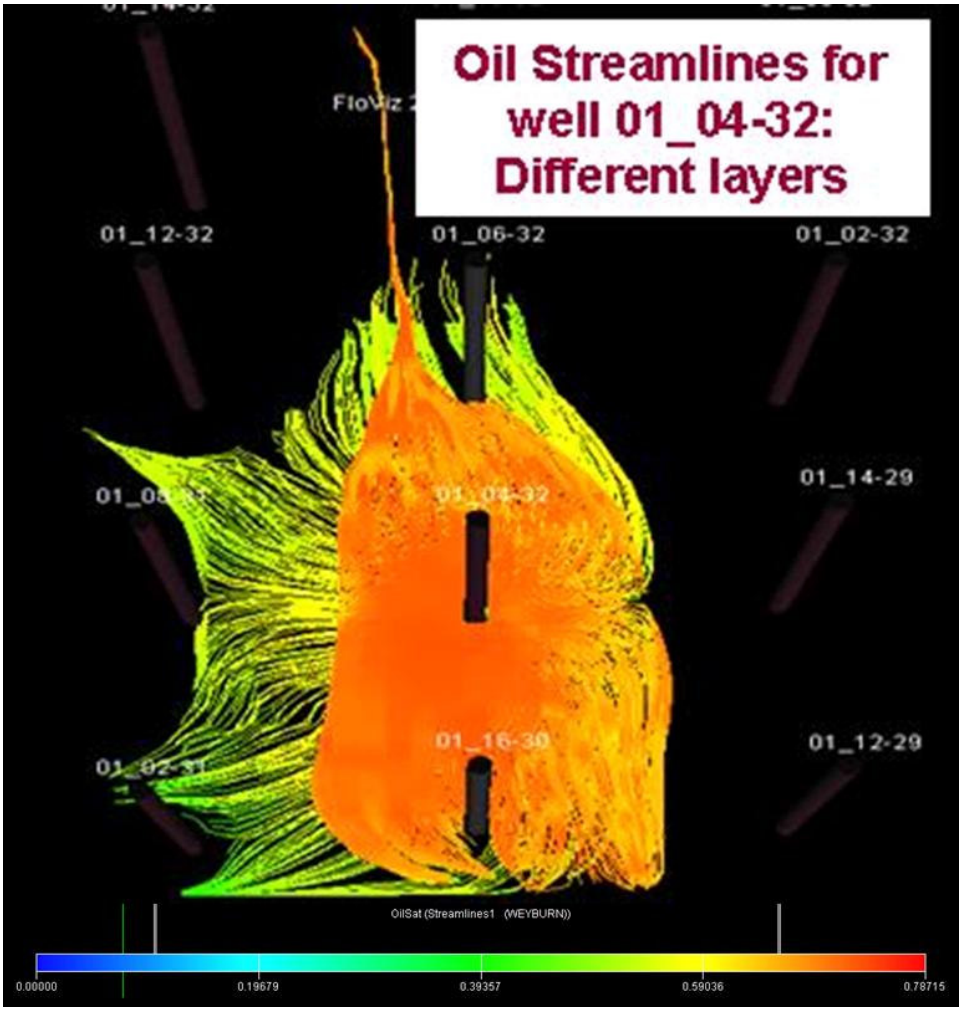

Fig. 54 – Oil Streamlines for a Particular Well: Can Be Used for Estimating Layer Contributions and Drainage Area in Each Layer (Traced from Producers as Sinks, Oil Saturation Mapped on Streamlines)

From the **Fig. 54** it can also be observed that the area of drainage is different in different layers and so oil streamlines can be used to map the oil drainage area in different layers.

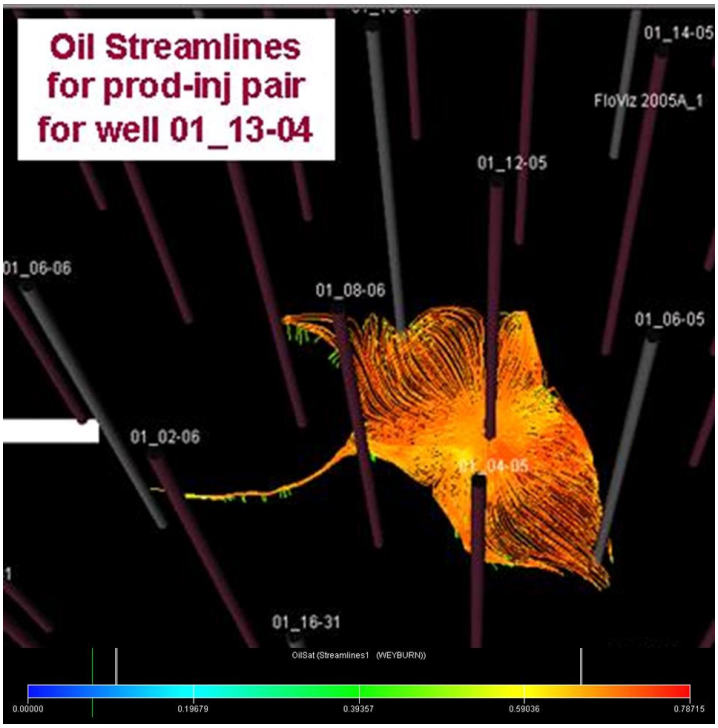

Fig. 55 – Oil Streamlines For Producer-Injector Pair: Allow Estimation of Oil Rate Allocation of Producers to Corresponding Injectors (Traced from Producers as Sinks, Oil Saturation Mapped on Streamlines)

In **Fig. 55**, oil streamlines have been shown for a producer, which is being pressure supported by water injection from two wells. Using the fraction of streamlines

for these two pairs we can estimate how much oil production of the well, under consideration, can be allocated to each of the injectors. This kind of dynamic allocation has been done previously using total velocity streamlines but they did not furnish any information about the contributions of the individual phases in flow, i.e. from total velocity streamlines one can not conclude the contribution of injector A to the water production of producer B or the contribution of injector C to the oil rate of producer B.

Traditionally the total flux streamlines have been used for mapping the drainage and swept area for a well. Here we would like to demonstrate that the phase streamlines can also be used to map the drainage area contributing to the production and the drainage area corresponding to different phases can be different from each other and from the total flux streamlines. In **Figs. 56** and **57** the streamlines for a time-of-flight cut-off of 10,000 days and the corresponding swept grid cells are presented in areal and vertical perspectives for a time-step corresponding to waterflood regime around an injector.

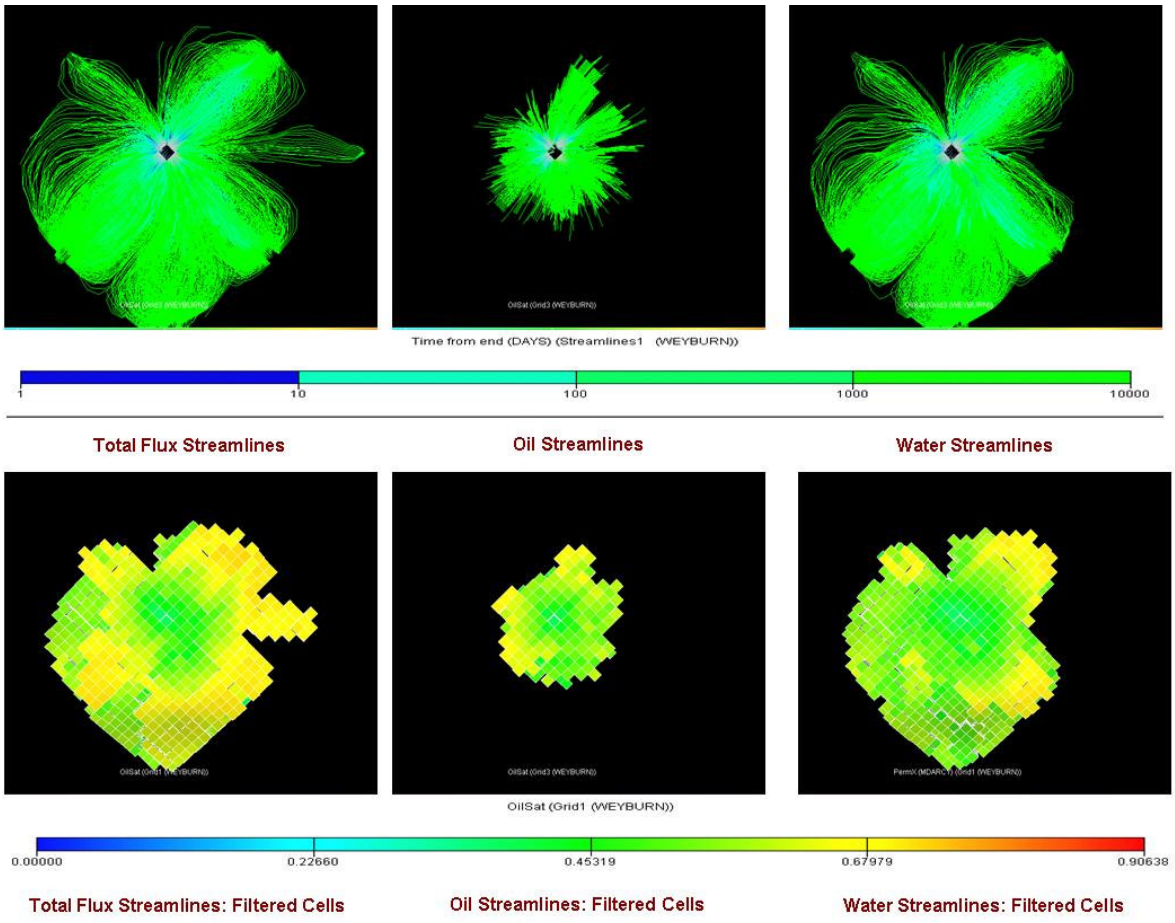

Fig. 56 – Streamlines Corresponding to an Injector Traced Using Total Flux, Oil Flux, and Water Flux With TOF Threshold of 10,000 Days and Corresponding Filtered Grid Cells. (Top View)
(Traced from Cells as Sinks, TOF mapped on the Streamlines)

Here it can be observed that the as water is being injected in the lower layers they constitute the bulk of flow there and they provide the pressure support to the production of the producer from bottom. The regions of the dominant flow of phases can be identified independently both in terms of areal expansion as well as the vertical distribution. They can be used to identify the left over oil in layers and also to identify thief zones taking lot of water without effecting any meaningful displacement.

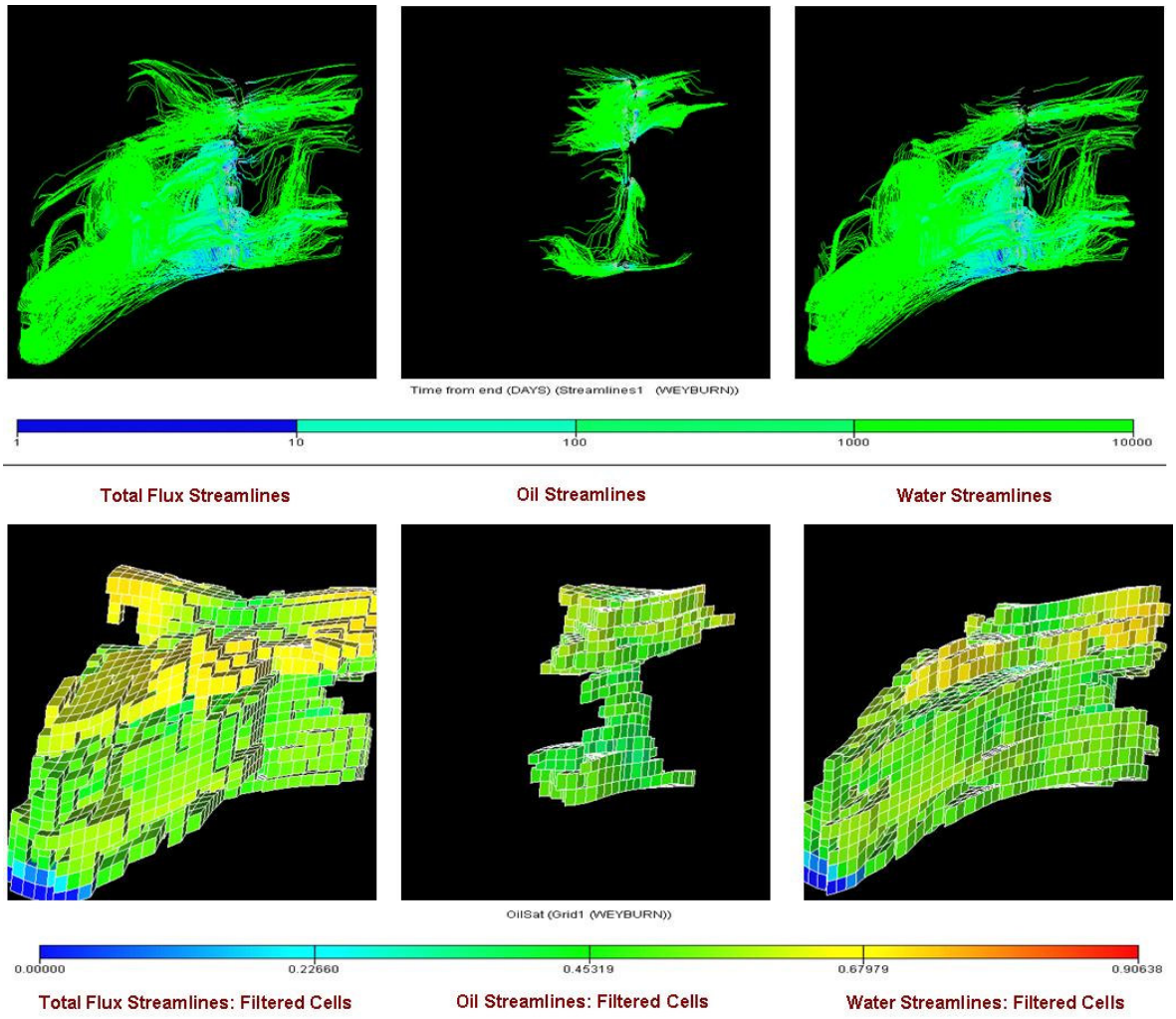

Fig. 57 – Streamlines Corresponding to an Injector Traced Using Total Flux, Oil Flux, and Water Flux With TOF Threshold of 10,000 Days and Corresponding Filtered Grid Cells. (Side View)
(Traced from Cells as Sinks, TOF mapped on the Streamlines)

CHAPTER VI

CONCLUSIONS

1. The phase and components streamline tracing has been successfully demonstrated and the power and utility of these have been analyzed using synthetic and field cases.

2. For forward flow simulation, industry standard black oil and compositional simulators have been used to obtain fluxes and a post processing tool has been used for tracing streamlines corresponding to total flux, phase fluxes and component fluxes.

3. Phase and component streamlines overcome some of the shortcomings of the streamlines traced using total velocities, particularly in terms of flow visualization and understanding reservoir flow.

4. Uses of phase and component streamlines are as follows:

    4.1 As a source of additional information towards understanding of reservoir drive mechanism.

    4.2 Phase streamlines have been successfully used for identification of the dominant phase(s) in flow in different regions of the reservoir. Based on their trajectories the area swept for any particular phase can be identified as well as the effects of permeability channels or high permeability streaks on the distribution of phase flows can be identified.

4.3 The phase streamlines have also been used for depiction of appearance and disappearance of phase(s) in reservoir. Thus, they can be used to explain high gas oil ratio in some wells vs. others having low GOR.

4.4 The use of phase streamlines (for the phase which is being injected, e.g. water streamlines corresponding to water injection wells) for study of effects of reservoir parameters on the flow of fluid being injected have been demonstrated. They have also been used for locating regions which are not benefiting from the current injection program. Thus they can be used for optimization of location of injection well and the injection rates. Also, oil streamlines have been successfully used to identify the regions unswept of oil so they can be used to identify the location of infill wells to maximize the recovery from the reservoir. Thus, the phase streamlines are of potential significance in secondary recovery processes like waterflooding.

4.5 As the component streamlines have been demonstrated to be capable of tracking the movement of components like CO_2 or other gases which can be used during tertiary recovery processes, the location of infill wells for production and injection can be optimized based on them. So they have been proved to be a promising tool for tertiary field development and management.

4.6 As phase streamline delineated regions have been shown to be more localized than the total velocity streamlines, so use of phase streamlines would have a better tendency to preserve the prior model and therefore they

can be used as an improvement over the total velocity streamline during assisted history matching.

4.7 As CO_2 dissolved in any phase, including water, can be tracked using the formulation presented, the component streamlines corresponding to CO_2 along with the total and phase streamlines can be used for CO_2 sequestration management where CO_2 is injected in aquifers for long time storage. Also component streamline can be used to track movement of components.

4.8 The use of phase streamlines to allocate the contribution of any layers in any phase flow has been demonstrated. The oil streamlines have been used to back allocate the production to different producing layers. Following similar rationale, the intake capacity of the layers or zones in any reservoir can be estimated. These are useful in identify the thief zones and the cross flow in reservoir.

4.9 Using phase streamlines the total rate allocation using total velocity streamlines can be further broken down to individual phase rates. This use has also been demonstrated.

REFERENCES

1. Datta-Gupta, A., King, M.J.: *Streamline Simulation: Theory and Practice*, SPE Publications, Richardson, Texas (2007).

2. Datta-Gupta, A.: "Streamline Simulation: A Technology Update," Paper SPE 65604 presented as 1999-2000 SPE Distinguished Author Series.

3. Thiele, M.R.: "Streamline Simulation," keynote address presented at the 2001 International Forum on Reservoir Simulation, Schloss Fuschl, Austria, 3-7 September.

4. King, M.J. and Datta-Gupta, A.: "Streamline Simulation: A Current Perspective," *In Situ* (1998), **22**, No. 1, 91.

5. Samier, P., Quettier, L., and Thiele, M.: "Applications of Streamline Simulations to Reservoir Studies," *SPE Reservoir Evaluation & Engineering* (August 2002) 324.

6. Baker, R.O., Kuppe F., Chugh, S., Bora, R., Stojanovic, S., and Batycky, R.: "Full-Field Modeling Using Streamline-Based Simulation: Four Case Studies," *SPE Reservoir Evaluation & Engineering* (April 2002) 126.

7. Li, Dacun: "Comparative Simulation Study of Water Flood," Paper SPE 88459 presented at the 2004 SPE Asia Pacific Oil and Gas Conference and Exhibition, Perth, Australia, 18-20 October.

8. Kurelenkov, Sergey Kh., and Ryazanov, A.V.*:* "Efficiency Evaluation of Non-Uniform Upgridding Method Based on Streamlines Approach: Western Siberia Field Example," Paper SPE 104347 presented at the 2006 SPE Russian Oil and Gas Technical Conference and Exhibition, Moscow, Russia, 3-6 October.

9. Jimenez, E.: "The Impact of Grid Geometry on Displacement Calculations," M.S. Thesis, Texas A&M University, College Station, TX (August 2004).

10. Jimenez, E., Sabir, K., Datta-Gupta, A., and King, Michael J.: "Spatial Error and Convergence in Streamline Simulation," *SPE Reservoir Evaluation & Engineering* (June 2007) 221.

11. Pollock, D.W.: "Semi-analytical Computation of Path Lines for Finite Difference Models," *Ground Water*, (November-December 1988) **26,** 6.

12. Cordes, C., and Kinzelbach, W.: "Continuous Groundwater Velocity Fields and Path Lines in Linear, Bilinear and Trilinear Finite Elements," *Water Resources. Res.* (1994) **30**, No. 4, 965.

13. ECLIPSE File Formats Reference Manual, 2005A, Schlumberger Information Solutions.

14. ECLIPSE Reference Manual, 2005A, Schlumberger Information Solutions.

15. ECLIPSE-300 Reference Manual, 2005A, Schlumberger Information Solutions.

16. Alhuthali, A.H., Oyerinde, D., and Datta-Gupta, A.: "Optimal Waterflood Management Using Rate Control," Paper SPE 102478 presented at the 2006 SPE Annual Technical Conference and Exhibition, San Antonio, Texas, 24 - 27 September.

17. Grinestaff, G.H., and Caffrey, D.J.: "Water Management: A Case Study of the Northwest Fault Block Area of Prudhoe Bay, Alaska, Using Streamline Simulation and Traditional Waterflood Analysis," Paper SPE 63152 presented at the 2000 SPE Annual Technical Conference and Exhibition held in Dallas, Texas, 1-4 October.

18. Thiele, M. R. and Batycky, R. P.: "Using Streamline-Derived Injection Efficiencies for Improved Waterflood Management," *SPE Reservoir Evaluation and Engineering* (April 2006) 187.

19. Naguib, M. , Sikaiti, S. , Balushi, H. , Barrio, C., Mahrooqi, S. and Batycky, R.: "Results of Proactively Managing a Heavy-Oil Waterflood in South Oman Using Streamline-Based Simulation," Paper SPE 101195 presented at 2006 SPE Asia Pacific Oil & Gas Conference and Exhibition, Adelaide, Australia, 11-13 September.

20. Spath, J., and McCants, S.: "Waterflood Optimization Using a Combined Geostatistical – 3D Streamline Simulation Approach: A Field Example," Paper SPE 38355 presented at 1997 SPE Rocky Mountain Regional Meeting, Casper, Wyoming, 18-21 May.

21. Grinestaff, G. H.: "Waterflood Pattern Allocations: Quantifying the Injector to Producer Relationship with Streamline Simulation," Paper SPE 54616 presented at 1999 SPE Western Regional Meeting, Anchorage, Alaska, 26-27 May.

22. Giordano, Ronald M., Jayanti, S., Chopra, A., Yuan, H., Asakawa, K., Suleimani, Ali, Gheithy, Ali, and Edwards, C.: "A Streamline Based Reservoir Management Workflow to Maximize Oil Recovery," Paper SPE 111143 presented at the 2007 SPE/EAGE Reservoir Characterization and Simulation Conference, Abu Dhabi, UAE, 28-31 October.

23. Ibrahim, Muhammad N., Clark, Robert A. Jr., and Al-Matar, Bader S.: "Streamline Simulation for Reservoir Management of a Super Giant: Sabiriyah Field North Kuwait Case Study," Paper SPE 105069 presented at the 2007 SPE Middle East Oil and Gas Show and Conference held in Kingdom of Bahrain, 11-14 March.

24. He, Z., Parikh, H., Datta-Gupta, A., Perez, J., and Pham, T.: "Identifying Reservoir Compartmentalization and Flow Barriers Using Primary Production: A Streamline Approach," Paper SPE 77589 presented at the 2002 SPE Annual Technical Conference and Exhibition, San Antonio, Texas, 29 September - 2 October.

25. Park, C., Kang, J.M., Jung, Y., and Kim, S.: "Streamline-Based Simulation To Investigate Interwell Connectivity and Tracer Transport in 3D Discrete Fractured Reservoir," Paper SPE 100216 presented at the 2006 SPE Europec/EAGE Annual Conference and Exhibition, Vienna, Austria, 12-15 June.

26. Beraldo, V.T., Blunt, M.J., Schiozer, D.J., and Qi, R.: "Streamline Simulation With an API Tracking Option," Paper SPE 107496 presented at the 2007 EUROPEC/EAGE Conference and Exhibition, London, U.K., 11-14 June.

27. Turan, H., Brand, P., Grinestaff, G., and Trythall, R.: "Forties CO_2 IOR Evaluation Integrating Finite Difference and Streamline Simulation Techniques," Paper SPE 78298 presented at the 2002 SPE 13th European Petroleum Conference, Aberdeen, Scotland, U.K., 29-31 October.

28. Ruan, F., Carhart, S., Giordano, R.M., Grinestaff, G.H., Bratvedt, F., and Olufsen, R.: "An Overview of Streamline Tracer Modeling of Miscible/ Immiscible WAG Injection IOR," Paper SPE 75198 presented at the 2002 SPE/DOE Improved Oil Recovery Symposium, Tulsa, Oklahoma, 13-17 April.

29. Agustsson, H., Grinestaff, G.H.: "A Study of IOR by CO_2 Injection in the Gullfaks Field, Offshore Norway," Paper SPE 89338 presented at 2004 SPE/DOE Fourteenth Symposium on IOR, Tulsa, Oklahoma, U.S.A., 17-21 April.

30. Cheng, H, Khargoria, A., He, Z., and Datta-Gupta, A.: "Fast History Matching of Finite-Difference Models Using Streamline-Derived Sensitivities," *SPE Reservoir Evaluation and Engineering* (October 2005) 426.

31. Cheng, H., Oyerinde, D. Datta-Gupta, A. and Milliken, W.: "Compressible Streamlines and Three-Phase History Matching," *SPE Journal* (December 2007) 475.

32. Oyerinde, A., Datta-Gupta, A., and Milliken, W.: "Experiences With Streamline-Based Three-phase History Matching," Paper SPE 109964 presented at the 2007 SPE Annual Technical Conference and Exhibition, Anaheim, California, U.S.A, 11-14 November.

33. Batycky, R.P., Seto, A.C., and Fenwick, D.H.: "Assisted History Matching of a 1.4-Million-Cell Simulation Model for Judy Creek 'A' Pool Waterflood/HCMF Using a Streamline-Based Workflow," Paper SPE 108701 presented at the 2007 SPE Annual Technical Conference and Exhibition, Anaheim, California, U.S.A, 11-14 November.

34. Agarwal, B., and Blunt, M. J.: "A Streamline-Based Method for Assisted History Matching Applied to an Arabian Gulf Field," *SPE Journal* (December 2004) 437.

35. Vasco, D.W., Datta-Gupta, A., He, Z., Behrens, R., Rickett, J., and Condon, P.: "Reconciling Time-Lapse Seismic and Production Data Using Streamline Models: The Bay Marchand Field, Gulf of Mexico," Paper SPE 84568 presented at 2003 SPE Annual Technical Conference and Exhibition, Denver, Colorado, 5-8 October.

36. Wang,Y., and Kovscek, A.R.: "Streamline Approach for History Matching Production Data," *SPE Journal* (December 2000) 353.

37. Caers, J., Krishnan, S., Wang, Y., and Kovscek, A.R.: "A Geostatistical Approach to Streamline-Based History Matching," *SPE Journal* (September 2002) 250.

38. Agarwal, B., and Blunt, M. J.: "Full-Physics, Streamline-Based Method for History Matching Performance Data of a North Sea Field," Paper SPE 66388 presented at the 2001 SPE Reservoir Simulation Symposium, Houston, Texas, 11-14 February.

39. Gilman, James R., Meng, Hai-Zui, Uland, Michael J., Dzurman, Peter J., and Cosic, S.: "Statistical Ranking of Stochastic Geomodels Using Streamline Simulation: A Field Application," Paper SPE 77374 presented at 2002 SPE Annual Technical Conference and Exhibition, San Antonio, 29 September – 2 October.

40. Al-Khalifa, M.A.: "Advances in Generating and Ranking Integrated Geological Models for Fluvial Reservoir," Paper SPE 86999 presented at the 2004 Asia Pacific Conference on Integrated Modeling for Asset Management, Kaula Lumpur, Malaysia, 29-30 March.

41. Wang. Y., and Kovscek, A.R.: "A Streamline Approach for Ranking Reservoir Models that Incorporates Production History," Paper SPE 77377 presented at the 2002 SPE Annual Technical Conference and Exhibition, San Antonio, TX, 29 September – 2 October.

VITA

Name:	Sarwesh Kumar
Address:	c/o Prof. Akhil Datta-Gupta 3116-TAMU-702 Dept of Petroleum Engineering, Richardson Building Texas A&M University, College Station TX-77843
Email Address:	sarwesh.ism@gmail.com
Education:	B.Tech., Petroleum Engineering, Indian School of Mines, Dhanbad, India, 2003 M.S., Petroleum Engineering, Texas A&M University, 2008
Experience:	Petroleum Engineer, Reliance Ind. Ltd., India. 2003-2006 Research Assistant, Texas A&M University, 2006-2008 Summer Intern, Chevron NAEP, Houston, (Summer) 2007